Fly ash based alkali-activated materials cured under ambient conditions

Oscar Tarique

A project report submitted in partial fulfilment of the requirements for the degree of

MASTERS OF ENGINEERING (STRUCTURAL ENGINEERING)

in the

FACULTY OF ENGINEERING, BUILT ENVIRONMENT AND INFORMATION TECHNOLOGY

UNIVERSITY OF PRETORIA

OCTOBER 2019

DISSERTATION SUMMARY

FLY ASH BASED ALKALI-ACTIVATED MATERIALS CURED UNDER AMBIENT CONDITIONS

OSCAR TARIQUE

Supervisor: Doctor Maxim Kovtun

Department: Civil Engineering

University: University of Pretoria

Degree: Master of Engineering (Structural Engineering)

In South Africa, approximately 35 million tonnes of fly ash (FA) gets produced annually of which only 7% are recycled. The rest gets discarded to massive landfills. This poses several environmental issues such as air pollution and heavy metals leaching into the groundwater. The National Development Plan 2030 is one of the most strategic initiatives of South Africa. The plan has placed a specific attention to reduce the waste-to-landfill problem in the country. Thus, to reduce the FA landfill issue, a nationwide need for its consumption and usage has to exist.

Alkali-activated materials (AAM) are building materials that utilise source materials rich in Al and Si, it provides an opportunity to use by-products such as FA, silica fume (SF) and granulated blast furnace slag (GBFS). Therefore, since AAM can utilise FA as waste material, it will not only recycle FA but also provide a building material with good mechanical properties and provide a drive towards a reduction in global CO_2 emissions caused by cement manufacture.

However, AAMs need controlled environments to produce, can be costly and are highly variable due to the binder's chemical composition. To achieve sufficient strength and mechanical properties, it is often required that FA based AAM's be cured under elevated temperature conditions. This impedes its range of application and drives consumers away from its acceptance as a suitable alternative binder to cement. Thus, the main objective of this study was to create suitable FA based AAM blends that can be cured under ambient conditions.

One solution was to replace a portion of FA with SF and use calcium hydroxide (CH) and sodium carbonate (SC) as activators. These activators are 2-3 times cheaper than activators the commonly used for FA activation (sodium hydroxide and sodium silicates) while also being non-hygroscopic (critical property in production of dry powder AAMs), low impact and safer to handle (less corrosive). Combination of this with SF's high reactivity, this proposed system has potential to address the issues.

The experiment was conducted to test the aptitude of the FA|SF|CH|SC blend by determining the influence of each mix component on the strength development. This was followed by characterization techniques to study the mineralogical and microstructural properties.

The FA|SF|CH|SC blends gained 44.2 and 14.2 MPa as the highest and lowest strength at 28 days, respectively. The main trend noticed is that samples that gained the higher strengths at 28 days had a low strength at 3 days and samples that gained high strength at 3 days did not gain significant strength at 28 days. The characterization techniques suggest that there is either an early reaction occurring or a delayed reaction depending on the content of the two activators. Furthermore, the techniques also revealed that gaylussite and calcite are dominant in the mixtures which serves to aid in creating more denser microstructures.

ABSTRACT

FLY ASH BASED ALKALI-ACTIVATED MATERIALS CURED UNDER AMBIENT CONDITIONS

OSCAR TARIQUE

Title: Fly ash based alkali-activated materials cured under ambient conditions

Author: Oscar Tarique

Supervisor: Doctor Maxim Kovtun

Department: Civil Engineering

University: University of Pretoria

Degree: Master of Engineering (Structural Engineering)

The disposal of fly ash into landfills is quickly becoming a cause of concern. Alkali-activated materials (AAM) can utilise fly ash as source material to create building materials that can perform on par with cement. However, it is often required that fly ash AAM's be cured under elevated temperatures. The chosen blend consisted of using low impact activators that gained highest strength of 44.2 MPa at 28 days. The two trends noticed were the samples had either low or rapid strength development from a high and low 3-day strength, respectively. Microstructural and mineralogical studies suggest that reactions occur at different times depending on the content of the activators. Furthermore, mixtures contained prominent amounts of gaylussite and calcite, which provided a beneficial effect of creating denser microstructures.

.

DECLARATION

I, the undersigned hereby declare that:

- I understand what plagiarism is and I am aware of the University's policy in this regard;
- The work contained in this dissertation is my own original work;
- I did not refer to work of current or previous, lecture notes, handbooks or any study material without referencing;
- Where other people's work has been used this has been properly acknowledged and referenced;
- I have not allowed anyone to copy any part of my dissertation;
- I have not previously in its entirety or in part submitted this dissertation at any university for a degree.

DISCLAIMER:

The work presented in this report is that of the student alone. Students were encouraged to take ownership of their projects and to develop and execute their experiments with limited guidance and assistance. The content of the research does not necessarily represent the views of the supervisor or any staff member of the University of Pretoria, Department of Civil Engineering. The supervisor did not read or edit the final report and is not responsible for any technical inaccuracies, statements or errors. The conclusions and recommendations given in this report are also not necessarily that of the supervisor, sponsors or companies involved in the research.

Signature of student:

Name of student: **Oscar Tarique**

Student number: **11078554**

Date: **October 2019**

ACKNOWLEGEMENT

I wish to express my appreciation to the following organisations and persons who made this project report possible:

a) The Civil Engineering Department of the University of Pretoria for financial support, the provision of data and the use of laboratory facilities during the course of the study.

b) Dr Maxim Kovtun, my supervisor, for his guidance and support.

c) The laboratory personnel at the University of Pretoria for their assistance throughout the course of the study.

d) Wiebke Grote and Jeanette Dykstra for their assistance in performing XRD and XRF analyses and Prof Coville for conducting FTIR analysis. The assistance with SEM studies provided by André Botha and Alan Hall are gratefully acknowledged.

e) My family and friends for their encouragement and support during the study.

Table of Contents

List of Figures

List of Tables

1 INTRODUCTION

1.1 Background

Concrete poses a significant impact on the environment due to its high CO_2 emissions that occur from cement manufacture. This is caused by the universal utilization of concrete in the construction industry, which promotes the increased consumption of cement. Cement production contributes 5-7% of all anthropogenic CO_2 emissions worldwide. One ton of cement manufacture produces approximately 0.7-0.9 ton of CO_2 emissions. In Southern Africa, Pretoria Portland Cement (PPC) reported that CO_2 emissions were 753 kg per ton of cement manufactured (PPC, 2017).

Therefore, it becomes important that alternative binders be produced to reduce the carbon footprint. Alkali-activated materials (AAM) are one of those alternative binders that have shown similar and at times better mechanical properties than Portland cement with lower carbon emissions. Since AAM utilize source materials rich in Al and Si, it provides an opportunity to use by-products from different process such as fly ash (FA), silica fume (SF) and granulated blast furnace slag (GBFS).

Fly ash is a fine powder that is created as a by-product through the burning of pulverized coal in thermal power plants for producing electricity. However due to rapid industrial development and urbanization, the amount of fly ash generated is large and a majority of it ends up in landfills. In South Africa, Eskom is the entity responsible for generating electricity for the country and is the largest coal consumer. The company reports that the production of FA is approximately 35 million tonnes yearly, of which only 7% gets recycled. This poses several serious environmental and health hazards due its very fine particles and toxic heavy metals. South Africa has implemented a plan known as The South African National Development Plan 2030 (NDP), which places a specific attention to reduce the waste-to-landfill problem in the country. Since AAM requires by-products such as FA for its production, it gives value to FA and increases its recyclability whilst providing an adequate building material. This will not only promote a drive towards the strategic initiative set out by the NDP but also towards a global reduction in CO_2 emissions.

Fly ash based AAM are dubbed by some researchers as the "cement of the future". However, it does have its fair share of disadvantages which hamper its acceptance level in the industry. The chemistry of AAM is not yet fully understood nor documented as mix design guidelines like OPC. This, coupled with the conservatism of engineers and the industry, affects its reception.

Another major setback is that FA based AAM require elevated temperature curing to attain sufficient mechanical properties, which researchers suggests are on par and even at times better than OPC.

Ambient (25 °C) cured FA based AAM is a possibility but not practical due to delayed setting, intensive efflorescence formation, very slow strength development, relatively low strength at 28 days and large strength deviation. This significantly affects its industrial application. Ordinary Portland cement (OPC) concretes can be made at ambient temperatures on a construction site, in-situ. Thus, it relegates FA based AAM to the pre-cast industry.

This is further aggravated by cost implications. Although FA is relatively cheap, AAM can be expensive to implement due to the alkaline solutions used for activation, which are most commonly sodium hydroxide (NaOH) and sodium silicate (Na_2SiO_3). Moreover, there are additional concerns about environmental impacts from manufacturing such solutions. They are caustic and difficult to handle, which poses several health and safety concerns on site.

Therefore, in order for FA based AAM to be able to covert a harmful waste material into a cost-effective, environmentally friendly building material that the industry will be receptive to, it needs to consist largely of FA; be cured under ambient conditions; utilise low-impact activators and the process to create it should not deviate from current practices with OPC.

One solution is to replace a portion of FA with SF and use calcium hydroxide (CH) and sodium carbonate (SC) as activators. These activators are 2-3 times cheaper than the commonly used activators while also being dry, low impact and easier to handle. This study investigated and reported on the performance of such a blend.

1.2 Objectives of the study

The main objective of the proposed research project is to develop and investigate the potential strength and limitations of a FA based AAM cured under ambient conditions with the use of low impact activators.

The specific study objectives include:

- Test the aptitude and evaluate the fly ash-silica fume-calcium hydroxide-sodium carbonate (FA-SF-CH-SC) mixtures for acceptable compressive strength at early age (3 days) and 28 days with suitable workability.
- Study the strength development of the mixutres and provide insight on the trends observed and determine the influence of each mix component on the strength.
- Investigate the mineralogical and microstructural development of the mixtures through characterization techniques.

1.3 Scope of the study

Fly ash was the most dominant quantity in the mix (≥64.3 wt%). All mixtures only consisted of FA, SF, CH and SC in dry powder form to which only water was added. Coarse or fine aggregates were omitted from any experiment. All samples were cured under ambient conditions at 25 ºC. Compressive tests were conducted on 40 x 40 x 160 mm samples. Compressive tests beyond 28 days were not conducted. Mineralogical and microstructural analyses were performed on select samples aged 3 and 28 days, based on observed results of strength development.

1.4 Methodology

To test the performance and capacity of the proposed FA-SF-CH-SC blend cured under ambient condtions, the samples were tested for compressive strength at 3, 7 and 28 days. A central composite design was chosen to perform statistical analysis such as ANOVA, regression and residual analysis. Thereafter, the strength development was evaluated to determine the influence and trends of each mix component. This was followed by studying the mineralogical and microstructural properties of the blend by performing characterisation techniques such as heat flow calorimeter, X-ray diffraction (XRD), Fourier Transform Infrared Spectroscopy (FTIR), Thermal Gravimetric Analysis (TGA), Scanning Electron Microscopy (SEM) with backscattered electron (BSE) imaging and Energy Dispersive Spectroscopy (EDS) on fractured and polished samples. All experimental results were compared with literature.

1.5 Organisation of the report

The structure of the dissertation can be summarised as follows:

- **Chapter 1** includes the background, objective and scope of the study as well as the methodology and organization of report.
- **Chapter 2** chapter gives an overview of the origin and formation of alkali-activated materials as well as information on various types of unary and binary AAMs.
- **Chapter 3** details the experimental setup, information on materials and sample preparation as well as testing procedures.
- **Chapter 4** focuses on representation, interpretation and discussion of results.
- **Chapter 5** outlines the conclusion of the study and provides recommendations for future research.
- **Chapter 6** contains a list of references.

2 LITERATURE SURVEY

2.1 The problem with ubiquitous use of cement

Global utilization and consumption of concrete is only second to water. It is the crucial building material to give rise to society's infrastructures all around the world. Approximately 25 billion tonnes of concrete are produced annually on a global scale. This is equivalent to over 1.7 billion truck loads per year or about 6.4 million truck loads a day or over 3.8 tonnes per person around the globe each year (WBSCD, 2009; Madlool et al., 2011).

Thus, there is a high volume of concrete produced, which significantly increases the consumption of cement. Cement acts as an adhesive to bind the constituents in the concrete mix. It comprises of approximately 5-20% of concrete. The manufacture of cement, however, is a significant contributor to global CO_2 emissions. The production of clinker, an intermediate product in cement manufacture, is the most energy-intensive step that accounts for roughly 80% of the cement production (Zhu, 2011). Approximately 50% of carbon emissions, during the fabrication process, originate from decomposition of raw materials to form clinker. Combustion of fossil fuels in pyro-procession units release 40% of emissions. The last 10% are due to transportation of raw materials and electricity consumed by electrical motors and facilities (Ali et al., 2011; Turner & Collins, 2013; Benhelal et al., 2013). Figure 2-1 represents the points of CO_2 release during various stages of cement manufacture.

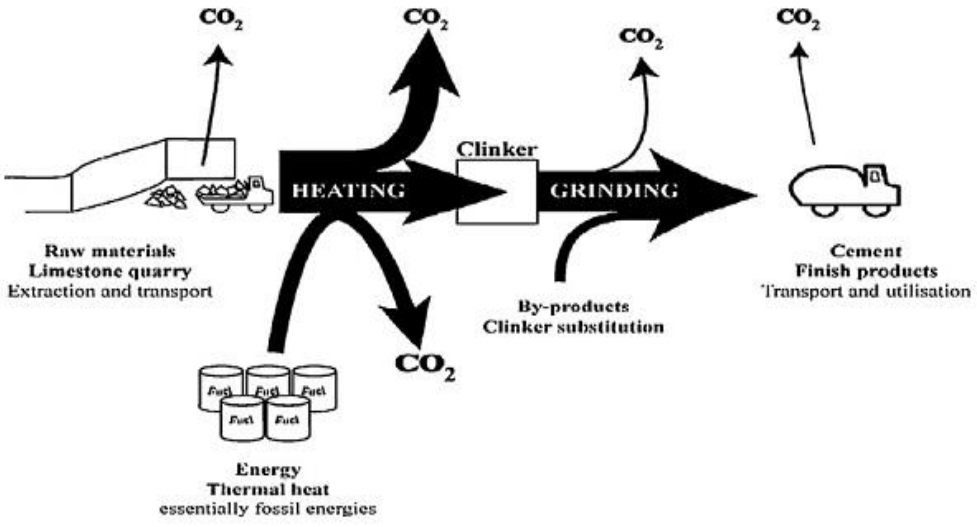

Figure 2-1: Schematic representation of cement fabrication process and CO_2 release point (Ali et al., 2011)

A large portion of CO_2 is released during calcination of limestone at 900 °C. It converts carbonates to oxides and CO_2 forms as a by-product in the chemical reaction. The simplified stoichiometric relationship can be expressed as:

$$CaCO_3 + heat \rightarrow CaO + CO_2 \uparrow \quad (1)$$

About 64-67% of clinker comprises of calcium oxide (CaO) while the rest are iron oxides and aluminium oxide. This amounts to roughly 0.5 kg of CO_2 that is produced per kilogram of clinker and emissions are dependent on clinker to cement ratio. Furthermore, it is estimated that 0.65-0.9 tonnes of CO_2 are produced per ton of cement depending on the type of fuel used, modern technology and equipment (Turner & Collins, 2013; Ali et al., 2011; Gibbs et al., 2000; Gao et al., 2014).

There is a significant impact of the environment due to the ubiquitous use of cement in civil construction and rapid increase in its production. Cement production contributes 5-7% of all anthropogenic CO_2 emissions worldwide (IEA & WBSCD, 2009). In South Africa, Pretoria Portland Cement has reported that in 2017 their CO_2 emissions were 1 055 kg per tonne of clinker and 765 kg per tonne of cement (PPC, 2017).

Since CO_2 emissions contribute to 65% of global warming, it has become imperative that alternative methods be established to reduce the carbon footprint. To further justify the need for substitutes, ordinary Portland cement (OPC) is subjected to certain limitations. These limitations include durability issues due to its intrinsic properties, high permeability that can cause carbonation and corrosion problems and alkali-silica reactions (Torgal et al., 2008).

An alternative to OPC cements is blended cements, which is expected to significantly reduce cement use. Cement is partially replaced by supplementary cementitious binder materials based on waste by-products such as fly ash (FA) and granulated blast furnace slag (GBFS). Another alternative method to produce a cementitious binder is the alkali activation of aluminosilicate materials (Turner & Collins, 2013; Rashad, 2014). This report will focus on the second alternative.

2.2 Brief history of alkali-activated materials

The alkali activation of aluminosilicate materials has become an integral topic of investigation due to its lower environmental impact and superior durability over OPC. The process involves chemically reacting alkaline solutions with silicon (Si) and aluminium (Al) from source materials of geological origins to produce binders. Therefore, these binders are known to emit very little CO_2 due to the absence of limestone and high temperature processes (Provis & Bernal, 2014; Rangan, 2010).

There is a rich history in the development of these alternative binders which dates back as early as the 1940's with the work of Purdon. The author activated blast furnace slag with sodium hydroxide and was the first to publish an extensive laboratory study on binders utilizing slag and alkali. In the late 1950's and early 1960's, Glukhovsky from the Soviet Union discovered, investigated and concluded that the binders in Roman and Egyptian construction were composed of aluminosilicate calcium hydrates (zeolite) and a natural rock known as analcite. These ancient mortars or concrete have been shown to be unaffected by severe corrosive conditions for 2 000 years whilst OPC can last only 10 years under the same conditions. This suggests that the formation of amorphous zeolitic compounds and presence of analcite vastly improves the durability of the binder. Based on those investigations, Glukhovsky created binders utilizing low-calcium or calcium-free aluminosilicate precursors activated by alkaline solutions and termed them as "soil-cement". The word "soil" is used as it appeared like a ground rock and "cement" due to its cementitious qualities (Torgal et al., 2008; Provis & Bernal, 2014; Roy, 1999).

In the 1970's, research and investigation in regard to alkali-activated cement saw an exponential rise due to the working of a French author named Davidovits. The author developed and commercialised binders that were prepared by alkali activation of metakaolin, a calcined product of the clay mineral kaolinite. He termed it as "geopolymer". This term defines a family of mineral binders or inorganic polymers that have a chemical composition similar to those of zeolites but with an amorphous structure. The binder is an adjusted and improved process that was used by Romans and Egyptians. Geopolymers have polymers that harden, polymerize and transform at low temperature but they are also inorganic, hard and stable at elevated temperatures (Torgal et al., 2008; Roy, 1999; Rangan, 2010; Silva et al., 2013).

2.3 The process behind the formation of alkali-activated materials

Alkali-activated materials involve a polymerization process. The main concept is the polymerization of Si-O-Al-O bonds that occurs when source materials consisting of Si and Al is dissolved in alkaline solutions such as sodium hydroxide (NaOH) and/or sodium silicate (Na_2SiO_3) (Das et al., 2014). The Al-O-Si polymeric structures form the building blocks of a geopolymeric structure. The alkali activation gives rise to 3-D cross-linked poly(siliate) chains and ring structures which result from the hydroxylation and polycondensation reaction of natural minerals (Khale & Chaudhary 2007). Three types of geopolymer structures occur: poly(sialate) (-Si-O-Al-O-), which was later termed as "geopolymer", poly(sialate-siloxo) (-Si-O-Al-O-Si-O-) and poly(sialate-disiloxo) (-Si-O-Al-O-Si-O-Si-O-). The latter two are more rigid, stable and stronger than poly(sialate) structures (Mustafa Al Bakri et al., 2011; Das et al., 2014). The images in Figure 2-2 and 2-3 represent the poly(sialate)

structures according to Davidovits and a computer molecular graphics of the framework, respectively.

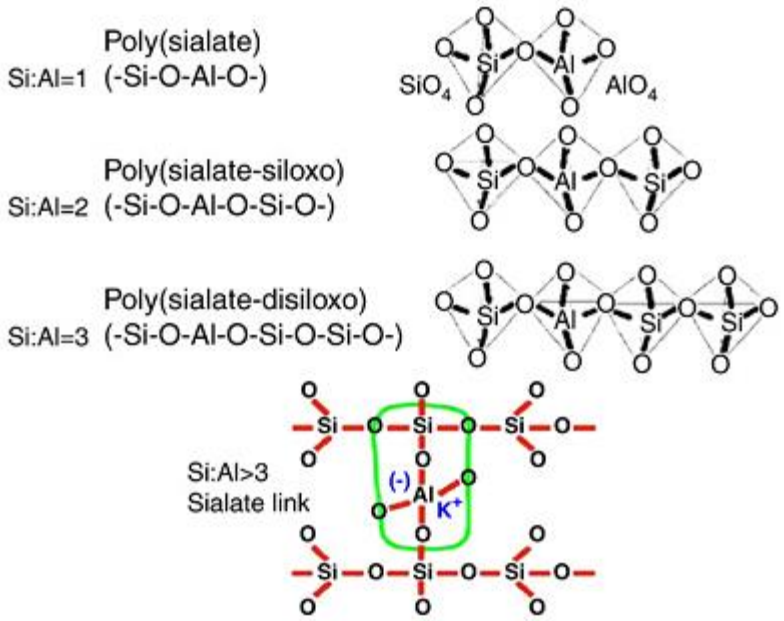

Figure 2-2: Poly(sialate) structures according to Davidovits (Li et al., 2010)

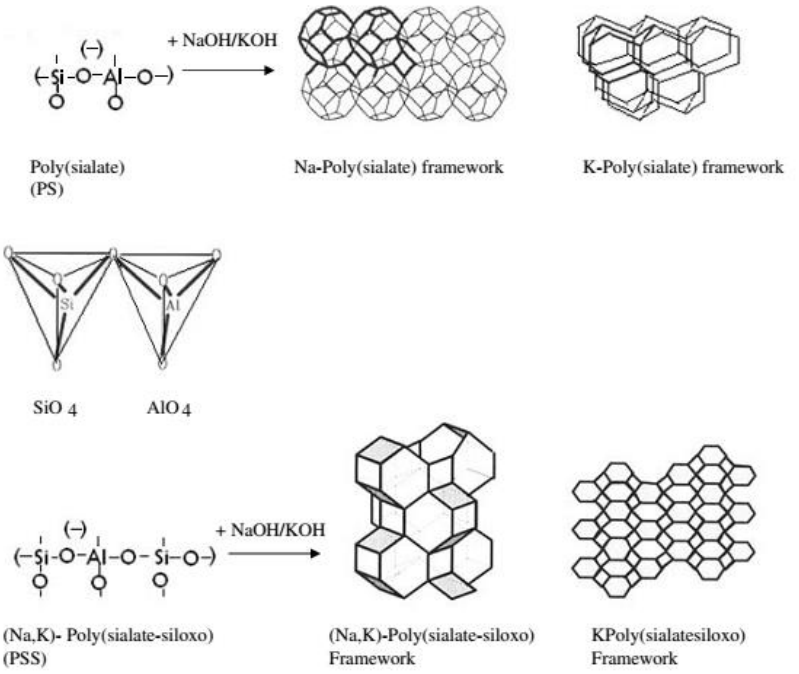

Figure 2-3: Computer molecular graphics of frameworks (Khale & Chaudary, 2007)

The image in Figure 2-4 represent the chemical reactions for geopolymerization (Khale & Chaudhary, 2007).

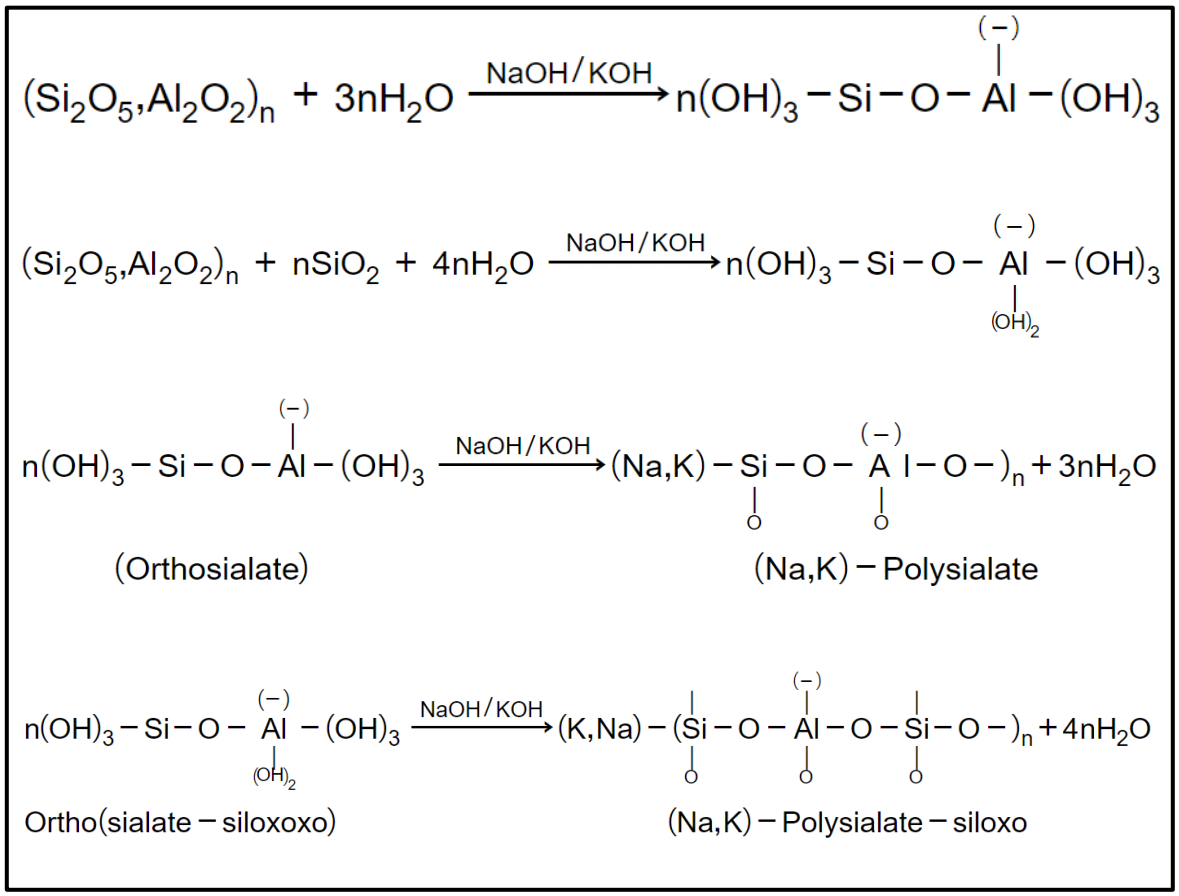

Figure 2-4: Chemical reactions during geopolymerization

The image in Figure 2-5 represents a conceptual model for AAM formation.

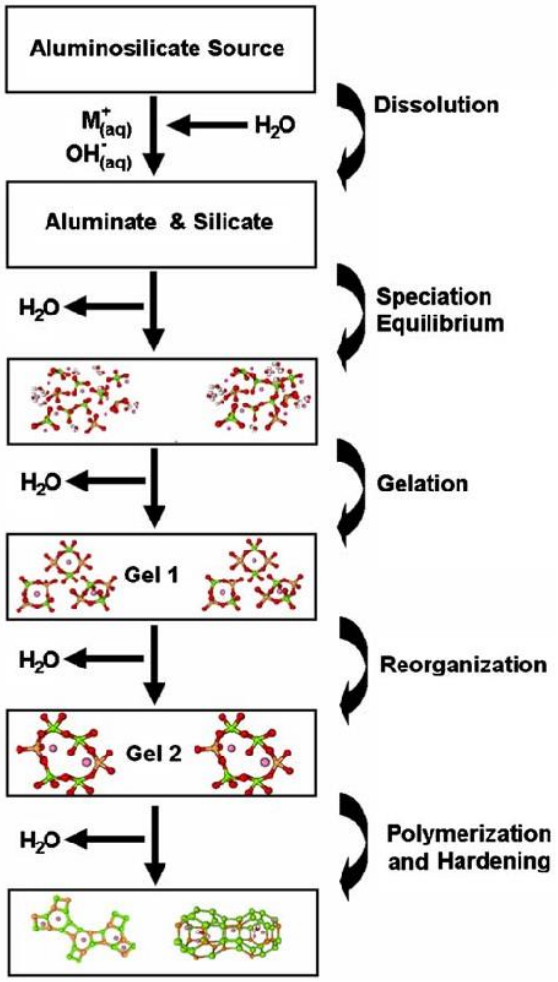

Figure 2-5: Conceptual model for AAM formation (Duxson et al., 2007)

The process for AAM formation is summarized as (Torgal et al., 2008; Silva et al., n.d.; Palomo et al., 1999):

- Exothermic process of dissolution of Si and Al atoms, from source materials, through the action of hydroxide ions (OH^-) from strong alkali solutions.
- Transportation, orientation and condensation of precursor ions/dissolved species into monomers during which heat is hardly released.
- Setting and polymerization (condensation and hardening) of monomers into inorganic polymeric structures with a poorly ordered structure but high mechanical strength. This is a strong exothermal step.

2.4 The role of alkaline activators in alkali-activated materials

The type of chemical activator can have a significant impact on the properties of the binder system such as durability, mechanical, physical, shrinkage and microstructure. Typically, a strong alkaline medium is necessary to increase the surface hydrolysis of the aluminosilicate particles present in the raw waste material. The concentration of the chemical activator has a distinct effect on the mechanical properties of the alkali-activated material (Part et al., 2015).

Glukhovsky classified alkaline activators into six groups, where M is the sodium/potassium ion (Pacheco-Torgal et al., 2008):

1. Alkalis; MOH
2. Weak acid salts; M_2CO_3, M_2SO_3, M_3PO_4, MF
3. Silicates; $M_2O{\cdot}nSiO_3$
4. Aluminates; $M_2O{\cdot}nAl_2O_3$
5. Aluminosilicate; $M_2O{\cdot}nAl_2O_3{\cdot}(2\text{-}6)SiO_2$
6. Strong acid salts; M_2SO_4

Komljenović et al. (2010) conceptualized five different type of alkali activators i.e. $Ca(OH)_2$, NaOH, NaOH + Na_2CO_3, KOH and Na_2SiO_3 to produce FA-based geopolymer mortars and inspect the influence of different types and concentrations of alkaline activators have on the mechanical properties of geopolymer mortars. Based on the mechanical strength results at a constant curing condition, the activator that attained the highest compressive strength was Na_2SiO_3, followed by $Ca(OH)_2$, NaOH, NaOH + Na_2CO_3 and KOH. The high activation potential of Na_2SiO_3 is due to the fact that it contains dissolved and partially polymerized silicon that readily reacts, incorporates into the reaction products and contributes to improving the mortar's characteristics. The lower activation potential of KOH compared to NaOH was due to the difference in ionic diameter between sodium and potassium. Furthermore, regardless of the types of alkali activators used, the compressive strength generally increased with the increase in activator's concentration. The higher the concentration of dissolved silicon in the system, the higher the strength obtained. The authors further concluded the optimum value of Na_2SiO_3 modulus was 1.5 as anything greater had a deleterious effect on the compressive strength value.

2.5 The role of waste materials in alkali-activated materials

Since AAM utilize source materials rich in Al and Si, it provides an opportunity to use waste materials such as fly ash, silica fume and granulated blast furnace slag. Strength development and properties of AAM concrete are highly dependent on the type of binder used. Palomo et al. (1999) suggested two models of alkali-activated binding system depending on the prime materials. The first model is represented by the alkali activation of slag (Si + Ca) with a mild alkaline solution. Many investigations were focused on this model. Slag is a waste material which forms, during the production of pig iron, when slagging agents are added to iron ore to remove impurities. It is high in calcium content and the main hydration product is accepted to be calcium silicate hydrate (CSH). The presence of calcium can play a significant role on the physical properties of the final hydration products. It can also enhance many aspects of AAM concrete durability due to its role of reducing permeability, which extends the serviceability life of concrete (Provis & Bernal, 2014; Li et al., 2010).

The second model is the alkali activation of metakaolin or FA (Si + Al) with medium to high alkaline solution. The binders in this model are low in calcium and form geopolymer gels or sodium (alumino)silicate hydrate (NASH) gels, which have excellent chemical and thermal resistance (Provis & Bernal, 2014). Fly ash is a by-product due the combustion of pulverized coal in thermal power plants. Due to rapid industrial development and urbanization, the amount of fly ash generated is large and a majority of it ends up in landfills. Eskom, one of the largest coal consumers in South Africa, produced 32.6 million tonnes of FA of which only 8.5% were recycled in 2017 (Eskom, 2017). The remainder were dumped in massive landfills. This has become a great concern due to the numerous hazardous health and environmental impacts due to the leaching of the ash's toxic heavy metals and trace elements. This toxicity can cause deleterious effect to human health; impact grazing animals, livestock and wildlife as well as contaminate groundwater and surface water. (Jambhulkar et al., 2018). It also contributes to the loss of useable land. Fly ash has limited use but a partial solution was to utilize these in OPC mix designs, ranging from 30 to 50% cement substitution, due to their inherent cementitious properties. Despite this, large amounts are still being deposited in landfills. Another ecologically efficient way would be to reuse these waste materials as a cementing component by alkali activation (Rashad, 2013; Li et al., 2010; Khale & Chaudhary, 2007). Moreover, the National Development Plan 2030 of South Africa, one of the country's most strategic initiatives, has placed specific attention to reduce the waste-to-landfill problem (NPC, 2012). This further drives the usage of fly ash as it will not only provide a greener alternate binder but also aid in attaining the objective set out by the National Development Plan 2030.

2.5.1 Alkali-activated slag

Alkali-activated slag (AAS) was the first type of binder system under consideration that can provide considerably better strength and mechanical properties than OPC concrete. Chi (2012) investigated the mechanical and physical properties as well as the durability of alkali-activated slag concrete (AASC). The author concluded by stating that in hardened concrete the compressive strength, splitting tensile strength, drying shrinkage, total charge passed, high-temperature resistance and sulphate attack resistance of AASC were higher than that of OPC.

The mechanical properties of AAS is affected by curing condition (temperature) and type of activator. Chi (2012) states further that the properties and durability of AASC were significantly dependent on alkali dosage in activator solution and curing conditions. The properties and durability of AASC improved with an increased dosage of sodium oxide (Na_2O). AASC cured at relative humidity (RH) of 80% and temperature of 60 °C has the superior performance, followed by air curing and saturated limewater curing. Živic (2007) researched the effects of different activators at varying temperatures on setting time and workability of fresh AAS cement. The author reported that sodium silicate, sodium hydroxide and sodium carbonate in dosages of 3, 5 and 7 wt% accelerated setting and decreased the workability of AAS cement mixtures. The author also concluded that a relatively significant influence had been recorded due to the increase in ambient temperatures (20-31 °C). It caused reduced setting time and decreased workability. The effect shows AAS cement mixtures are highly sensitive to ambient temperature changes. Bakharev et al. (1999) addressed the effect of elevated curing temperature on microstructure, shrinkage and compressive strength of AAS. They commented that heat treatment considerably accelerated strength development, reduced shrinkage and caused a more open microstructure when compared to OPC.

However, the decreased workability and setting time are potential problem areas. Pratt et al. (1995) mention that additional practical problems were occurrence of alkali-silica reactions, efflorescence formation, shrinkage, micro-cracks and strength variation. Some of these limitations can be alleviated by temperature changes. Ya-min et al. (2015) researched on effects of ambient and lower temperatures on the setting time, strength development, shrinkage and microstructure of AAS. The authors concluded that curing at below-normal temperatures (7-15 °C) can retard setting time to increase workability but at the cost of reduced early age strength. Moreover, curing at below normal temperatures retards shrinkage and thus reduces the potential risk of micro-cracks. Furthermore, Altan and Erdogan (2012) state that AAS mortars cured under ambient conditions can attain equal and greater strengths than mortars cured at elevated temperatures at the cost of early age strength. Mortars cured at 5 °C for numerous weeks can gain strength comparable to OPC.

2.5.2 Alkali-activated fly ash

Although AAS can obtain strength comparable to OPC under ambient condition, GBFS can be costly and is not available in large quantities. Fly ash is a relatively cheaper binder than GBFS and is also available in abundance. Wardhono et al. (2017) compares engineering properties of AAS and AAFA. Alkali-activated slag, when compared to alkali-activated fly ash (AAFA), had a higher compressive and tensile strength, modulus of elasticity and lower permeation characteristics during the initial 90 days. However, after testing the samples again after 540 days the authors discovered that the performance of AAS sample reduced but increased for AAFA samples. Alkali-activated slag samples only showed a 2% strength increase from the 90-day test whereas the AAFA sample's strength increased by 48%. Over this time, the fly ash samples' modulus of elasticity increased whilst that of the slag decreased. The author concluded that the effect of disjoining pressure combined with self-desiccation due to the continuing reaction and CSH gel formation caused the propagation of micro-cracks and is the reason for the long-term reduction in engineering performance of the AAS concrete.

Similar to AAS, significant factors that affect the mechanical strength are temperature and type of activator. Alkali-activated fly ash (AAFA) is favourable for gaining high compressive strength, better mechanical properties and can be cost effective than OPC concrete. Olivia & Nikraz (2012) produced AAFA concrete that was steam cured for the first 12-24 h and then air cured at room temperature. The samples were then compared to OPC concrete. Their results showed tensile strengths 8-12% higher; flexural strength 1.4 times higher and moduli of elasticity 14.9-28.8% lower than OPC concrete. Furthermore, the AAFA concrete exhibited less expansion, drying shrinkage and water absorption but sorptivity increased. Ryu et al. (2013) examined the effects of chemical changes on cementless alkali-activated concrete by using 100% fly ash for binder. The authors state that higher concentrations of NaOH provide higher compressive strength as well as a considerable increase in early-age strength gain. They achieved a compressive strength of 47 MPa and commented that it can be deemed as a potential replacement for OPC as 40 MPa is known as the threshold for high strength concrete. Rangan (2010) also researched AAFA and its properties. The researcher remarked on the economic benefits of geopolymer concrete stating that the price of one ton of FA is only a fraction of one ton of cement. Even after taking into consideration the price of alkaline solutions, the cost of FA based geopolymer concrete is 10-30% cheaper than OPC concrete.

However, it is stated that elevated temperature curing is a necessity to reach optimal mechanical characteristics for AAFA. Alkali-activated fly ash has a slow rate of dissolution at low temperatures and cannot attain satisfactory strength. Shekhovtsova et al. (2014) commented that curing at 25 °C was a possibility but not practical due to delayed setting, intensive efflorescence formation, very slow

strength development, relatively low strength at 28 days and large strength deviation. This limits AAFA use in pre-cast industry and impedes its range of application in the concrete industry. Unlike OPC concrete, which has freedom in curing conditions and can be cast on site, AAM require controlled environments to be a useful alternative.

Rangan (2010) concluded that heat-cured samples showed excellent resistance to sulphate attack, good acid resistance, low creep and suffer very little drying shrinkage. Silva et al. (2013) studied AAFA concrete and its properties. The authors noticed rapid strength gain in 3 days for heat-cured samples and a large amount of time taken for strength gain in ambient cured samples. Mustafa Al Bakri et al. (2011) investigated the effects of temperature on physical and chemical properties of AAFA. They concluded that optimum curing temperature of 60 °C produced the highest compressive strength of 67 MPa. The lowest compressive strength (22.9 MPa) was produced at room temperature. Higher temperatures caused moisture loss limiting further strength gain. It also induced cracks in the samples. Shekhovtsova et al. (2014) found similar results and also concluded that 60 °C was the optimum temperature. At 80 °C, excessive moisture loss took place during curing which led to a compressive strength decrease at 91 days.

2.5.3 Binary alkali-activated material blends

As with unary blends of AAS and AAFA, binary blends also show favourable outcomes when compared to OPC since CSH type gels can coexist with geopolymeric gels and contribute to the overall strength gain of the system (Part et al., 2015). Nath & Sarker (2014) replaced up to 30% of total binder with GBFS in FA based geopolymer concrete cured at ambient temperature and compared it to OPC. They noticed reduced workability and setting time whilst achieving compressive strength of concrete and mortar of 55 MPa and 63 MPa in 28 days, respectively.

Since GBFS is high in calcium content, partial replacement of FA with GBFS can aid in accelerating the hardening process and increase strength gain (Kim, 2012). Marjanović et al.(2015) investigated the physical-mechanical and microstructural properties of alkali-activated binary blend of FA and GBFS. Increase in GBFS content, activator modulus and concentration enhanced compressive and flexural strength. Elevated temperature curing significantly reduced drying shrinkage. Jang et al. (2014) investigated the fresh and hardened properties of alkali-activated slag/FA pastes with superplasticisers. They reported that setting time and compressive strength was significantly affected with the addition of GBFS. High levels of slag content (70–100%) increased strength but caused rapid setting and crack formation due to autogeneous shrinkage. Deb et al. (2014) studied the effect of GBFS blended with FA in geopolymers. They manufactured geopolymer concrete with 20%

GBFS and 80% FA in binder with a strength of 51 MPa at 28 days cured at 20 °C. Addition of GBFS improved setting time as well at ambient temperature. Chi & Huang (2013) researched on the binding mechanism and properties of alkali-activated fly ash/slag mortars (AAFS). The authors commented that higher compressive strength (110.6 MPa), flexural strength (9.32 MPa) and lower water absorption were achieved when compared to OPC mortars. Moreover, the greater the percentage of FA in binder content, the lower the drying shrinkage of AAFS mortars.

Another common by-product is silica fume (SF) and attempts have been made to introduce it as a secondary binder in either AAFA or AAS. Silica fume is a by-product of the smelting process in the production of metallic silicon or ferrosilicon in the alloys industry (Xu et al., 2016). It is a highly reactive pozzolanic material due to its higher silicon dioxide content as well as its very small particle size. Unary SF blends are not economically feasible as it costs considerably more than FA and GBFS. Besides its high reactivity, SF can act as a filler material that can fill in the voids of pores and aid in increasing mechanical strength by densification of the structure (Dutta et al., 2010).

Rashad & Khalil (2013) tested the performance of AAS blended with SF at elevated temperatures when activated with Na_2SiO_3. The authors concluded that up to 15% replacement of slag with SF, in pastes, proved beneficial towards strength gain and lower porosity. Sayed & Zeedan (2012) aimed to create cementless binding material by alkali activation of slag and SF with NaOH and Na_2SiO_3. They reported that up to 25% replacement of slag with SF was reasonable for adequate strength gain and economical point of view. Compressive strength results of vapour cured pastes were superior to the results of corresponding pastes cured at room temperature. Aydin (2013) activated slag mortars, using NaOH and Na_2SiO_3, blended with different binders. The author partially replaced slag with 10% and 20% SF. The results indicated that 10% replacement caused a 4.2% increase in compressive strength but a 15.2% decrease for 20% replacement. However, the flexural strength decreased by 29.6% for 10% replacement and 32.7% for 20% replacement.

Nuruddin et al. (2010) replaced FA with SF at levels of 0, 3, 5 and 7% in AAM concrete and tested strength in different curing conditions. The authors concluded that 3% was optimal for ambient curing (30.3 MPa) and 7% for direct sunlight curing (42.3 MPa). Furthermore, they state that SF impacts early age strength gain due to its very fine particles causing immediate reaction. Dutta et al.(2010) investigated the effect of SF addition to FA geopolymer on the porosity and compressive strength. They concluded that increasing replacement of FA with SF caused compressive strength decrements in pastes but increments in mortar specimens. The reasoning was stated to be the notable variations of porosity which increased in pastes but decreased in mortars. This was directly correlated

to water absorption of the specimens. Songpiriyakij et al. (2011) also replaced FA with SF at levels of 0, 10, 20, 30 and 40%. They reported that the blend of FA and SF significantly enhanced the compressive and bonding strengths of geopolymer pastes. Increasing SF content gave increasing strength values. Moreover, they also observed the change in setting times. Inclusion of SF increased initial setting time by 17.9% but decreased final setting time by 20%.

Furthermore, SF can help imbue the material with durability properties. Okoye et al. (2017) investigated effect of SF on the mechanical properties of FA based geopolymer concrete. The authors found that the presence of SF decreases the workability of the paste but improves the compressive, tensile and flexural strengths when compared to the control mixture. The authors also tested durability properties of FA based geopolymer in the presence and absence of SF in corrosive atmosphere of 2% H_2SO_4, 5% NaCl and 5% Na_2SO_4 solutions and compared it to a control OPC concrete mix. The authors reported that visual observations revealed that there was surface erosion and cutting of edges in the case of OPC concrete but no erosion in the case of geopolymer concrete containing 20% SF when exposed to 2% H_2SO_4 and 5% NaCl solution for 90 days. Mixtures containing 2% H_2SO_4 was found to be more corrosive when compared to 5% NaCl solution. Compressive strength losses in the case of geopolymer concrete containing 20% SF were negligible in the presence of 2% H_2SO_4 and 5% NaCl solutions. Geopolymer concrete in presence of 20% SF possessed excellent long-term durability properties capable of resisting chemical attack.

2.6 Acceptance of alkali-activated materials into the industry

Even though alkali-activated binders have been under investigation, the widespread use of AAM has not taken place. This stems from the fact that OPC concretes have been thoroughly researched, understood and tested for plethora of years. Most companies in the industry still choose OPC concrete as there is a certain level of confidence in its use. Alkali-activated binders and their chemistry are not fully understood. There is a significant lack of procedures or set guidelines to create AAM with certain characteristics. The main driver in AAM acceptance is the carbon conscious market (van Deventer et al., 2012).

Mclellan et al. (2011) performed a comparison analysis on cost and carbon emissions between AAM and OPC. They suggest that AAM have 44-64% reduction in greenhouse gas emissions over OPC while financial costs can be 7% lower to 39% higher than OPC. However, Turner & Collins (2013) investigated the same matter and found that AAM only have a 9% decrease in CO_2 footprint compared to OPC, which was significantly different from the estimation concluded in previous researches. Habert et al. (2011) performed an environmental evaluation. The authors concluded that

AAM have slightly lower impact on global warming as opposed to ordinary Portland cement. However, they also conclude that AAM usually have a greater environmental impact other than global warming. The process of producing alkali-activated binders has its drawbacks that prevent the process from being accepted in the industry: the use of highly alkaline activators like NaOH and Na_2SiO_3 to attain alkali activation possess problems pertaining to handling and storage (Dakhane, et al., 2017).

2.7 Conclusion of literature survey

The advantages of unary and binary AAM blends include (Rashad 2013; Provis & Bernal 2014; Wang et al. 1995):

- better flexural and compressive strength, both early and final as well as rapid hardening;
- low water requirement due to water release during chemical reaction;
- low permeability;
- high-temperature resistance, including thermal insulating properties;
- stability under chemical (including acid) attack;
- excellent resistance to sulphate attack;
- low drying shrinkage;
- dimensional stability in service;
- strong adhesion to metallic and non-metallic surfaces;
- effective passivation of reinforcing steel;
- low permeability to fluids and chloride ions;
- low cost and energy saving (only for AAS and GBFS/FA binary blends);
- beneficiation and/or valorisation of industrial wastes;
- low CO_2 emissions footprint;
- low heat release and
- freeze-thaw resistance.

Limitations of unary and binary AAM include (Wang et al. 1995):

- quick setting (impedes the allowable time for application);
- occurrence of efflorescence (white deposits on surface due to leaching of free alkali with evaporating water);
- shrinkage and microcracks;
- strength variation;
- most application only in precast industry (mostly for AAFA blends);

- cost and environmental impact of producing alkaline solution, NaOH and Na_2SiO_3; and
- energy expenditure due to elevated temperature curing.

Even though the beneficial properties seem to outweigh the limitations, the acceptance of AAM is still low in the industry. The production of unary fly ash based AAM with sufficient strength and mechanical properties require curing at elevated temperatures. This limits its application to the pre-cast industry. To alleviate the issue, focus was shifted to creating binary blends with FA and GBFS. This allowed for ambient curing to take place but it uses a relatively small amount of FA. Since one of the National Development Plan 2030 strategic objectives is to reduce landfilling by recycling waste, successful utilization of FA can only be achieved if a nationwide need exists for it. Therefore, the amount of FA in the AAM system needs to be increased.

Moreover, there is a cost implication. Although FA is relatively cheap, AAM can be expensive to implement due to the alkaline solutions used for activation, which are most commonly sodium hydroxide and sodium silicate. Furthermore, it raises concerns about environmental impacts from manufacturing such solutions and due to their high pH toxicity (Turner and Collins, 2013).

Therefore, in order for FA based AAM to be able to covert a harmful waste material into a cost-effective, environmentally friendly building material that industry will be receptive to, it needs to consist largely of FA; be cured under ambient conditions; utilise low-impact activators and the process to create it should not deviate from current practices with OPC.

One solution is to replace a portion of fly ash with silica fume and use calcium hydroxide plus sodium carbonate as activators.

Calcium hydroxide can be an alternative activator due to its lower pH content (less than 14) and also being much cheaper than NaOH or Na_2SiO_3. Pozzolanic materials (FA and SF) require a source of lime to attain its cementitious properties, which is provided by CH. However for AAM, like the name suggests, a strong alkaline medium is necessary for sufficient dissolution of its source materials (FA) for strength gain (Fraay and Bejen, 1989). Due to the low pH of CH, the activation of FA with CH has low strength development. An additive activator needs to be introduced to help increase the pH of the system and promote early activation. Shi & Day (2000) used different chemical activators to improve the strength development of FA-CH binder system. The authors incorporated sodium sulphate (Na_2SO_4) to increase the pH of the solution as its the addition with calcium hydroxide gives the chemical reaction:

$$Na_2SO_4 + Ca(OH)_2 + 2H_2O \leftrightarrow CaSO_4 \cdot 2H_2O \downarrow + 2NaOH \quad (2)$$

The formation of NaOH is responsible for increasing the pH of the solution, promoting an increase in the degree of early activation. However, the use of Na_2SO_4 produces durability problems such as sulfate attack; and thus Jeon et al. (2015) incorporated the use of sodium carbonate. The authors found that the same pH increasing effect was present and there was a noticeable improvement in the compressive strength. The authors state the strength was approximately 4-5 times higher than samples containing no sodium carbonate.

Sodium carbonate is a naturally occurring mineral and can be obtained from trona and sodium carbonate-rich brines or chemical processes such as the Solvay process. The worldwide total of natural occurring sodium carbonate amounts to 24 billion tonnes (USGS, 2017). Moreover, SC is reported to be 2-3 times cheaper than NaOH or sodium silicate. In addition to the low cost of this activator compared to conventional ones, it is safer to handle and can yield lower drying shrinkage (Jin & Al-Tabbaa, 2015). Thus, the use of SC as an activator can contribute to the development of more sustainable AAMs (Abdalqader et al., 2016).

The incorporation of SF is being highly reactive to CH, due to its nature. This can create additional binders or act as a micro-filler.

In most cases with AAM you have to prepare the alkaline solution in controlled environments, which, on a construction site, can pose several health and safety concerns. However, in the proposed system, all the materials, including the activators, are dry and much safer to handle. Due to this, it provides the possibility of mixing them together and stored in bags or silos. This is extremely similar to current practices with OPC, where the only component required for activation is water.

Jeon et al. (2015) had a similar blend system (FA-CH-SC) to the proposed system and attained noticeable strength improvements. However, their system was cured under elevated temperatures. This study will focus on the proposed system of FA-SF-CH-SC that is cured under ambient conditions to test its aptitude and report on its feasibility.

3 EXPERIMENTAL PROGRAM

3.1 Introduction

The experiment tested different mixes with varying amounts of each component: fly ash (FA), sodium carbonate (SC), calcium hydroxide (CH) and silica fume (SF) by performing a detailed analysis of the binding system by mathematical design of experiments. The effect of each part on the mechanical strength was noted in order to attain a better understanding of its dynamic and feasibility.

This was followed by performing characterisation techniques such as Heat flow calorimeter, X-ray Diffraction (XRD), Scanning Electron Microscope (SEM), Fourier Transform Infrared (FTIR) and Thermogravimetric (TGA) analysis.

3.2 Experimental setup

Central composite designs (CCD), also known as Box-Wilson designs, are highly efficient and flexible. They allow for modelling and analysis of the response of interest as well as providing satisfactory information on the experimental variables and their effects plus error with minimal number of runs.

Central composite designs include an embedded factorial or fractional factorial design with centre points that is augmented with a group of axial/star points that allows curvature estimation. This type of design can be used to estimate the first- and second- order terms/effects as well as model a response variable. Using a 2-level CCD example, it will contain a centre point (circle), four factorial points at its corners (the +1 and -1 coded variable levels shown by triangles) and four axial/star points (diamond) that lie a distance +α and -α on each axis. This is shown in Figure 3-1.

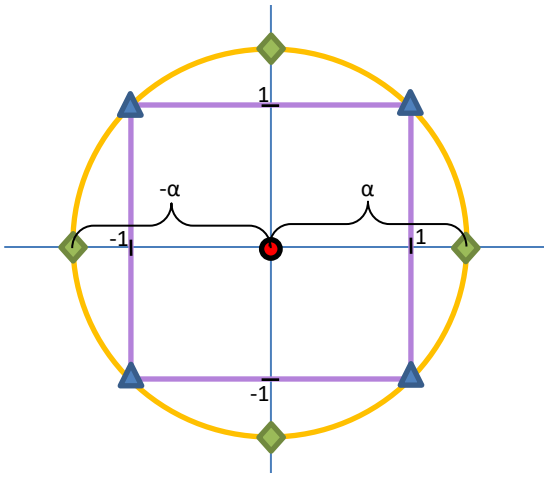

Figure 3-1: 2-level CCD design space

There are three kinds of CCD (inscribed, circumscribed, faced) where each type uses a different α value. For this experimental design, a face-centred CCD (α = ±1) was chosen as the region of interest encompasses the extremities and a 3^k level CCD was chosen. A visual representation of the box is shown in Figure 3-2.

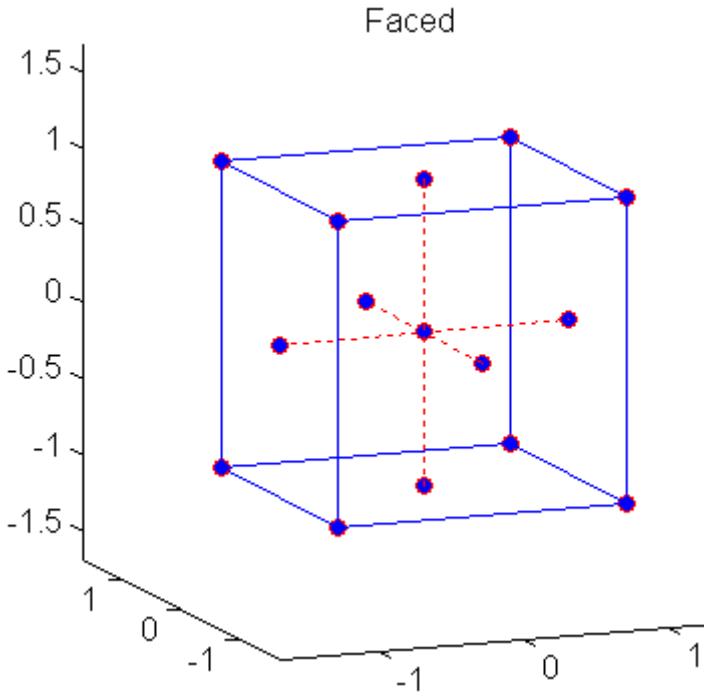

Figure 3-2: 3-level face-centred CCD design space (MathWorks, 2019)

Table 3-1 and 3-2 show the coded/uncoded control variables and constant parameters.

Table 3-1: Coded and uncoded control variables

Control variables*	**-1**	**0**	**+1**
SC**, wt%	6	9	12
CH, wt%	10	15	20
SF, wt%	5	10	15

* wt% = calculated as a percentage of FA content
** Calculated as a Na_2O_{eq} %

Table 3-2: Constant parameter values

Curing condition	25±1 ^{o}C & relative humidity of 85±5%.
w/b ratio*	0.27
Mixing time	5 minutes

* Binder = FA+SF+CH+SC.

Jeon et al. (2015) investigated the effect of SC in a FA-CH system and concluded that the strength was 4-5 times greater than systems with no SC. Thus, to further quantify the effect, this experimentation used different amounts of CH and SC to see the variability in the results.

Furthermore, in the authors' investigation, the system was cured at an elevated temperature of 60 °C. However, the aim of this research was to produce a binder than can be cured at ambient conditions on site. Thus, curing conditions were limited to ambient temperatures.

The water-to-binder ratio (W/B ratio) was derived from trial tests. W/B ratio of 0.27 was chosen for the experiment because it provided paste with moderate workability and no issues during compaction by vibration.

As components of the binding system were dry, it allowed for dry mixing. Thus, a ball mill was used to combine the materials and dry mix was stored until casting date. To limit the effect of grinding on the performance of the binding system, a mixing time of 5 minutes was used during the experiment.

Table 3-3 gives the sample mixture quantities in coded format.

Table 3-3: Experimental mixture design

Mix ID	SC	CH	SF
SC12|CH20|SF15	+1	+1	+1
SC12|CH20|SF5	+1	+1	-1
SC12|CH10|SF15	+1	-1	+1
SC12|CH10|SF5	+1	-1	-1
SC6|CH20SF|15	-1	+1	+1
SC6|CH20|SF5	-1	+1	-1
SC6|CH10|SF15	-1	-1	+1
SC6|CH10|SF5	-1	-1	-1
SC12|CH15|SF10	+1	0	0
SC6|CH15|SF10	-1	0	0
SC9|CH20|SF10	0	+1	0
SC9|CH10|SF10	0	-1	0
SC9|CH15|SF15	0	0	+1
SC9|CH15|SF5	0	0	-1
SC9|CH15|SF10	0	0	0
SC9|CH15|SF10	0	0	0
SC9|CH15|SF10	0	0	0

SC - Sodium Carbonate; CH - Calcium Hydroxide; SF - Silica Fume

Number represents wt% of respective material

The replication of the centre point runs provides an estimate of the experimental error. The face-centred CCD was performed in random order to eliminate the possibility that one run depends on the conditions of the previous run or have an influence of subsequent runs.

3.3 Materials

Fly ash, sodium carbonate, chemical grade hydrated lime and silica fume were procured from local distributors in South Africa. Table 3-4 represents the chemical composition of FA and SF.

Table 3-4: Chemical composition of source materials

%	Fly ash	Silica fume
SiO_2	56.23	88.86
TiO_2	1.57	0.01
Al_2O_3	30.67	0.60
Fe_2O_3	4.45	4.63
MnO	0.04	0.13
MgO	0.49	1.03
CaO	4.54	1.86
Na_2O	0.27	0.28
K_2O	0.81	2.03
P_2O_5	0.24	0.08
Cr_2O_3	0.03	0.01
SO_3	0.37	-
LOI	0.28	4.58
TOTAL	99.99	99.54

3.4 Sample preparation and testing procedures

Binder pastes were mixed in a Hobart mixer. Dry binder was added to a damp bowl and then water was added with the mixer running. This was done for 5 minutes and then mixer was stopped and all leftover dry material was scrapped off the bowl surface within 30 seconds. The mixer was run again for another 5 minutes until the paste was completely mixed.

Workability of the pastes were measured using standard flow table test (ASTM C1437-14). The paste was placed onto the flow table cone disk in two layers, each layer being compacted with short strokes 20 times over the cross-section of the mould with a tamping rod. Excess paste was skimmed off the top of the cone and then the cone was slowly lifted up vertically. The mould of the paste was then raised and dropped from a height of 12.5 mm by the flow table 25 times in approximately 15 seconds. The flow of the paste (diameter) was then measured in two directions at right angles to one another using a Vernier calliper.

Prismatic moulds were used to cast 40x40x160 mm samples. Prepared pastes were placed in the moulds, compacted on a vibrating table until there were no air bubbles, covered in film and left to set at 25±1 °C overnight. The samples were then demoulded the following day and cured in a room with an ambient temperature of 25±1 °C and relative humidity of 85±5%. The samples were first

weighed in air then weighed in water before strength tests were conducted. Compressive strength tests were carried out on three half prism samples at 3, 7 and 28 days. The test procedure was done in accordance to SANS 50196-1.

3.4.1 Statistical analysis

The first stage of statistical analysis deals with interpreting the variable effects. This aids in providing necessary information on which variables and interactions may prove to be important terms to include in the model.

Thereafter, the initial model is formed which is a full model with all factors and interactions included. For this investigation, a full quadratic model was chosen to include possibility of curvature. Then analysis of variance (ANOVA) is applied to test the significance of the model. This is quantified by looking at the p-value, which is the converted F-statistic that is derived from the mean squares. If the p-value is less than 0.05, the model (and its terms) is deemed significant. If it is greater than 0.1, then the model terms are statistically insignificant. The next stage deals with model refinement where insignificant terms in the model are removed and ANOVA tests run until only significant terms remain in the model.

Thereafter, residual plots are analysed to confirm model assumptions and check its adequacy. This is an important part of the statistical analysis as it examines whether the model in question provides an adequate representation of the true system and it does not violate the least squares regression assumptions. The least squares regression assumptions are:

1. Normality;
2. Constant variance;
3. Independence.

The normality assumption is checked with the normal probability residual plot. If the graph follows a straight line then the assumption holds true and the model follows a normal distribution. If there is a s-shape or any abnormal shape then the normality assumption is violated.

The constant variance assumption is validated by the residuals versus predicted response graph. This plot should show a random scatter to satisfy the assumption. A presence of any sort of trend such as

a megaphone shape indicates the assumption does not hold true and suggests an inequality of variance.

Plotting the residuals versus experimental run validates the independence of assumption, which again should show a random scatter with no noticeable trends. If all the assumptions hold true then the model can be deemed adequate and analysis of response surfaces and contour plots can be performed (Montgomery, 2011).

3.4.2 Characterization techniques

Characterization techniques of X-Ray Diffraction (XRD), Fourier-Transform Infrared Spectroscopy (FTIR), Thermal Gravimetric Analysis (TGA), Scanning Electron Microscopy (SEM) with Energy Dispersive Spectroscopy (EDS) were performed. These techniques were used to evaluate the microstructural and mineralogical changes over time for selected samples at 3 and 28 days. This provides information on the different compressive strength values observed during the study.

The samples were prepared before the characterisation techniques could be conducted. After being tested for strength at 3 and 28 days, representative samples for selected binders were collected, then they were dehydrated to prevent further material evolution. This was achieved by placing the samples in acetone to stop the hydration and then transferred to a vacuum chamber to filter out the acetone. Thereafter, the samples were placed in a desiccator at 25 °C to completely dry the sample until testing date (Ismail, et al., 2013). Samples for XRD, FTIR, and TGA require the material to be in powdered form. This was attained by hand milling the dried samples using a pestle and mortar.

Heat flow calorimeter can aid in evaluating early hydration mechanisms. Generally, the hydration reaction can be divided into initial reaction, induction period, acceleration, deceleration and decay (Rashad et al., 2013). A custom-made calorimeter was used to study the heat flow evolution of selected binders. To equalize temperature, binder samples and water for the test were kept in the room with the calorimeter for at least 24 hours before testing. On a testing day, 1.5 g of binder was put into copper pots which were placed in the calorimeter. After 30 minutes of temperature stabilisation, 0.75 g of water (W/B ratio of 0.5) was injected into the copper pots and heat flow evolution was measured for 72 hours.

X-Ray diffraction analysis (XRD) allows for crystalline phase determination. The samples were prepared according to the standardized PANalytical back-loading system, which provides nearly random distribution of the particles. The samples were analyzed using a PANalyticalX'Pert Pro

powder diffractometer in θ–θ configuration with an X'Celerator detector and variable divergence- and fixed receiving slits with Fe filtered Co-Kα radiation (λ=1.789 Å). The phases were identified using X'PertHighscore Plus software. The data was recorded in the angular range 5° < 2Θ < 90°. The relative phase amounts (weight%) were estimated using the Rietveld method (X'PertHighscore Plus software).

Microstructure evolution can be further studied with Fourier-Transform Infrared Spectroscopy (FTIR). This characterisation technique provides information on the vibrations generated by the chemical bonds in a material. Lee and Van Deventer (2002) comment that it is necessary to follow the progressive change of chemical bonds within a structure and then correlate that with the physical characteristics observed. Criado et al. (2012) discovered a correlation between the pendulum movement of the main band of the FTIR spectra and compressive strength development of alkali-activated fly ash, over time.

The FTIR of the selected samples was recorded on a solid state by a VERTEX 70v spectrometer equipped with the Golden Gate diamond ATR cell (Bruker). FTIR was recorded on the 4000-400 cm^{-1} spectral region, with 32 acquisitions at a 4 cm^{-1} resolution. Chemical bonds that correspond to the spectra bands were identified according to literature.

Thermal Gravimetric Analysis (TGA) can quantify the gel of the material by evaluating the relative weight loss of the samples. It was noticed that an increase in the amorphous content corresponded to an increase in the relative weight loss of the sample (Nedeljkovic et al., 2016). Thermal Gravimetric Analysis on samples were carried out using a Thermal Analyser Instrument Q600 SDT, the samples were heated from 30 to 1200 °C at a heating rate of 20 °C/min, under 100 ml/min nitrogen purge.

The SEM and EDS analyses were conducted on Zeiss Ultra plus SEM at an accelerating voltage of 1 kV for SEM imaging and 15 kV for EDS and backscattered electron imaging (BSE). The SEM images were captured for both fractured and polished samples while EDS and BSE were done only on polished samples. Samples were polished using diamond pads (66, 28.8 and 16 μm) and diamond suspensions (9, 3, 1 and 0.25 μm). Thereafter, the polished samples were coated with a single layer of carbon such that it provides a minimal thickness that would be undetectable during EDS scanning.

4 RESULTS AND DISCUSSION

4.1 Workability and compressive strength

The initial flow of binder pastes is shown in Figure 4-1.

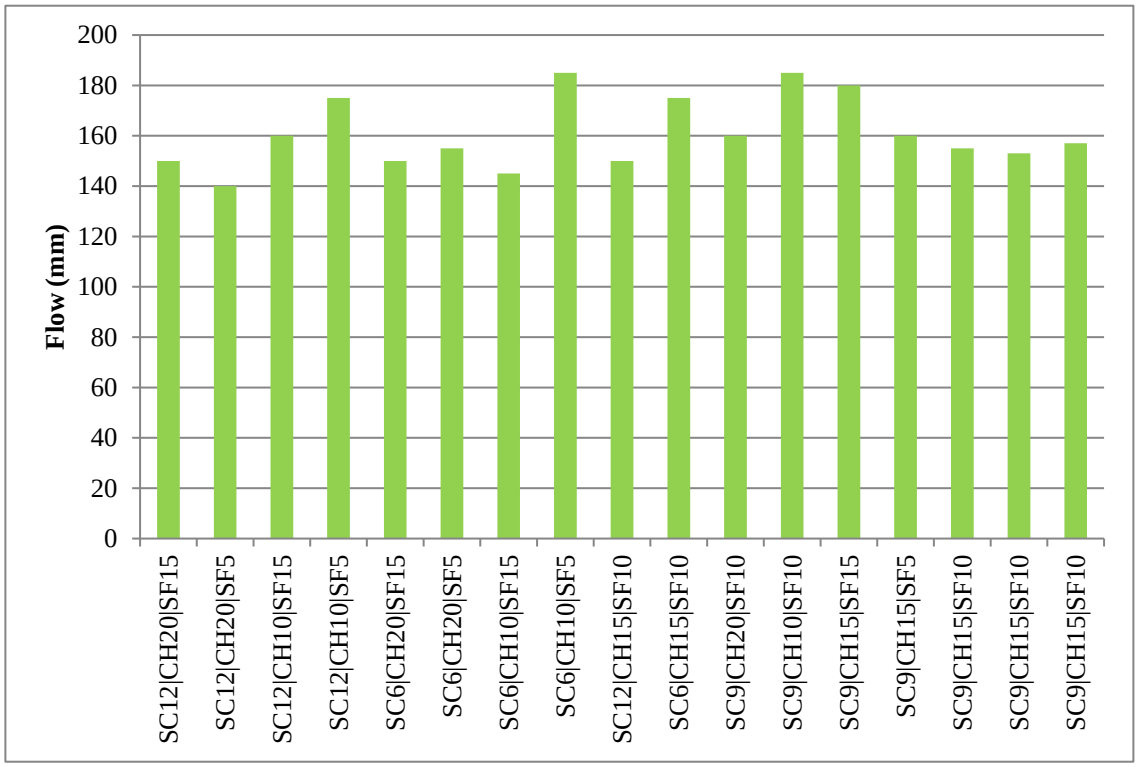

Figure 4.1a: Initial flow of samples

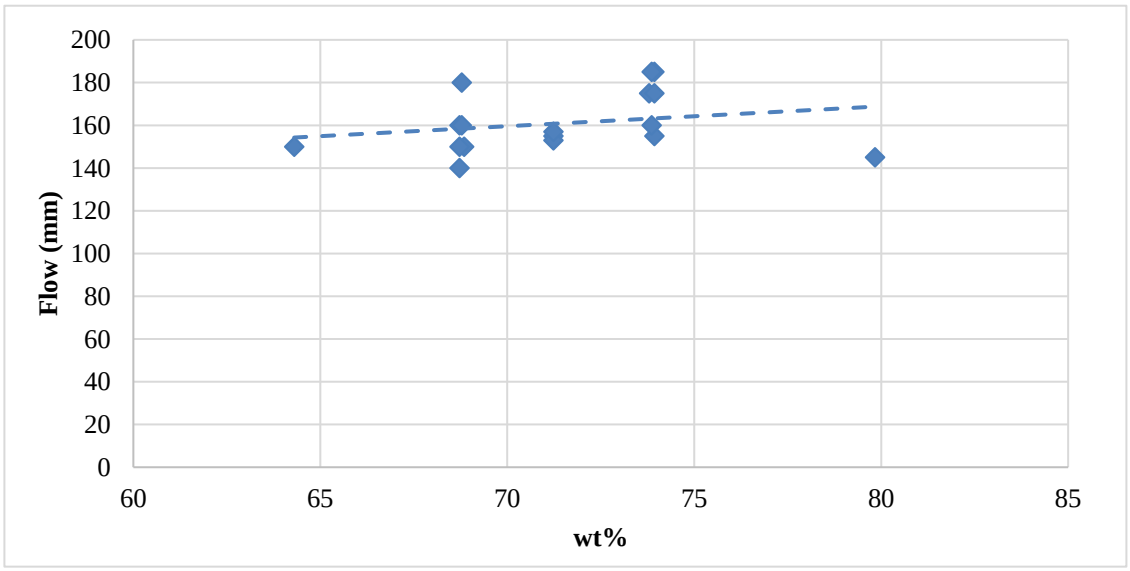

Figure 4.1b: Effect of fly ash on workability

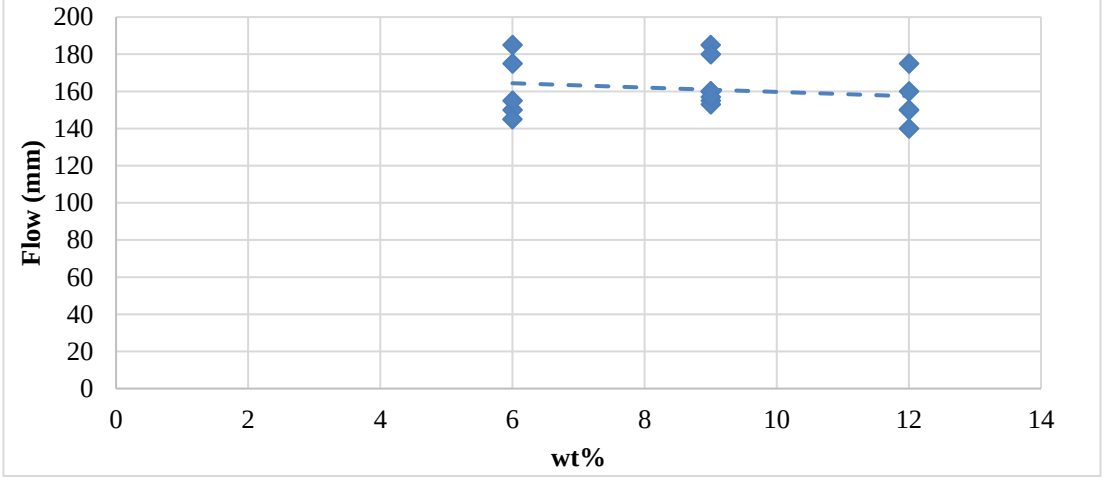

Figure 4.1c: Effect of sodium carbonate on workability

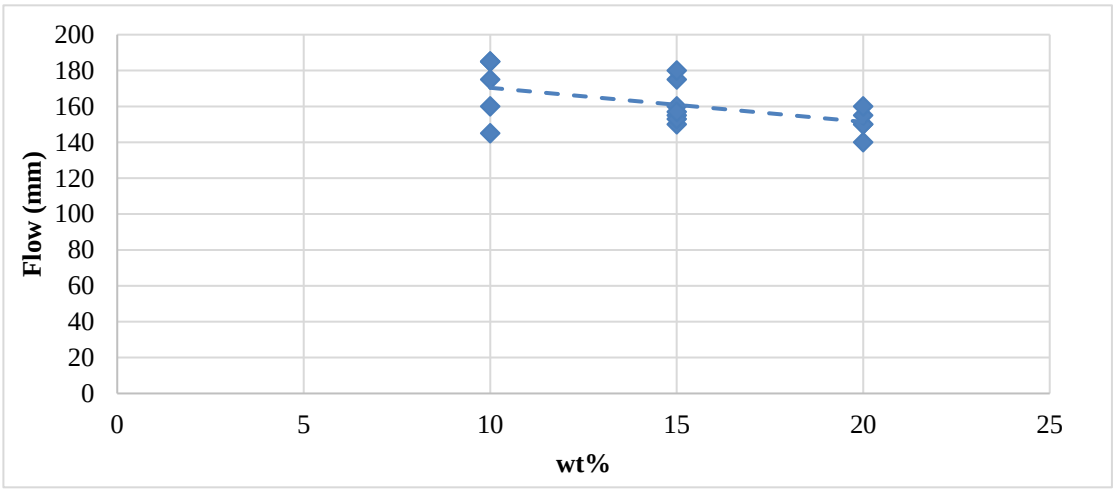

Figure 4.1d: Effect of calcium hydroxide on workability

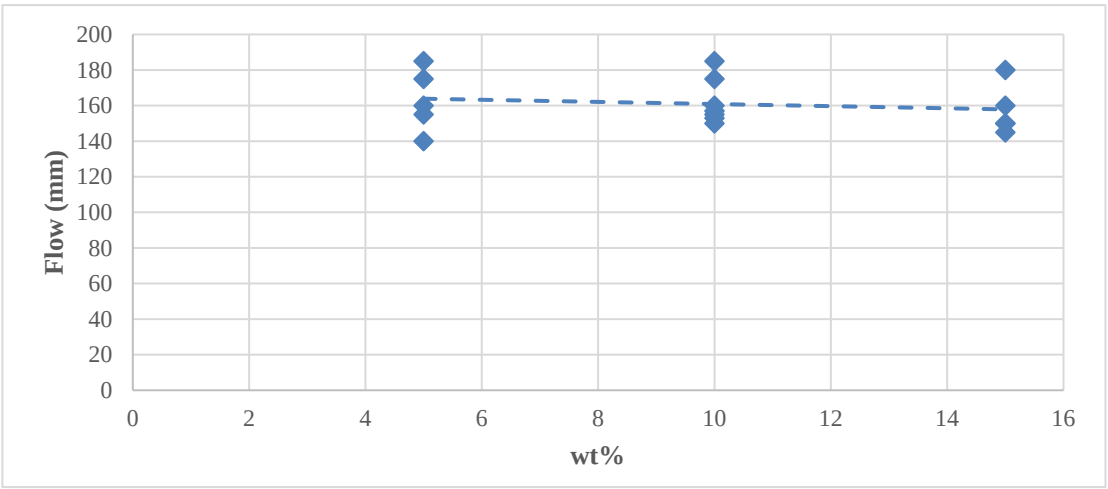

Figure 4.1e: Effect of silica fume on workability

Figure 4-1: Workability and effect of mix components of samples

Figure 4-1a show the workability was more or less similar for all the mixes. There were no signs of pseudo flash-setting. Looking at Figure 4.1c-4.1d, the effect of increasing SC, SF and CH content decreased the workability. Nonetheless, all samples had good workability with medium cohesiveness (a putty-like consistency) and were easy to trowel. An example is shown in Figure 4-2.

Figure 4-2: Representative of workability for samples

The graph in Figure 4-3 shows the strength development of the samples.

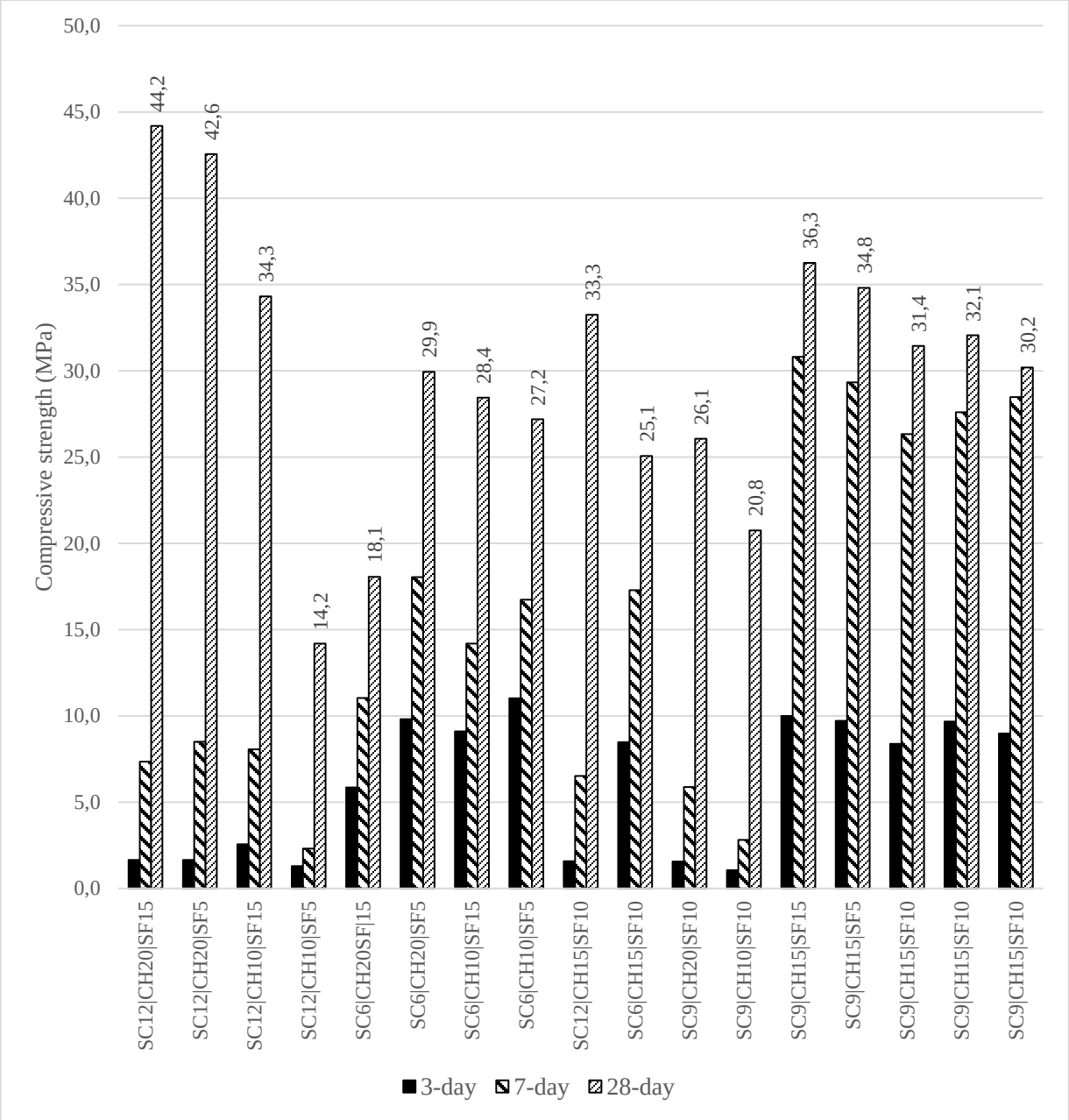

Figure 4-3: Strength development

4.2 Face-centred CCD results and analysis

The computer software, Minitab® 17.1.0, was used to assist in the design, analysis and interpretation of the 3^k face centred central composite design. To test the presence of curvature in the system, a full quadratic model was analysed first consisting of first order, second order and interaction terms.

It is often required that the impact of different factors be expressed as effect sizes and represented graphically. This helps in understanding which factor did or did not significantly influence the

response, which was the compressive strength at 28 days. The main factor effects can be calculated as the difference between the factor average and the grand mean. This is represented graphically in Figure 4-4.

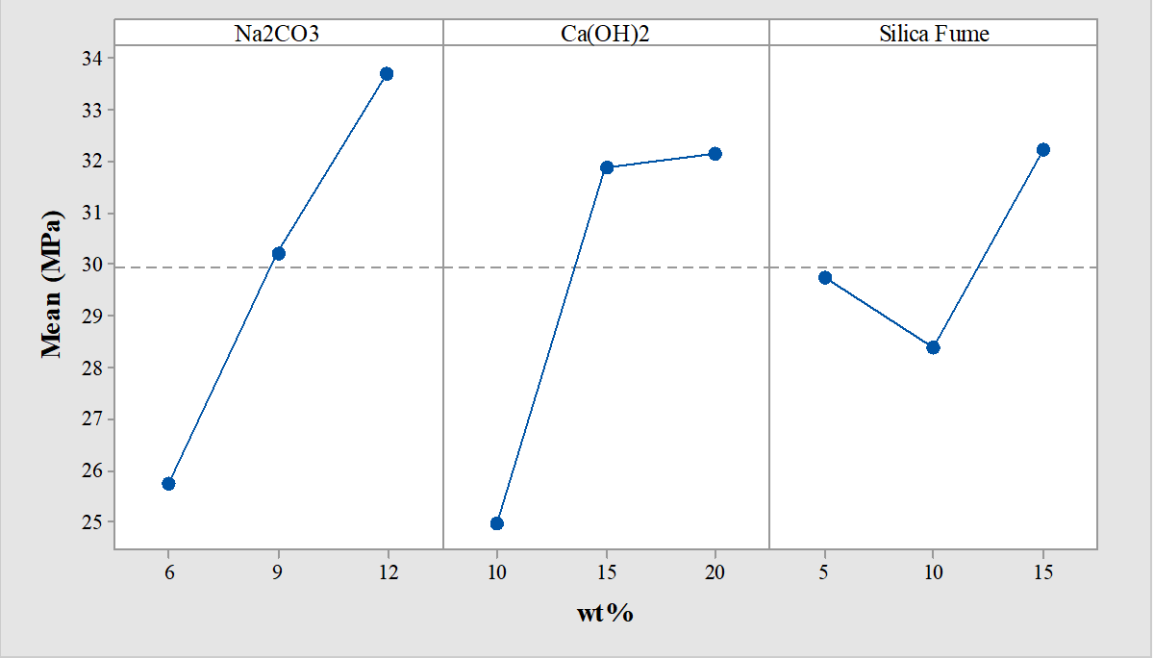

Figure 4-4: Main effect of variables

The graph in Figure 4-4 is known as a main effects plot. It gives a visual representation of the relationship between the response and the independent variables. The dashed horizontal line represents the grand mean and the dots show the response mean at each factor level. The slope of each line visually indicates the impact. A horizontal line (parallel to the x-axis) implies no main factor effect and the response mean is the same across all factor levels. Non-horizontal lines imply there are main factor effects. The steeper the slopes of the line, the larger the effect and thus a greater impact on the response.

From Figure 4-4, it can be noticed that Na_2CO_3 and $Ca(OH)_2$ have a positive impact on the compressive strength. Silica fume, on the other hand, has a negative impact at one factor level but a positive effect at another. Sodium carbonate has increasing slope at each factor level showing that higher quantity of Na_2CO_3 provides a beneficial effect towards strength development. Calcium hydroxide has a large effect on the strength when increasing from 10 to 15 wt% but a much smaller yet still positive effect from 15 to 20 wt%. Silica fume shows a negative impact when amount is

increased from 5 to 10 wt% but it is counteracted with a larger positive effect when increased from 10 to 15 wt%.

If there are significant interaction terms then it is not possible to fully interpret the main effects without looking at the interaction plots.

An interaction plot shows the relationship of how one factor and the response depend on the value of another factor. For interaction plots, analysis is conducted by looking at both lines of an interaction and compared. If both lines are parallel then the interaction effect is concluded to be zero. However, the more different and steeper the slopes become, the greater the influence it has on the results. Furthermore, if the lines cross each other, it is known as disordinal interactions and if they do not then they are called ordinal interactions (Stevens, 2000). Each criterion alters how the factors are interpreted. Figure 4-5 show the interaction plot between $Ca(OH)_2$ and Na_2CO_3.

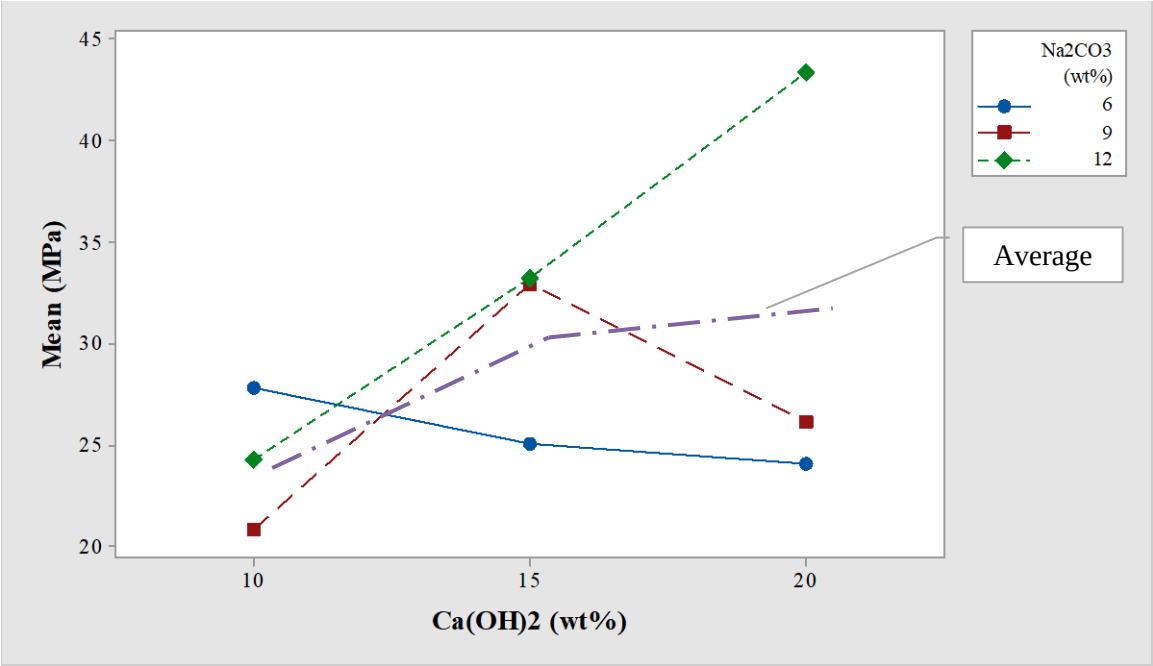

Figure 4-5: Interaction plots between $Ca(OH)_2$ and Na_2CO_3

From Figure 4-5, it can be noticed that none of the lines are parallel. Sodium carbonate at 12 wt% gives higher mean strength at 15 and 20 wt% factor levels of $Ca(OH)_2$. However, at 10 wt% of $Ca(OH)_2$, Na_2CO_3 at 6 wt% gave a higher mean value than at 12 wt%. Sodium carbonate at 12 wt% factor level is always higher than at 9 wt% factor level. At 9 wt% factor level, it is higher than 6 wt% except for 10 wt% $Ca(OH)_2$ factor level and even crosses the other lines. This shows that there is a

possibility of a significant interaction as the relationship between $Ca(OH)_2$ and strength is dependent on the value of Na_2CO_3.

As there are interaction effects, it is possible to deduce simple main effects and check whether it is significant or not. This is evaluated by looking at the average of mean strength (the circle, diamond and square points) at each factor level on the x-axis and comparing them. This is shown by the purple long dash dot line in Figure 4-5. If there is a large enough change between each factor level, then the main effect can be deemed possible. The average of the points of $Ca(OH)_2$ at each factor level show that it generally increases, especially between 10 and 15 wt% but less between 15 and 20 wt%. This is confirmed with the main effects plot in Figure 4-4 and shows $Ca(OH)_2$ as a possible main effect.

From Figure 4-6, it can be again noticed that none of the lines are parallel. Silica fume at 15 wt% gives higher mean strength at two factor levels, 9 and 12 wt%, of Na_2CO_3 except at 6 wt%, where SF at 5 wt% gave a higher mean value. In fact, the 15 wt% of SF gives the lowest mean value at 6 wt% Na_2CO_3. This shows that there is a possibility of a significant interaction as the relationship between Na_2CO_3 and strength is dependent on the value of SF.

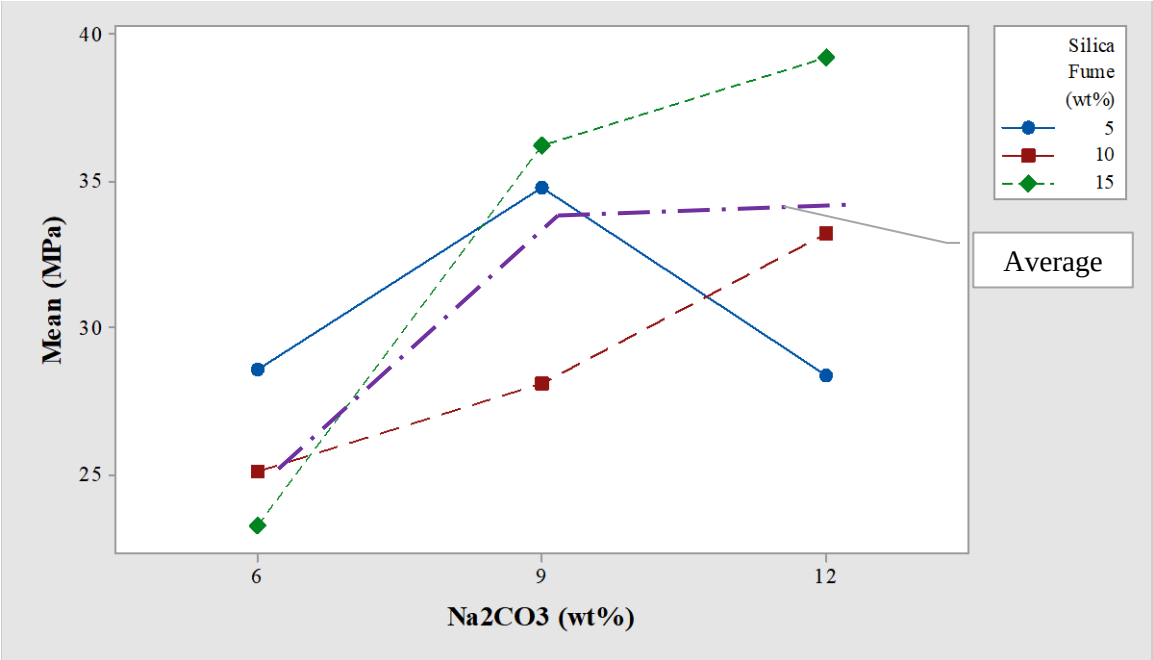

Figure 4-6: Interaction between Na_2CO_3 and SF

Evaluating the simple main effect of Na_2CO_3 by taking average mean strength (the square, diamond and circle points) at each factor level (purple long dash dot line in Figure 4-6) of Na_2CO_3 shows a large increase between 6 and 9 wt% but a very slight increase between 9 and 12 wt%, which is in correlation with the main effects plot in Figure 4.4. The main effect of Na_2CO_3 is a possibility.

From Figure 4-7, it can be again noticed parallel lines do not exist. Calcium hydroxide at 15 wt% gives higher mean strength at two factor levels, 10 and 15 wt%, of SF except at 5 wt%, where $Ca(OH)_2$ at 20 wt% gave a higher mean value. This shows that there is a possibility of a significant interaction as the relationship between SF and strength is dependent on the value of $Ca(OH)_2$. Calcium hydroxide at 10 wt% showed a lower mean value except at 15 wt% of SF where the mean value was similar to 20 wt% $Ca(OH)_2$ with 10 wt% $Ca(OH)_2$ being slightly higher. Moreover it can be noticed that at 5 and 10 wt% SF factor levels for 10 wt% $Ca(OH)_2$, there was almost no change in the mean values.

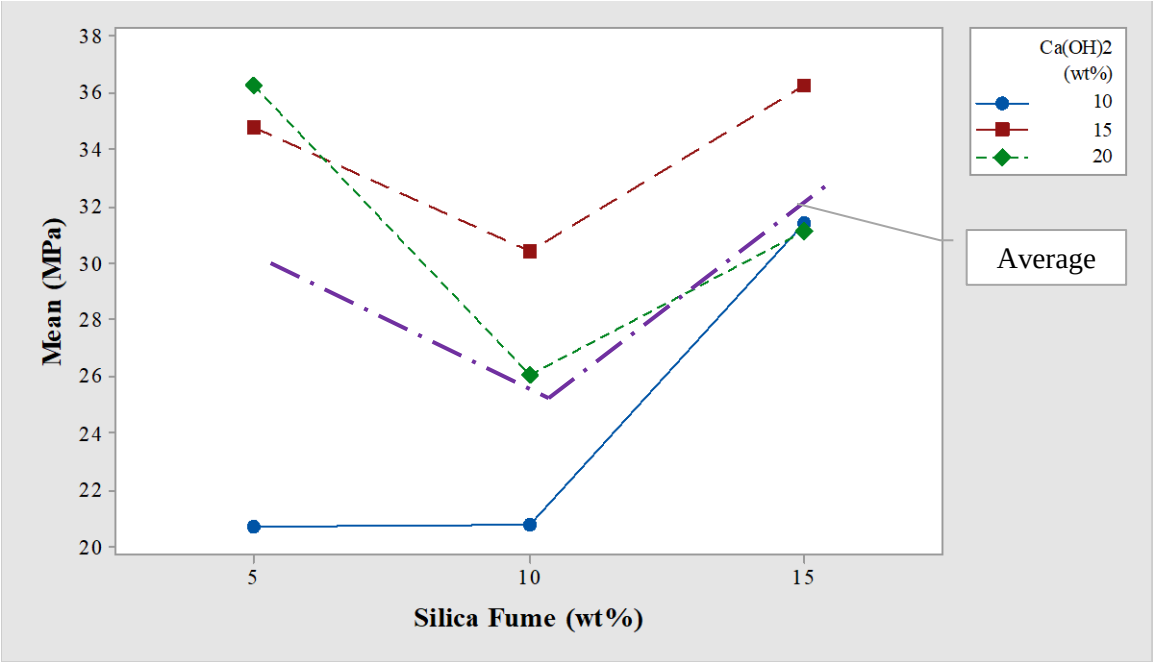

Figure 4-7: Interaction between SF and $Ca(OH)_2$

Evaluating the simple main effect of SF by taking average mean strength of the square, diamond and circle points at each factor level (purple dash dot line in Figure 4-7) shows that it decreases between 5 and 10 wt% but increases between 10 and 15 wt%, which is in correlation with the main effects plot in Figure 4-4. The main effect of SF is also another possibility.

The possible significance of the interactions and simple main effects will be checked via analysis of variance (ANOVA).

The analysis of variance (ANOVA) was computed first to test the adequacy of the model as shown in Table 4-1.

Table 4-1: Initial full quadratic model ANOVA result

Source	DF	Adj SS	Adj MS	F-Value	P-Value
Model	9	970.647	107.850	52.41	<0.0001
Linear	3	303.355	101.118	49.14	<0.0001
Na_2CO_3	1	158.484	158.484	77.02	<0.0001
$Ca(OH)_2$	1	129.096	129.096	62.74	<0.0001
Silica Fume	1	15.775	15.775	7.67	0.028
Square	3	148.133	49.378	24.00	<0.0001
Na_2CO_3*Na_2CO_3	1	0.443	0.443	0.22	0.657
$Ca(OH)_2$*$Ca(OH)_2$	1	101.561	101.561	49.35	<0.0001
Silica Fume*Silica Fume	1	95.432	95.432	46.38	<0.0001
2-Way Interaction	3	519.158	173.053	84.10	<0.0001
Na_2CO_3*$Ca(OH)_2$	1	263.122	263.122	127.87	<0.0001
Na_2CO_3*Silica Fume	1	131.058	131.058	63.69	<0.0001
$Ca(OH)_2$*Silica Fume	1	124.978	124.978	60.73	<0.0001
Error	7	14.404	2.058		
Lack-of-Fit	5	12.590	2.518	2.78	0.286
Pure Error	2	1.815	0.907		
Total	16	985.051			

As seen from Table 4-1, the F-value of the model is 52.41 implying that the model is significant and the probability that this value was due to noise is less than 0.01%. Furthermore, the lack-of-fit P-value is 0.286 which indicates that it is insignificant as $p > 0.05$. The insignificance of the lack-of-fit implies that the model fits the experimental data and the factors under consideration have a considerable impact on the response. However, it can be noticed that there is an insignificant term in the model (Na_2CO_3*Na_2CO_3) as $p > 0.05$. This was removed and the reduced model ANOVA results are shown in Table 4-2.

Table 4-2: Reduced model ANOVA result

Source	DF	Adj SS	Adj MS	F-Value	P-Value
Model	8	970.203	121.275	65.34	<0.0001
Linear	3	303.355	101.118	54.48	<0.0001
Na_2CO_3	1	158.484	158.484	85.39	<0.0001
$Ca(OH)_2$	1	129.096	129.096	69.56	<0.0001
Silica Fume	1	15.775	15.775	8.50	0.019
Square	2	147.690	73.845	39.79	<0.0001
$Ca(OH)_2$*$Ca(OH)_2$	1	120.013	120.013	64.66	<0.0001
Silica Fume*Silica Fume	1	102.938	102.938	55.46	<0.0001
2-Way Interaction	3	519.158	173.053	93.24	<0.0001
Na_2CO_3*$Ca(OH)_2$	1	263.122	263.122	141.77	<0.0001
Na_2CO_3*Silica Fume	1	131.058	131.058	70.61	<0.0001
$Ca(OH)_2$*Silica Fume	1	124.978	124.978	67.34	<0.0001
Error	8	14.848	1.856		
Lack-of-Fit	6	13.033	2.172	2.39	0.324
Pure Error	2	1.815	0.907		
Total	16	985.051			

The reduced model has a F-value of 65.34 which is greater than the initial model and still implies the model is significant. Moreover, the lack-of-fit is still insignificant ($p = 0.324 > 0.05$) which again shows the adequacy of the model. Table 4-3 gives a comparison of the summary statistics for ANOVA of the initial model vs. reduced model.

Table 4-3: Summary statistic comparison between initial and reduced model

Initial Model			
S	R-sq	R-sq(adj)	R-sq(pred)
1.43450	98.54%	96.66%	86.27%
Reduced Model			
S	R-sq	R-sq(adj)	R-sq(pred)
1.36235	98.49%	96.99%	88.12%

The R^2 of the reduced model indicates it can explain 98.49% of the model's variability. A large R^2 is usually a good indicator of the model's fit. However, the value of R^2 can be artificial increased as more predictors get included in the model without any real improvement to the system. Hence it is beneficial to compare the adjusted R^2 to the original R^2. The adjusted R^2 is a modified version of the normal R^2 and will only increase if the new term improves the model, if it has a strong correlation to the response. It decreases when the predictor does not have a strong correlation to the response. The adjust R^2 will always be less than R^2. From Table 4-10, the adjusted R^2 is 96.99% which is relatively high and further emphasises the model's adequacy and that non-significant terms have not been included.

The predicted R^2 is used, in conjunction with the adjusted R^2, to determine if there are too many predictors in the model and if it has been over-fit and is modelling random noise. An over-fit model will usually have a high R^2 value and low predicted R^2. From Table 4-4, the predicted $R^2$is 88.12% which shows the models high predictive capability and confirms that the model has not been over-fit. It is also within the acceptable margin of 0.2 from the adjusted R^2.

To further confirm the adequacy of the model, it is required to assess the residual plots. A residual is the difference between the observed value and its fitted value. Analysis of residual plots assists in confirming the assumption that the errors are approximately normally distributed with constant variance and whether additional terms would need to be added to the model (Montgomery, 2011).

The graph in Figure 4-8 represents the normal probability plot. Probability plots are used to assess whether the model has a fixed distribution. Most models are in the form,

Response = deterministic + stochastic

where the deterministic part is the fit and stochastic part is the error. The error part is most commonly assumed to be normally distributed. Therefore, a graph of a normal probability plot is generated from the residuals of the fitted model. Figure 4-8 shows that the residuals follow a straight line, which verifies the assumption that the residuals are normally distributed.

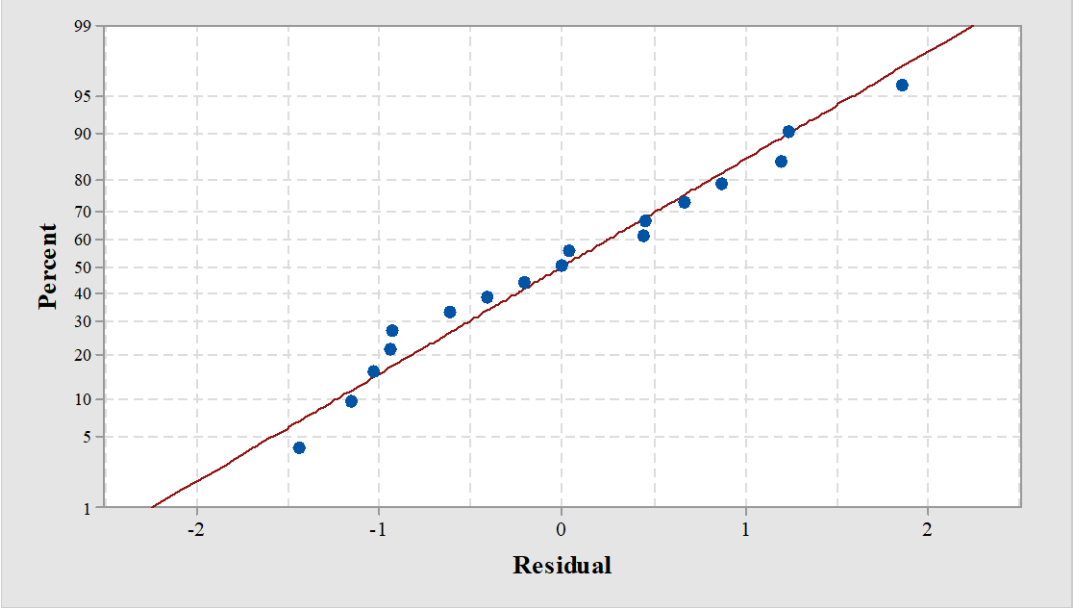

Figure 4-8: Normal probability plot

The graph in Figure 4-9 shows the residuals versus fits graph, which aids in confirming the assumption that the residuals constant variance and a mean of zero. As noticed, there are no visible trends in Figure 4-9 as the plots are scattered randomly around zero so the assumption that errors have a mean of zero is valid. Furthermore, there are no visible trends in and the vertical width of the scatter does not change significantly when moving along the fitted values, which shows that the assumption of residuals having a constant variance to be reasonable.

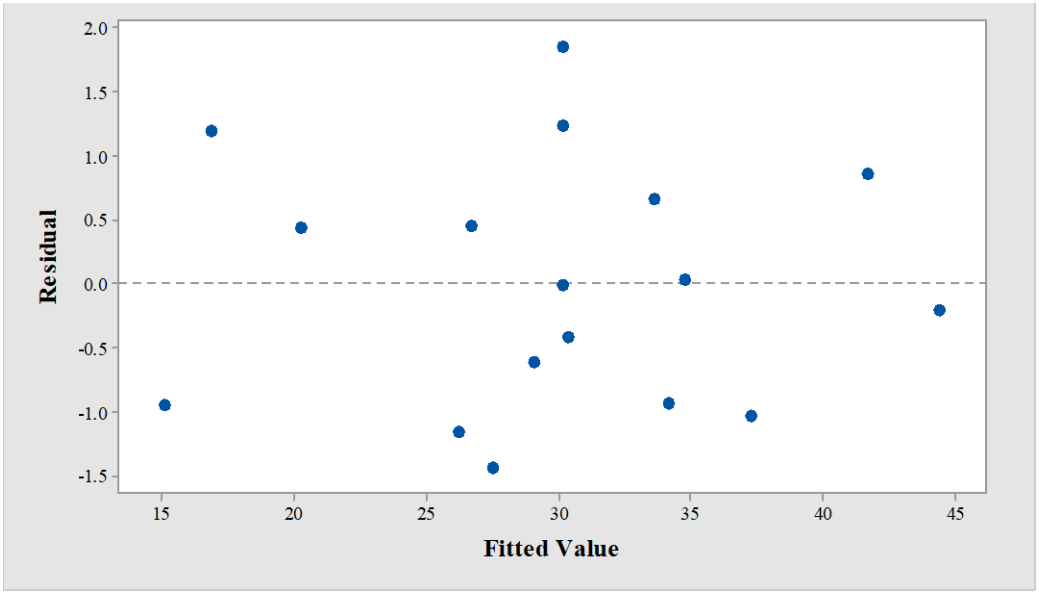

Figure 4-9: Graph of residuals versus fits

Another assumption required to be validated is where the errors are said to independent of each other. A plot of residual vs. order plot is required to validate this assumption, which is a plot of the residuals versus the order in which the data was collected. This is shown in Figure 4-10 for the model. For the assumption to hold true, it is required that the plots fluctuate randomly across the centreline of the graph, which is observed in Figure 4-10 showing the residuals are uncorrelated and the model is adequate.

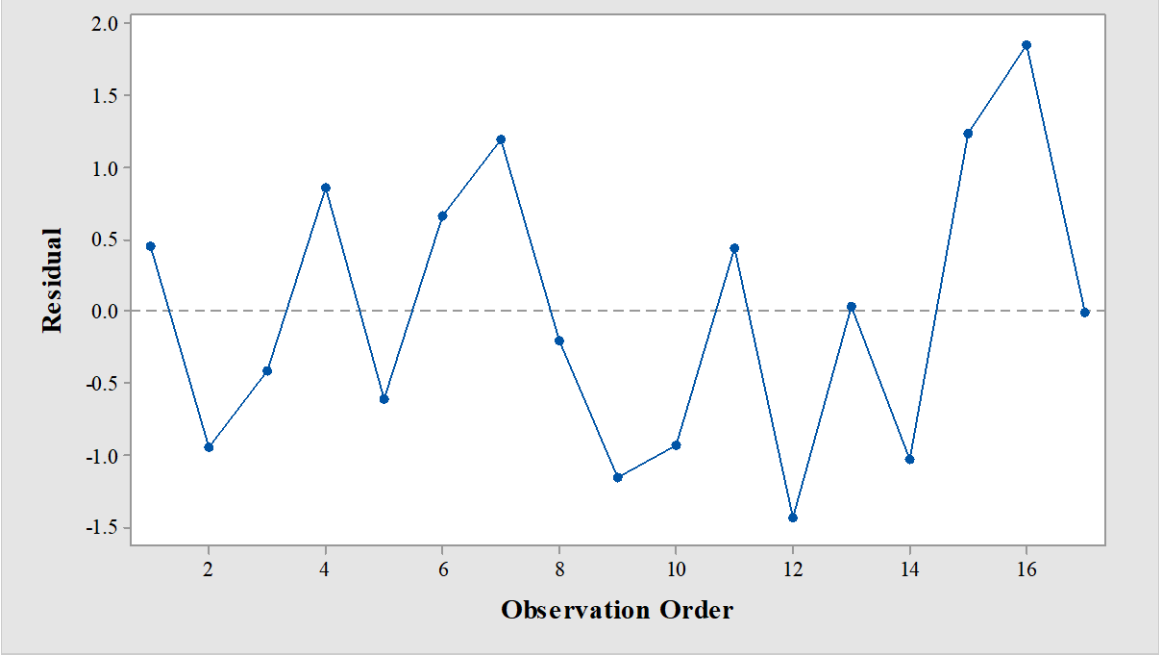

Figure 4-10: Graph of residuals versus order

With the model statistics and assumptions satisfied after analysis of the residuals, the final model can be used to navigate the design space.

The final empirical model equation is given in Eq. 3 and Eq. 4 as coded and actual units, respectively. Coded variables help with interpretation of the model and variable effects as the magnitude of the coefficients are given on a common scale.

$$Y = 30.200 + 3.981 \cdot A + 3.593 \cdot B + 1.256 \cdot C - 6.295 \cdot B^2$$
$$+5.830 \cdot C^2 + 5.735 \cdot A \cdot B + 4.047 \cdot A \cdot C - 3.952 \cdot B \cdot C \qquad (3)$$

where,

$Y - Compressive\ strength\ (MPa)$

$A - \ Na_2CO_3(wt\%), -1 \leq A \leq 1$

$B - \ Ca(OH)_2(wt\%), -1 \leq B \leq 1$

$C - \ Silica\ Fume\ (wt\%), -1 \leq C \leq 1$

$$Y = 23.82 - 7.106 \cdot A + 6.41 \cdot B - 4.471 \cdot C - 0.2518 \cdot B^2 + 0.2332 \cdot C^2 + 0.3829 \cdot A \cdot B + 0.2698 \cdot A \cdot C - 0.1581 \cdot B \cdot C \quad (4)$$

where,

$Y - Compressive\ strength\ (MPa)$

$A - \ Na_2CO_3(wt\%), 6 \leq A \leq 12$

$B - \ Ca(OH)_2(wt\%), 10 \leq B \leq 20$

$C - \ Silica\ Fume\ (wt\%), 5 \leq C \leq 15$

4.3 Influence of mix components on compressive strength

To get a better understanding of the system, it is imperative to look at how each component affects the strength. It should be noted that the test wt% amounts (taken as percentage of FA content) are different from what was actually in the samples (percentage of total solid weight) and this is shown in Table 4-4. The graphs in Figure 4-11 to 4-14 compares the actual and test weight percentages of each component in the samples and what their effects are on the compressive strength at 3 and 28 days.

Table 4-4: Actual vs test wt% in samples

Design Points	SC (wt%)		CH (wt%)		SF (wt%)		FA
	Test[1]	Actual*	Test[1]	Actual*	Test[1]	Actual*	
SC12|CH20|SF15	12.00	7.72	20.00	12.86	15.00	9.65	64.30
SC12|CH20|SF5	12.00	8.25	20.00	13.74	5.00	3.44	68.72
SC12|CH10|SF15	12.00	8.25	10.00	6.87	15.00	10.31	68.72
SC12|CH10|SF5	12.00	8.86	10.00	7.38	5.00	3.69	73.79
SC6|CH20SF|15	6.00	4.13	20.00	13.77	15.00	10.33	68.84
SC6|CH20|SF5	6.00	4.44	20.00	14.79	5.00	3.70	73.93
SC6|CH10|SF15	6.00	4.44	10.00	7.39	15.00	11.09	73.93
SC6|CH10|SF5	6.00	4.79	10.00	7.98	5.00	3.99	79.83
SC12|CH15|SF10	12.00	8.25	15.00	10.31	10.00	6.87	68.72
SC6|CH15|SF10	6.00	4.44	15.00	11.09	10.00	7.39	73.93
SC9|CH20|SF10	9.00	6.19	20.00	13.76	10.00	6.88	68.78
SC9|CH10|SF10	9.00	6.65	10.00	7.39	10.00	7.39	73.86
SC9|CH15|SF15	9.00	6.19	15.00	10.32	15.00	10.32	68.78
SC9|CH15|SF5	9.00	6.65	15.00	11.08	5.00	3.69	73.86
SC9|CH15|SF10	9.00	6.41	15.00	10.68	10.00	7.12	71.23
SC9|CH15|SF10	9.00	6.41	15.00	10.68	10.00	7.12	71.23
SC9|CH15|SF10	9.00	6.41	15.00	10.68	10.00	7.12	71.23

[1]Test values were taken as percentages of FA content
*Actual values are percentages of the total solid weight

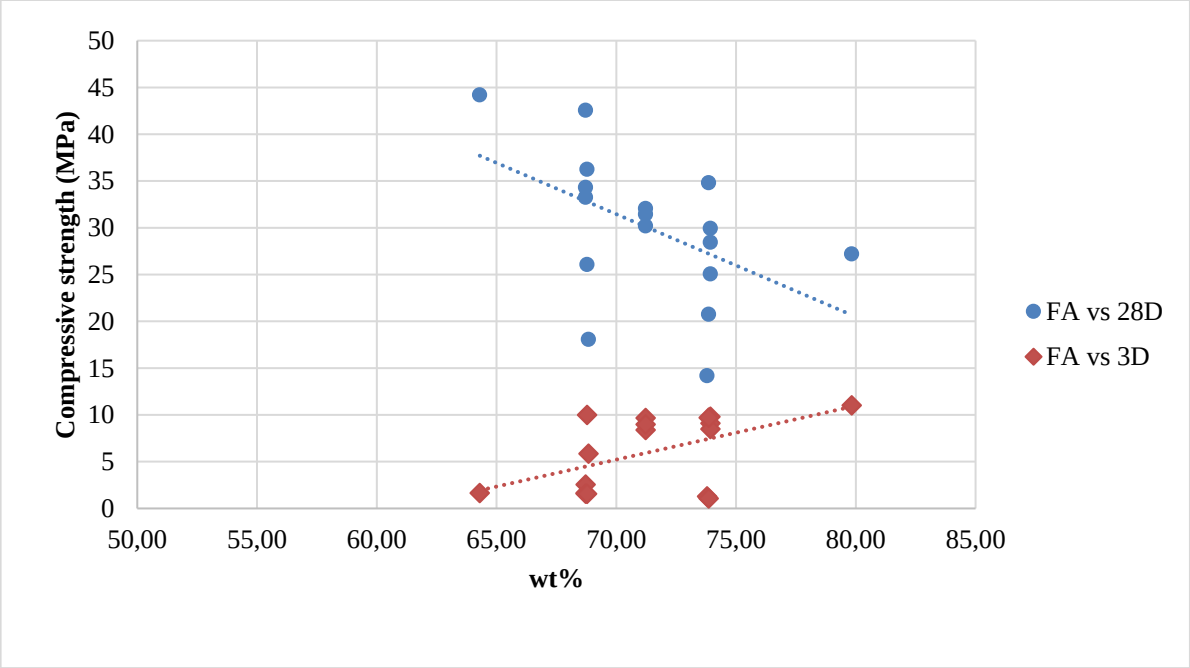

Figure 4-11: Test vs actual wt% for FA

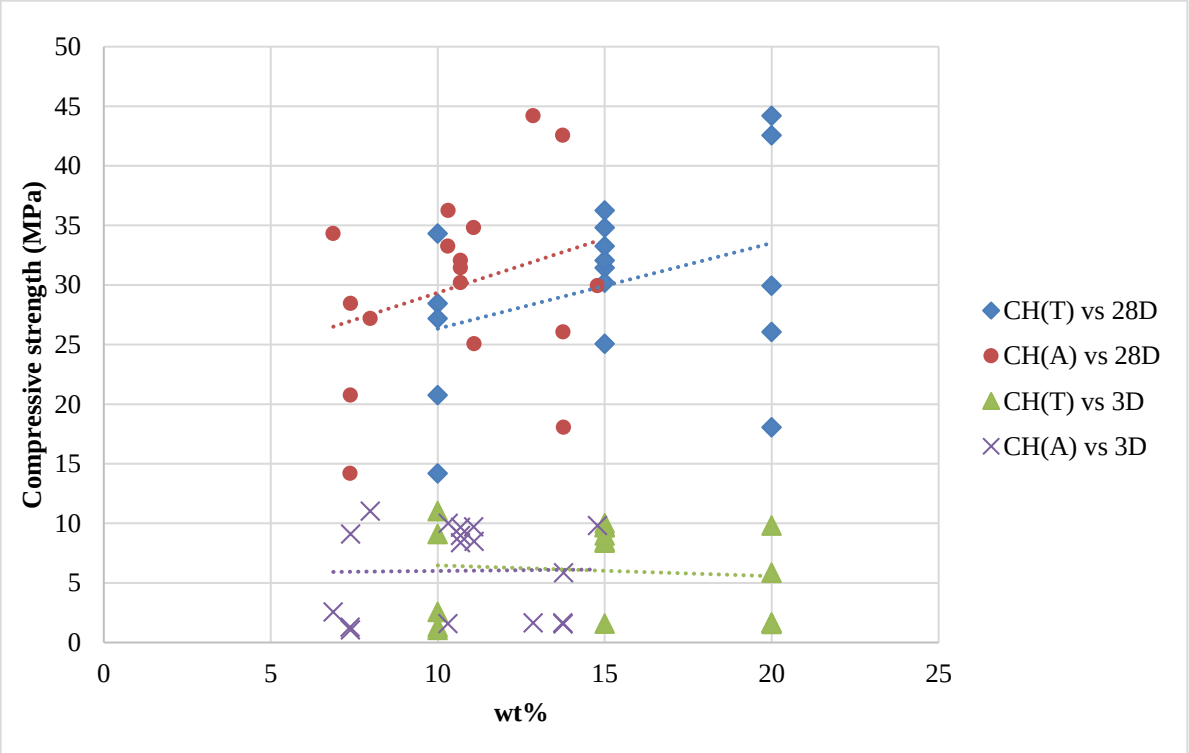

T = Test wt% / A = Actual wt%

Figure 4-12: Test vs actual wt% for CH

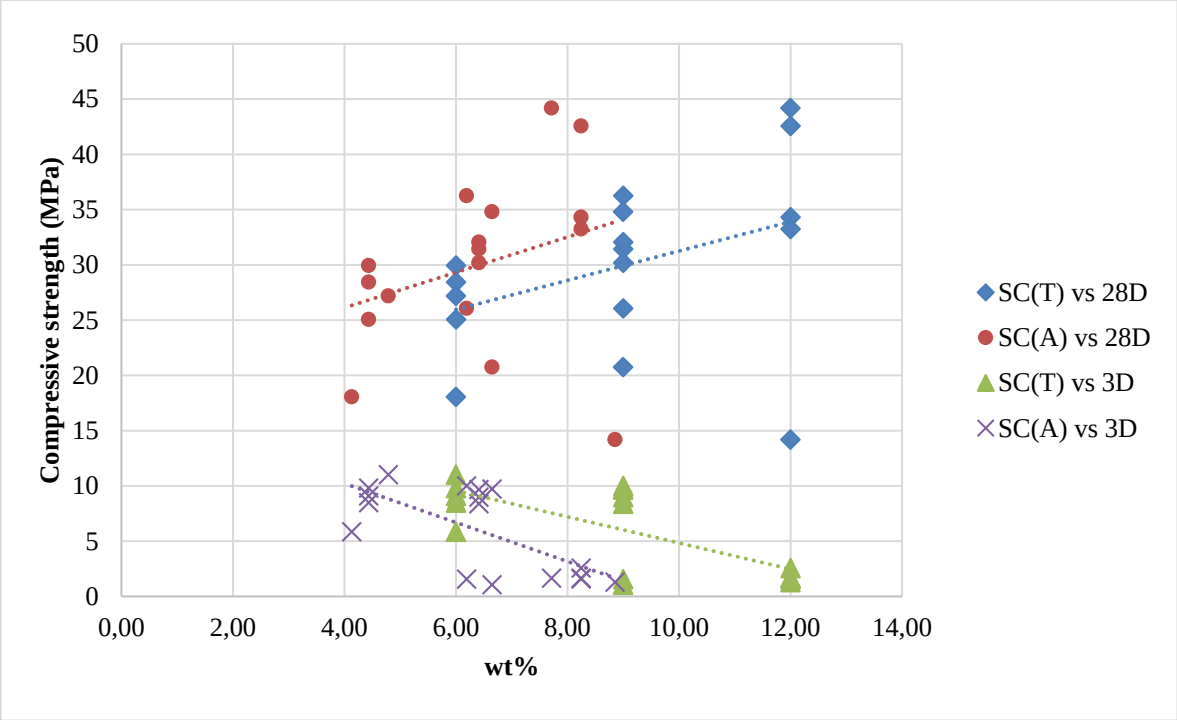

T = Test wt% / A = Actual wt%

Figure 4-13: Test vs actual wt% for SC

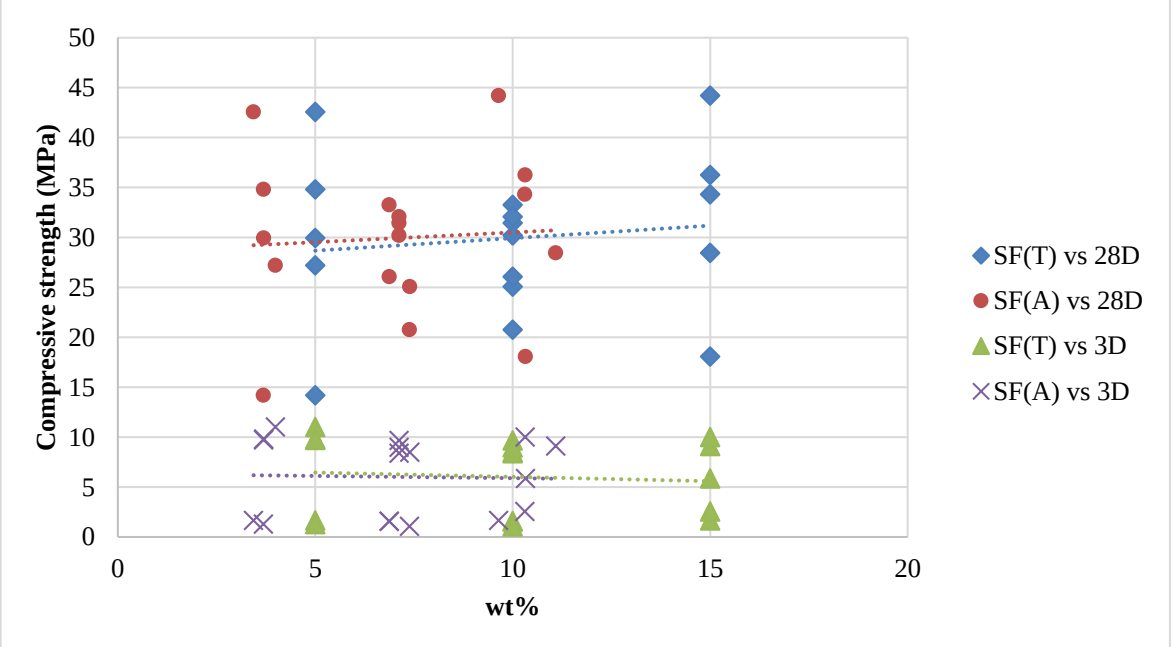

T = Test wt% / A = Actual wt%

Figure 4-14: Test vs actual wt% for SF

From Figure 4-11, it can be noticed that a lower amount of FA in the samples gains higher strength at 28 days. A lower FA content implies a greater quantity of activator, which increases the dissolution of its particles. This leads to increased gel formation which aids in attaining higher strength. However, it is worth noting the variance in strength values for the same FA content. This shows that the strength parameters are very much dependent on other factors, which was covered in the mathematical model.

From Figure 4-12 and Figure 4-13, an increase in the SC and CH wt% content positively affects the strength at 28 days, respectively. However, the inverse is true for strength at 3 days, similar to what was noticed with FA in Figure 4-11. The positive effect at 28 days is in good correlation with the result attained from the statistical analysis. Looking at Eq 3, the coefficient for both SC and CH are positive and of similar magnitude. This is further confirmed by the small difference in gradient of the line between test and actual wt% of SC and CH at 28 days, shown in Figure 4-12 and 4-13. Moreover, it is also interesting to note that SC was the dominant activator to influence the results. Sodium carbonate exhibited a greater effect on the strength values at 3 days when compared to CH, which showed an almost neutral effect.

From Figure 4-14, the effect of silica fume was fairly small and positive at 28 days, which is in good correlation with the statistical analysis as the coefficient and magnitude for SF in Eq. 3 is positive and small. Hence there was not a significant change in the gradient lines on Figure 4-14 when comparing the test and actual wt%. Considering the strength at 3 days, there was a neutral and almost negative effect with increasing wt% content. It is possible that SF reaction forms gels at the initial stages of hydration which agglomerates and reacts with CH to form CSH gels (Doughlas and Brandstetr, 1990).

Two noticeable trends are observed from Figure 4-3. The first trend is that a sample gains high strength at 3 days but is followed by a slow development in strength. For example, mix SC6|CH10|SF5 gained 11.0 MPa at 3 days and increased by 147% to 27.2 MPa at 28 days. Jeon et al. (2015) noticed a similar trend where the author's samples gained considerable strength at 3 days (28 MPa) but did not develop as aggressively and only increased in strength by 29% at 28 days (36 MPa).

The other trend is the exact opposite of the first trend. A sample gains low strength at 3 days but is followed by rapid strength development. For example, mix SC12|CH20|SF15 gained 1.6 MPa at 3 days and increased by 2578% to 44.2 MPa at 28 days.

The major factor contributing to the two trends was the amount of SC present in the samples. A higher content correlated to the first trend whilst a lower content correlated to the latter. This is due to the lower pH of SC. It can demonstrate a lower strength in the beginning but a higher strength at later stages due to the effect of CO_3^{2-} ions, which causes the formation of carbonated compounds that improves mechanical strength (Abdalqader et al., 2016; Wang et al., 1994; Fernández-Jiménez et al., 1999; Li and Sun, 2000). This is further explored in Section 4.4.

Calcium hydroxide activated FA systems were generally composed of CSH type gels but gained low compressive strength as observed by Huang and Cheng (1986). The authors mentioned that in a FA-$Ca(OH)_2$-H_2O system, the hydration rate was low. The system's hydration rate increased by 1.5% in 7 days and was less than 20% after 180 days. The reasoning stated was that unlike slag, FA has a lower content of CaO; higher aluminium and silicon content, which requires a higher degree of polymerization. Thus, the hydration activation is much less than that of slag. Furthermore, in a system of FA-$Ca(OH)_2$, the pH is less than 13. A pozzolan and lime system mixed with water undergoes hydrolyses and reaches a pH value of 12.5. However, this is a low pH to promote suitable dissolution. Fraay and Bejen (1989) demonstrated that a pH value of 13.3 is required for appropriate dissolution of alumina and silica species. Therefore, it is required that other additives be added to the system to increase the alkalinity (Li et al., 2000).

By combining SC with CH the following chemical balanced equation is formed:

$$Na_2CO_3 + Ca(OH)_2 \rightarrow 2NaOH_{(aq)} + CaCO_3 \qquad (5)$$

Similar to Equation 2, there is formation of NaOH in Equation 5. Although not a dominant factor, this increases the alkalinity of the mixture and promotes dissolution of the silica and alumina species in the FA, which is responsible for strength development due to increased gel formation in the samples (Wang et al, 1994; Li and Sun, 2000). Therefore, samples that contained the highest content of SC and CH (SC12|CH20|SF15 and SC12|CH20|SF5), and in extension lower FA content, obtained the highest strength at 28 days. The SC and CH would react first, accelerate the dissolution and increase the pozzolanic activity between CH and the pozzolans (Shi & Day, 2000).

Furthermore, there is formation of $CaCO_3$ as a secondary product from Eq. 5. Calcium carbonate has a pore refining effect that can reduce the porosity and promote better mechanical strength. Fine $CaCO_3$ also has a seeding effect that might promote early gel formation to improve strength (Bernal et al., 2015; Sato & Beaudoin, 2011). This is further explored in Section 4.4.

Authors (Nurrudin et al., 2010; Rashad & Khalil, 2013; Sayed & Zedan, 2013; Songpiriyakij et al., 2011) found that fine SF also has a packing effect that acts as a filler material for voids, which creates a more compact microstructure. They can also act as nucleation sites for further alkali reactions and greater formation of alkali-activated products. However, from Figure 4-7, the small effect implies that this packing effect is not significant enough to affect the strength.

Although, considering the Gibbs energy of the chemical equation, it can be argued that such a reaction (Eq. 5) does not occur under ambient conditions. But the complexity of the system could cause the reaction to occur or other reactions due to the inclusion of highly reactive SF. Jeon et al. (2015) had a similar blend system to the present study (FA + $Ca(OH)_2$ + Na_2CO_3). The authors mentioned there was significant formation of CSH type gels and subsequent pore-size refinement. However, their system was cured the system at 60 °C, which attained 36 MPa at 28 days. The highest strength sample in this study attained 44.2 MPa at 28 days under ambient conditions.

The following sections deal with the characterization techniques used to evaluate the microstructural and mineralogical changes over time for selected samples at 3 and 28 days. The selected samples were SC12|CH20|SF5-[H], SC12|CH10|SF5-[L] and SC6|CH20|SF5-[M], which gained high strength [H], low strength [L] and moderate strength [M] at 28 days, respectively.

4.4 Characterisation techniques

4.4.1 Heat flow calorimeter

The graph in Figure 4-15 represents the heat flow curves for SC12|CH20|SF5-[H], SC12|CH10|SF5-[L] and SC6|CH20|SF5-[M].

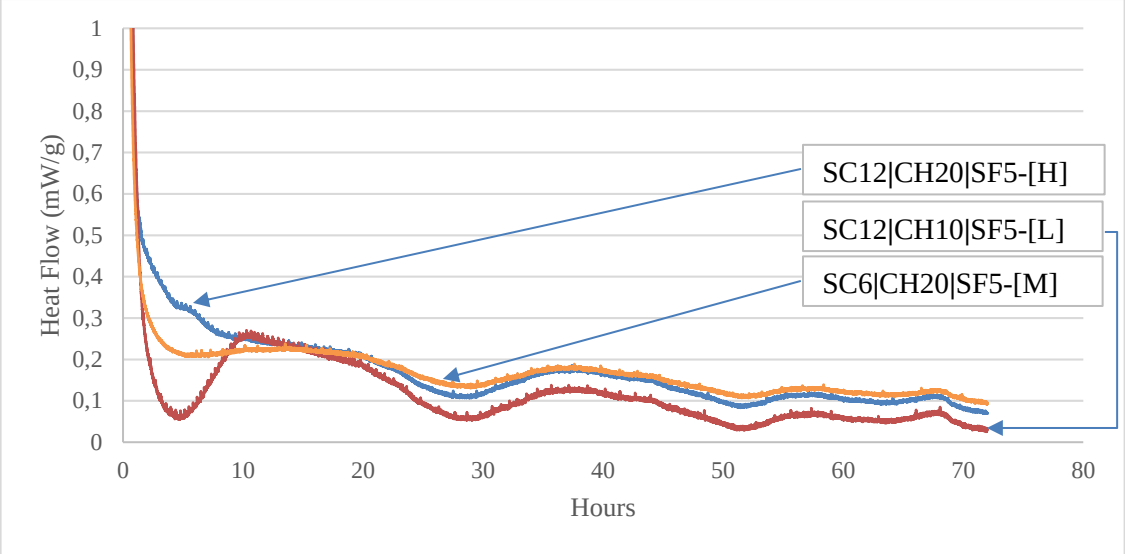

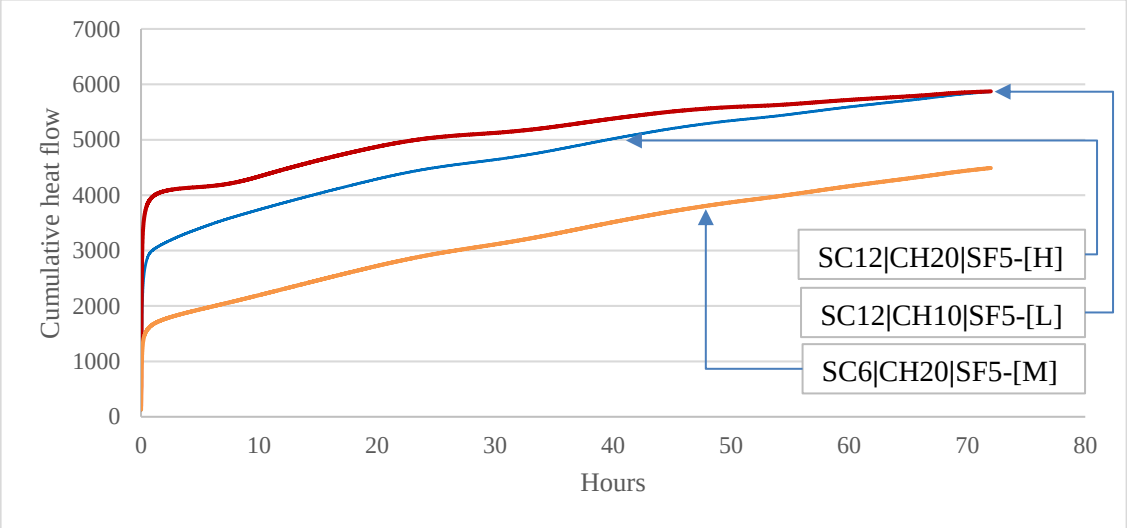

Figure 4-15: Heat flow and cumulative heat flow calorimeter curves

There are two broad humps that occur from 10-25 h and 30-50 h after a short induction period. This is related to the acceleration and deceleration processes that occur due to precipitation of reaction products/formation of gels (Rashad et al., 2013; Abdalqader et al., 2016). There is a difference in the heat flow during the short induction period. SC12|CH10|SF5-[L] has a low heat flow which is followed by a sharp rise whereas the other two samples had a more gradual change in its heat

evolution. The difference between the curves lie during the first 25 h, after which the curves show similar characteristics with the only difference being the heat flow. This could explain the difference in strength noticed between the samples with SC12|CH10|SF5-[L] gaining the lowest strength and had the lowest overall heat flow. SC12|CH20|SF5-[H] and SC6|CH20|SF5-[M] had similar heat flow curves with the exception of higher heat flow in the earlier stage for SC12|CH20|SF5-[H].

4.4.2 X-ray diffraction (XRD) analysis

The graphs in Figure 4-16 to 4-18 represents the diffractograms for samples SC12|CH20|SF5-[H], SC12|CH10|SF5-[L] and SC6|CH20|SF5-[M] at 3 and 28 days.

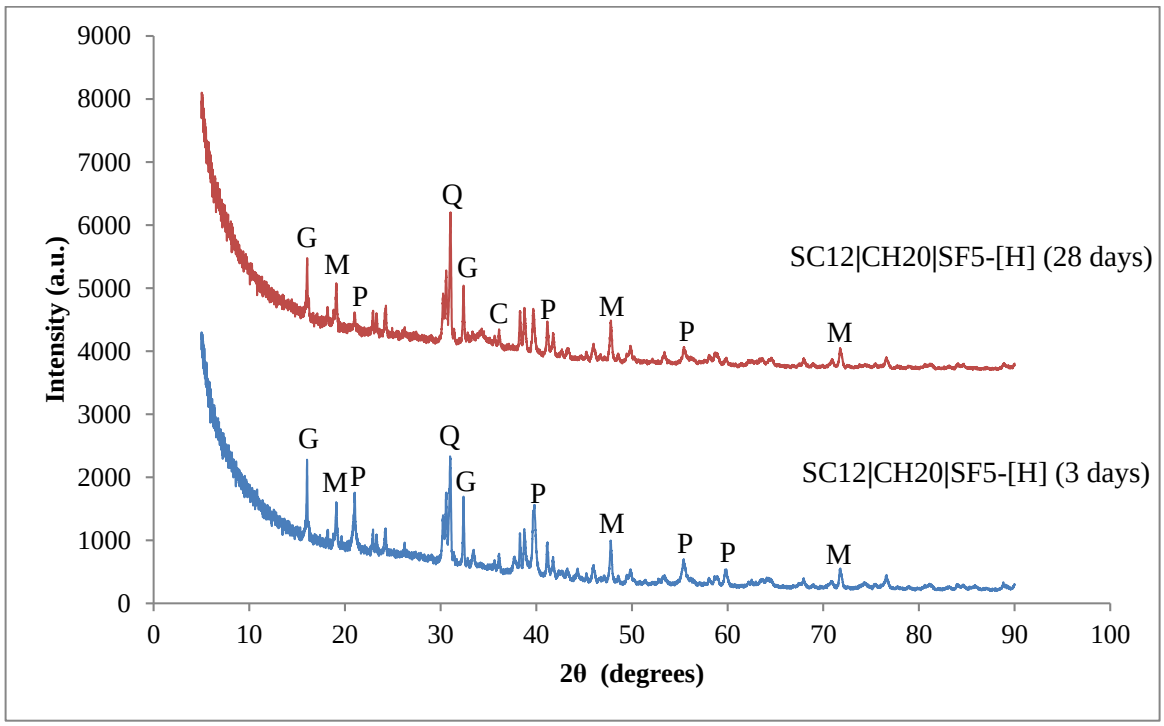

G - Gaylussite; M - Mullite; Q -Quartz; C - Calcite; P - Portlandite

Figure 4-16: X-ray diffractograms of SC12|CH20|SF5-[H] mix

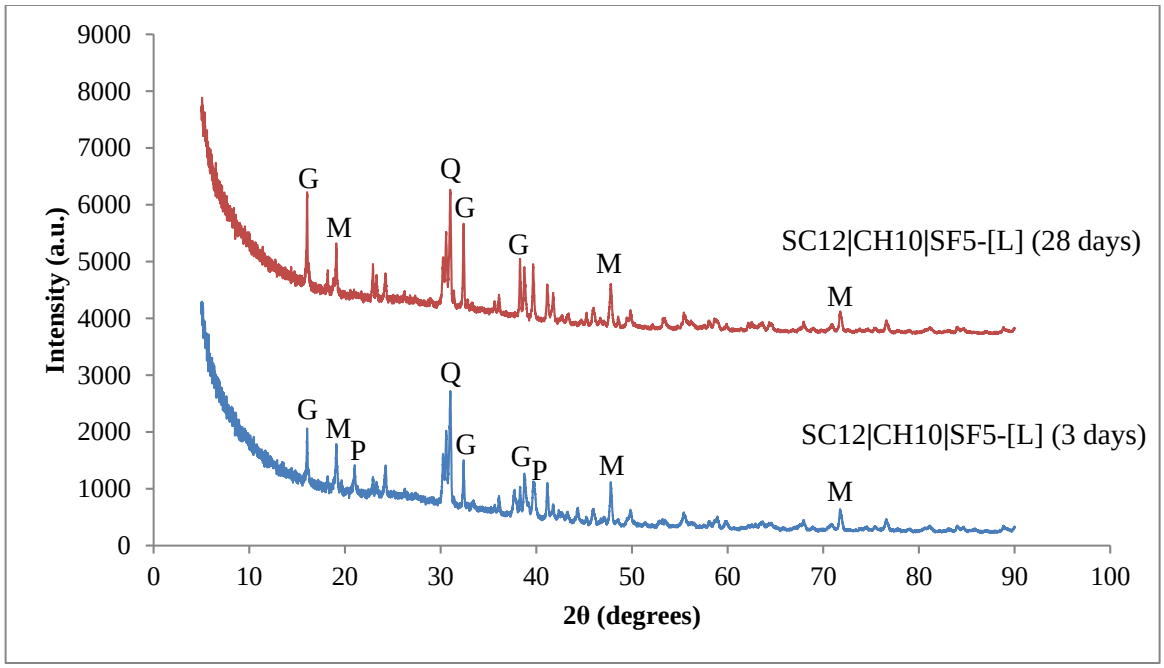

G - Gaylussite; M - Mullite; Q -Quartz; C - Calcite; P - Portlandite

Figure 4-17: X-ray diffractograms of SC12|CH10|SF5-[L] mix

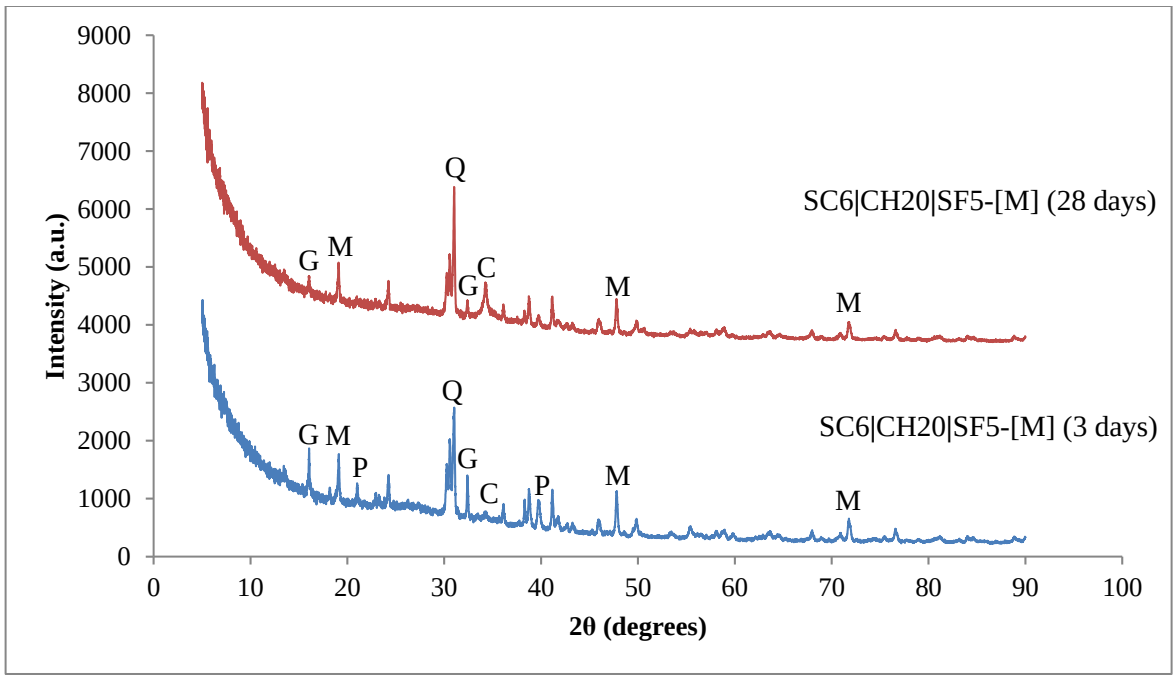

G - Gaylussite; M - Mullite; Q -Quartz; C - Calcite; P - Portlandite

Figure 4-18: X-ray diffractograms of SC6|CH20|SF5-[M] mix

Fly ash consists of stable but un-reactive crystalline phases such as mullite and quartz as well as reactive amorphous phases. Therefore, during reaction, the reactive part undergoes alkali activation whilst the un-reactive phases act as micro-aggregate in the final matrix (Kumar et al. 2017; Duxson et al. 2005). The major peak at approximately 31° is due to quartz that was present in the fly ash.

Portlandite, which is CH from the binder compositions, in the samples gets consumed and lower amounts are present at 28 days as seen in the XRD results (Figure 4-16 to 4-18). Sample SC12|CH20|SF5-[H] at 3 days (Figure 4-16), have peaks at 21° and 39.5° that represent portlandite, and it can be observed that the intensity of the peaks at 28 days is lower than at 3 days showing that full consumption has not completed. Moreover, mix SC12|CH10|SF5-[L] (Figure 4-17) and SC6|CH20|SF5-[M] (Figure 4-18) show the portlandite (CH) peaks in the 3-day samples but disappear completely in the 28-day samples.

Walkley et al. (2016) suggests that increasing the calcium content in precursors enables greater formation of low-Al, high Ca containing C-(N)-A-S-H with lower mean chain length (MCL) and AFm type phases with little evolution of binder chemistry at later stage. Authors mention that in general, increasing the Ca content in precursors impedes the formation of N-A-S-H and AFm type phases and in Al-rich samples, promotes the formation of portlandite and Al-rich reaction products. However, the diffractograms did not show any zeolitic formation and the hydration product for this type of binder system is most likely to be a CSH.

As the peaks of portlandite decrease/disappear with increasing age, there is progressive consumption which can be facilitated by lime-consuming CSH formation and due to the available silicon in the mixtures, forming additional gels (Jeon et al. 2015). The increase in calcite amount over the time can also decrease the amount of portlandite due to carbonation. This is proven by the calcite peaks noticed in the 28-day sample for SC12|CH20|SF5-[H] (Figure 4-16) and SC6|CH20|SF5-[M] (Figure 4-18) at position 34° in both diffractograms. In sample SC12|CH10|SF5-[L] (Figure 4-17) there was no calcite reflection at 28 days but the portlandite reflection at 3 days completely disappears, which can be most likely attributed to its consumption and formation of CSH type gels.

Carbonate salt gaylussite, sodium-calcium carbonate, was identified in the samples which indicate cation exchange reaction between the precursor and activator. In the alkali activation, the Ca^{2+} ions provided by calcium hydroxide must react with the CO_3^{2-} from sodium carbonate to form carbonate salts such as calcite and gaylussite (Eq. 5) such that the pH can be increased through the release of

OH^- ions. After gels start to precipitate, the gaylussite dissolves as a result of decreasing concentration of gaylussite CO_3^{2-} ions in the aqueous phase. The carbonate then re-precipitates as $CaCO_3$ polymorphs such as calcite. Thus, gaylussite is a transient phase that decreases/get consumed as more stable carbonates form at later stages as shown in Eq. 6 (Ke et al., 2016; Yuan et al., 2017; Bernal et al., 2014). Furthermore, the formation of gaylussite can be attributed to portlandite's (CH) consumption as well. This is in correlation with the XRD patterns. There is a notable decrease in gaylussite peak intensity from 3 to 28 days for all samples and in the case of SC12|CH20|SF5-[H] (Figure 4-16) and SC6|CH20|SF5-[M] (Figure 4-18), there is formation of calcite. Calcite acts as an inactive filler material and do not contribute to the formation of the gel structure (Aboulayt et al., 2017).

$$5H_2O + 2Na^+ + Ca^{2+} + 2CO_3^{2-} \rightarrow Na_2Ca(CO_3)_2.5H_2O\ (gaylussite) \quad (5)$$

$$Na_2Ca(CO_3)_2.5H_2O \rightarrow CaCO_3 + 2Na^+ + CO_3^{2-} + 5H_2O \quad (6)$$

In conclusion, the mechanism noticed is the formation of gaylussite due to the reaction Ca^{2+} with CO_3^{2-} for all samples. This releases hydroxide ions which aid in increasing the pH of the system and facilitate activation. Gaylussite transforms into carbonate phases at later age, noticed by the lower gaylussite peaks and formation of calcite peaks. The portlandite consumption can be tied to the formation of CSH type gels. This consumption, followed by calcite formation, can explain the difference in strength noticed for the three samples. Bernal et al. (2015) mentions that activation reactions proceeds once the CO_3^{2-} have been exhausted. This can be confirmed when looking at the strength gain trend of the samples in this study. Samples that contained a large quantity of SC had a low strength at 3 days but gained significant strength after 28 days. The opposite was true for samples containing lower quantity of SC. For example, sample SC12|CH20|SF5-[H] gained 1.65 MPa at 3 days but increased to 42.6 MPa at 28 days. Comparatively sample SC6|CH20|SF5-[M], which had the lower SC content, gained 9.81 MPa at 3 days and increased to 29.9 MPa. This shows that with higher quantities of SC, the exhaustion of CO_3^{2-} ions take longer but with the beneficial effect of increasing the pH due to the release of hydroxide ions and hence higher strength at later ages. With lower quantities, the CO_3^{2-} deplete earlier. Therefore, the activation mechanism begins earlier and hence the higher early age strength gain but a lower strength at later ages. This due to the lack of SC to form more hydroxide ions to increase the pH. When looking from construction material point of view, sample SC6|CH20|SF5-[M] is a great representative as an alternative building material. Not only did it gain sufficient early age strength but also had a 28 day mechanical strength that is comparable to what is recommended in most construction projects using ordinary Portland cement.

4.4.3 SEM/EDS analysis

Figure 4-19 shows SEM images of SC12|CH20|SF5-[H], SC12|CH10|SF5-[L] and SC6|CH20|SF5-[M] of samples at different curing ages.

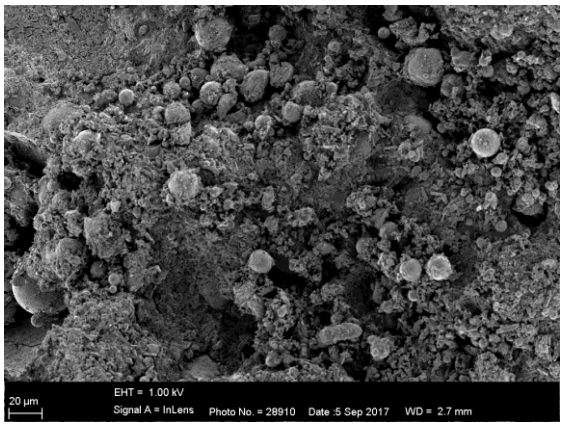

SC12|CH20|SF5-[H] (3D)

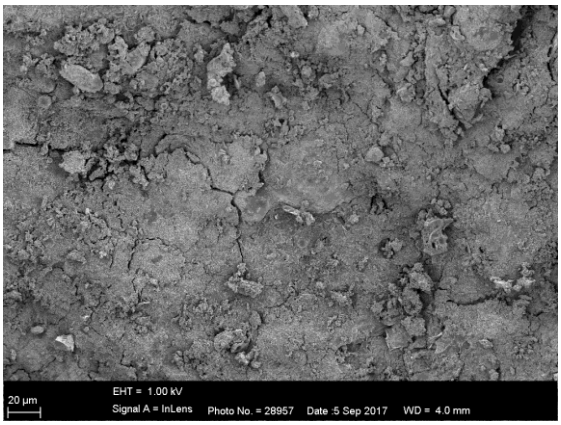

SC12|CH20|SF5-[H] (28D)

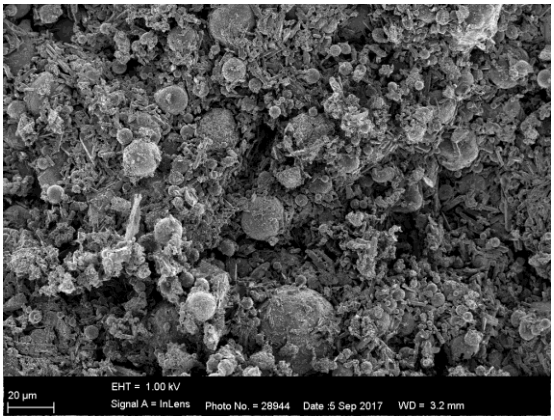

SC12|CH10|SF5-[L] (3D)

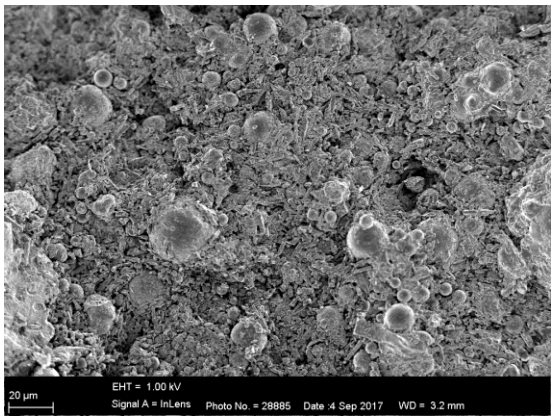

SC12|CH10|SF5-[L] (28D)

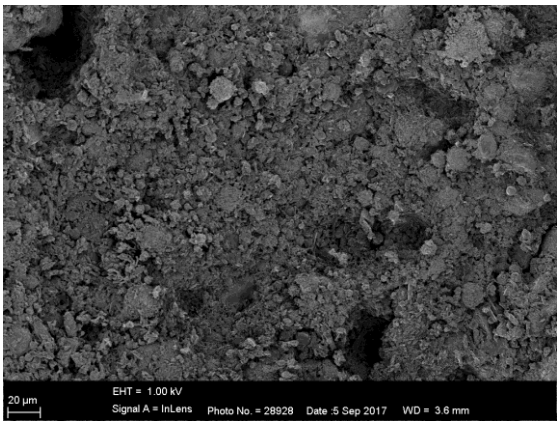

SC6|CH20|SF5-[M] (3D)

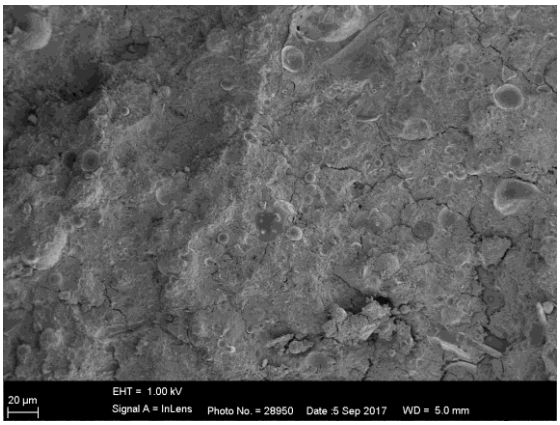

SC6|CH20|SF5-[M] (28D)

Figure 4-19: SEM images of chosen samples at 3 and 28 days

For the samples at 3 days, it can be noticed that there is a large disparity in the amounts of unreacted particles. Mix SC12|CH20|SF5-[H], which gained the second highest strength at 28 days but low strength at 3 days, has a noticeable amount of unreacted particles . Mix SC12|CH10|SF5-[L] showed similar characteristics to the sample SC12|CH20|SF5-[H] SEM image but the amount of unreacted particles were more prominent. However mix SC6|CH20|SF5-[M], which had one of the highest strength at 3 days of all the samples, showed a significantly lower amount of unreacted particles, comparatively. The SEM image of SC6|CH20|SF5-[M] (3D) shows a more developed microstructure with large amorphous area at early age compared to the other two, which can explain the higher strength at 3 days.

Investigating the samples at 28 days, SC12|CH20|SF5-[H] had scarce amounts of unreacted particles and mostly consisted of a dense amorphous microstructure. This shows that most of the unreacted particles noticed in the samples at 3 days had reacted and could be the reasoning behind on why it gained high strength at 28 days. Mix SC12|CH10|SF5-[L] which had similar characteristic to mix SC12|CH20|SF5-[H] at 3 days did not, however, show a similar trend. There are still copious amounts of unreacted particles. Sample SC6|CH20|SF5-[M] showed the same characteristic as its counterpart at 3 days but contained a larger quantity and size of unreacted particles when compared to mix SC12|CH20|SF5-[H]. This shows that it did not undergo a large dissolution phase unlike sample SC12|CH20|SF5-[H], which caused the strength value to be lower in comparison.

Comparing the microstructure of mix SC12|CH20|SF5-[H] between 3 and 28 days, it can be noticed the porosity of sample decreased over time. This reduction can be due to alkali activation and formation of reaction products. However, it can also possibly be attributed to the formation of calcite as mentioned in Section 4.4.2 and its formation noticed in the XRD diffractograms. Calcite can act as a pore-filling material as mentioned earlier. In SC12|CH20|SF5-[H], the XRD analysis show calcite formation only in the sample at 28 days. In the SC12|CH10|SF5-[L] sample, the XRD showed no formation of calcite in either samples at 3 and 28 days. However in SC6|CH20|SF5-[M], there was already calcite formation in the samples at 3 days, which only increased at 28 days and had the highest peak intensity amongst the studied samples. The more calcite formation, the less porous the microstructure. In Jeon et al. (2015) study, the authors noted that calcite does not contribute strength with its pore-filling characteristic but rather it is sodium carbonate that provides a pore-refining effect. However thus far the results in this study suggest that calcite formation can be related pore-refinement as per the XRD and SEM. This is in an area that could be further studied/investigated in the future.

Electron diffraction spectrometry (EDS) was performed to determine the elemental composition of the samples by selecting a number of points in different regions of each sample. Figure 4-20 shows spectrum 35 of an amorphous region on the SC12|CH20|SF5-[H] sample as an example to determine the type of gel forming. Table 4-5 gives the average quantity of the elements from EDS analysis done on various points.

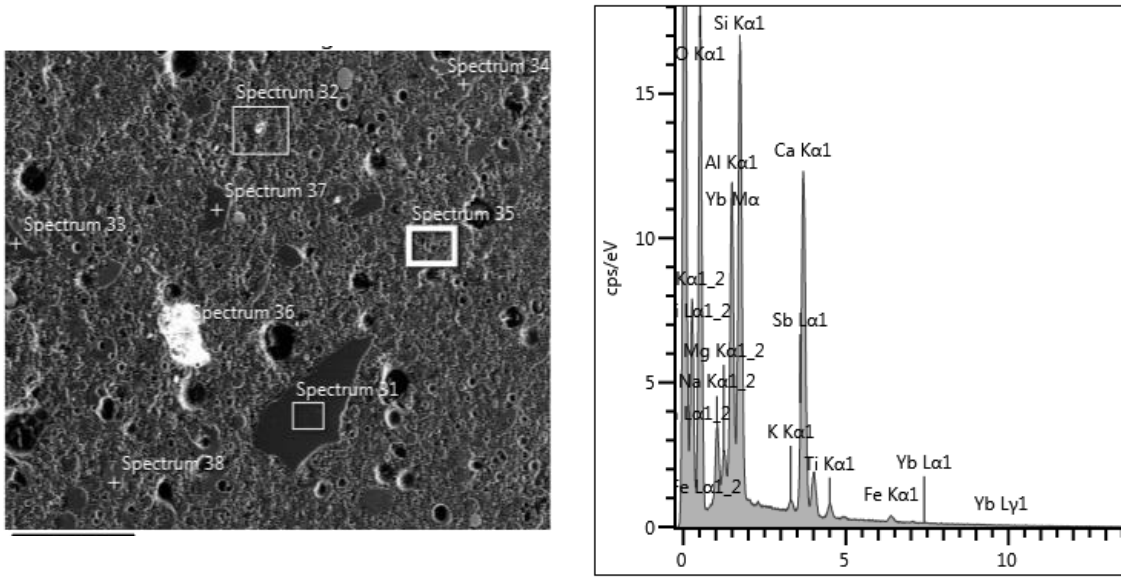

Figure 4-20: EDS spectrum 35 example

Table 4-5: Average element wt% of EDS spot analysis

C	O	Na	Mg	Al	Si	K	Ca	Ti	Fe
19.3	41.5	2.4	1.19	13.2	21.4	0.554	12.0	0.971	2.1

From Figure 4-20 and Table 4-5, it can be seen that it is abundant in Si and Al as well as Ca. This could suggest the type of binding gel forming is of CASH type. However, there are trace amounts of Na as well which could suggest a C(N)ASH type gel formation. This is in line with the theory stated in previous sections and will be validated in the following sections.

In conclusion, the SEM analysis correlated well with the XRD data. Sample SC6|CH20|SF5-[M] at 3 days had lower amounts of unreacted particles and a more homogenous microstructure, which can be attributed to the gaylussite transformation into carbonate species as it was the only sample to show calcite peaks at 3 days. This could also imply gel formation took place earlier and it did not gain additional strength unlike SC12|CH20|SF5-[H] which gained higher strength due to the denser microstructure at 28 days. SC12|CH10|SF5-[L] still had unreacted particles after 28 days showing

full dissolution had not taken place or was taking place at a slow rate. It was also the most porous sample which can possibly be tied to no calcite peaks noticed in the XRD data at 28 days in Figure 4-17.

4.4.4 FTIR analysis

Fourier transform infrared spectroscopy (FTIR) enables interpretation of the degree of polymerization of the reaction products and make conclusions about the types of structures present. The vibration of molecular bonds will differ depending on the absorption of photons at appropriate energies. Thus, allowing to relate structures to the energy that is absorbed and define the functional groups of the product. Molecular bonds will exhibit narrow peaks if the structure is highly crystalline. If the structure is amorphous, the IR spectra will show wider/broader bands/peaks (Dakhane et al., 2017).

Figures 4-21, 4-22 and 4-23 represents the IR spectrum from wavelength section 1500 to 500 cm^{-1} of SC12|CH20|SF5-[H], SC12|CH10|SF5-[L] and SC6|CH20|SF5-[M] for raw blended materials and at different ages, respectively. There were not any noticeable changes from 4000 to 1500 cm^{-1} and thus not included in the Figures, except some minor broad humps noticed in the region of 3600 to 3500 cm^{-1}, which can be attributed to the strength vibration of -OH (Jang & Lee, 2016).

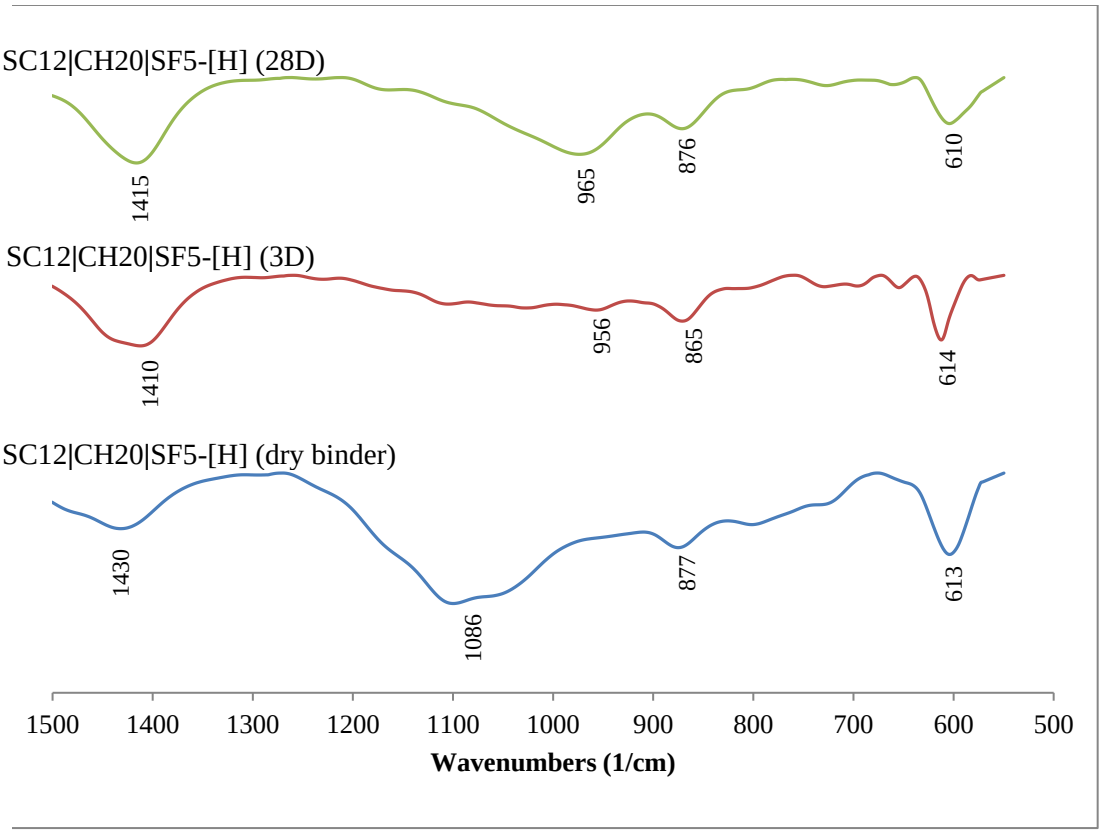

Figure 4-21: FTIR spectrum for SC12|CH20|SF5-[H] at different curing ages

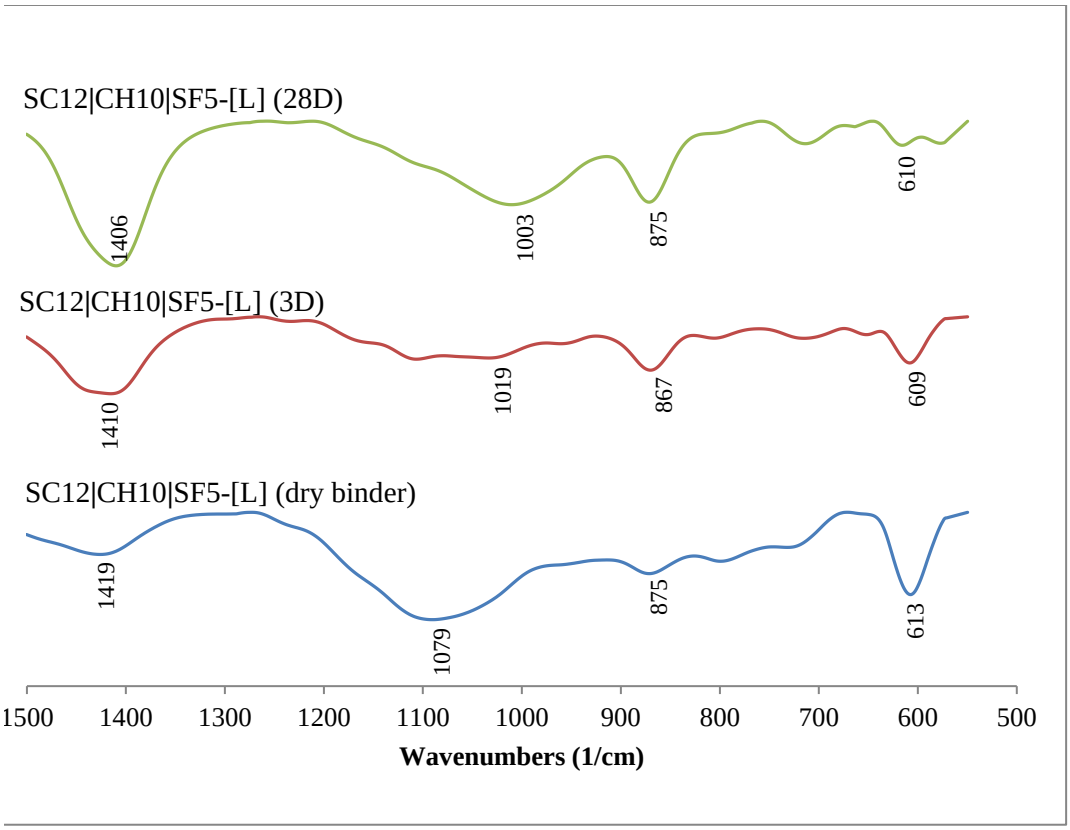

Figure 4-22: FTIR spectrum for SC12|CH10|SF5-[L] at different curing ages

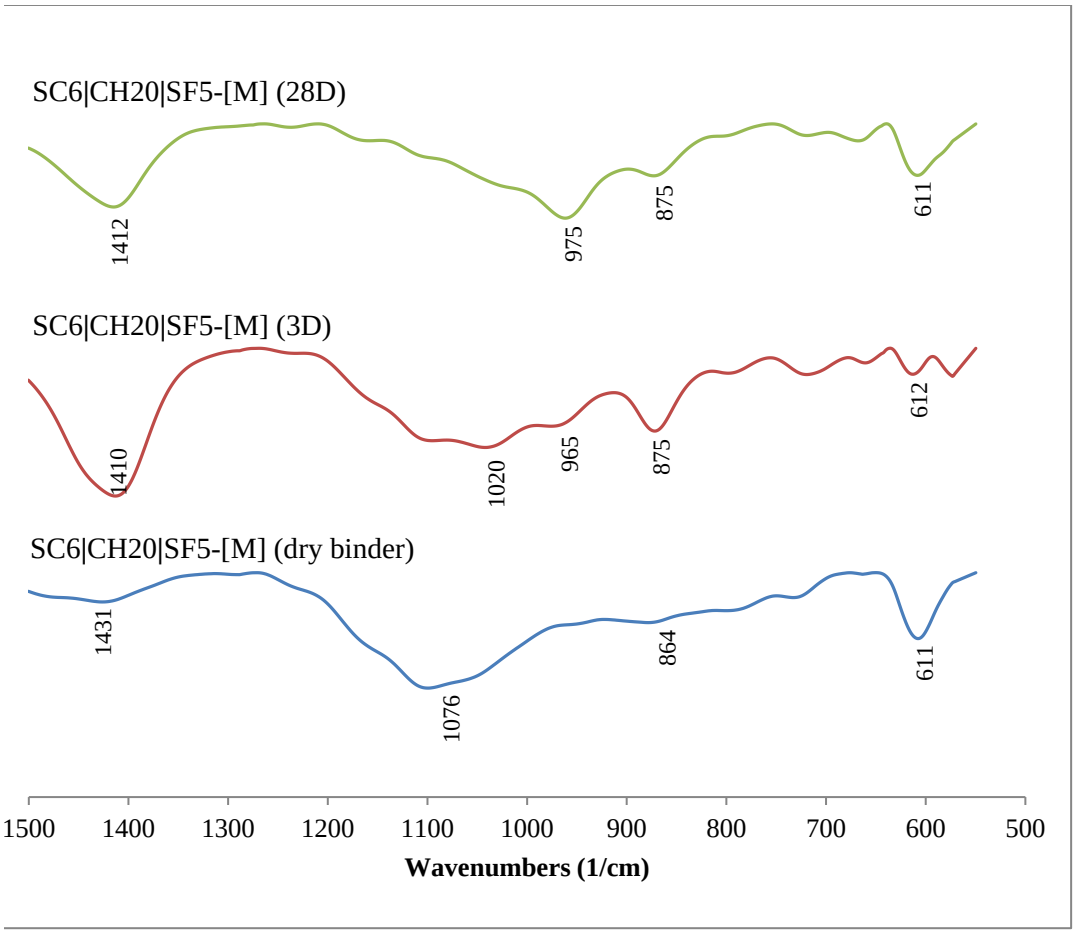

Figure 4-23: FTIR spectrum for SC6|CH20|SF5-[M] at different curing ages

There is a significant peak occurring in the region 1440 to 1410 cm^{-1} in all samples as well as a smaller peak around 880 to 865 cm^{-1} region. This can be associated with stretching vibrations of C=O or CO_3^{2-} anions, which confirms the formation of carbonate species (Peyne et al., 2017; Kumar et al., 2017; Lee et al., 2017; Abdel-Gawwad & Abo-El-Enein., 2014). The absorbance peaks at these two wavelengths indicate the formation of calcite and with increasing age, the intensity of the peaks increase.

Noticing the IR spectra of the raw blended mix for all samples, there is an absorbance band around 1080 cm^{-1} wavelength. This is attributed to asymmetric stretching vibration mode of Si-O-T (T = tetrahedral Si or Al) caused by the presence of FA in the blended mixture. For all investigated samples, this main band shifted to a lower wavelength with increasing age. This is known to be a common occurrence in FA based activated materials as it represents the extent of the reaction/formation of gels due to the effect of activators on the original material, fly ash (de Vargas et al., 2014; Jang and Lee, 2016; Siyal et al., 2016).

For SC12|CH20|SF5-[H] the main band in the blended mix appears at 1086 cm^{-1} and shifted to 954.7 cm^{-1} at 3 days and then to 965.4 cm^{-1} at 28 days (Figure 4-21). The initial shift to a lower frequency indicates the formation of Al-rich gel but the slight shift to a higher wavelength at a later stage indicates the transformation of the gel into a Si-rich gel. The shift to a lower wavelength is due to the reduced calcium content in the gel due to the incorporation of Al due to the dissolution of FA in the mixture. This shift imbues the material with beneficial mechanical properties (Jang and Lee, 2016; Criado et al., 2012; Abdalqader et al., 2015). Moreover, Garcia-Lodeiro et al. (2011) suggest that bands in the 950-970 cm^{-1} region represent CSH and CASH type gels whilst bands in the 1000 cm^{-1} represent NASH gels.

Therefore for SC12|CH20|SF5-[H], the reversal in band to a higher wavelength is noticed and is in the range of 950 to 970 cm^{-1} which implies it may have a C-A-S-H type gel. Similarly for SC6|CH20|SF5-[M], the main band appeared at 1076 cm^{-1} and moved to 965.6 cm^{-1} at 3 days and then to 975.2 cm^{-1} at 28 days (Figure 4-23). The final wavelength position for SC6|CH20|SF5-[M] is higher than that for SC12|CH20|SF5-[H] (965.4 vs. 975.2 cm^{-1}) which could be a possible reason for the higher strength gain in SC12|CH20|SF5-[H] than SC6|CH20|SF5-[M] at 28 days. The closer the wavelength is to 950 cm^{-1}, the gel gets most commonly attributed to CSH which gives better mechanical strength (Dakhane et al., 2017). This is evident in the higher amorphous nature of the microstructure as noticed in SEM/EDS analysis in Section 4.4.3.

For SC12|CH10|SF5-[L], the main band appeared at frequency 1079 cm^{-1} which shifted to 1019 cm^{-1} at 3 days but then moved to a lower 1003 cm^{-1} at 28 days (Figure 4-22). Therefore, this represents a possible NASH or N(C)ASH type gels which can contribute to its lower mechanical strength. It also implies the that polymerization reaction is still continuous and when it completes, the band should move towards a higher wavelength (Siyal et al., 2016). This is in good correlation with the EDS analysis from Section 4.4.3.

The series of small bands appearing around 790 cm^{-1} and 660 cm^{-1} can be attributed to symmetric stretching of O-Si-O bonds and the strong peaks appearing around 600 cm^{-1} can be associated with symmetric stretching of Al-O-Si bonds. This is related to the presence of quartz and mullite from the raw fly ash in the raw blended samples (Jang and Lee, 2016).

4.4.5 Thermal gravimetric analysis (TGA)

Figure 4-24 represents the TGA and DTG (Differential thermogravimetry) curves for SC12|CH20|SF5-[H], SC12|CH10|SF5-[L] and SC6|CH20|SF5-[M] at 28 days.

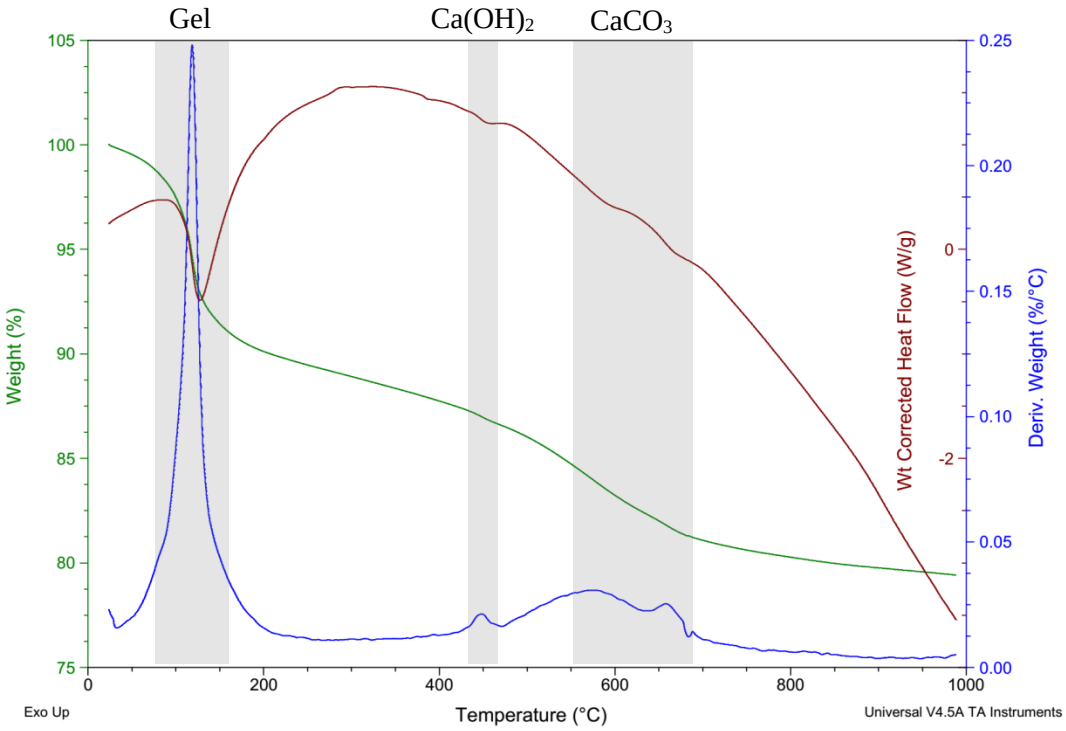

Figure 4-24a: TGA curve SC12|CH20|SF5-[H]

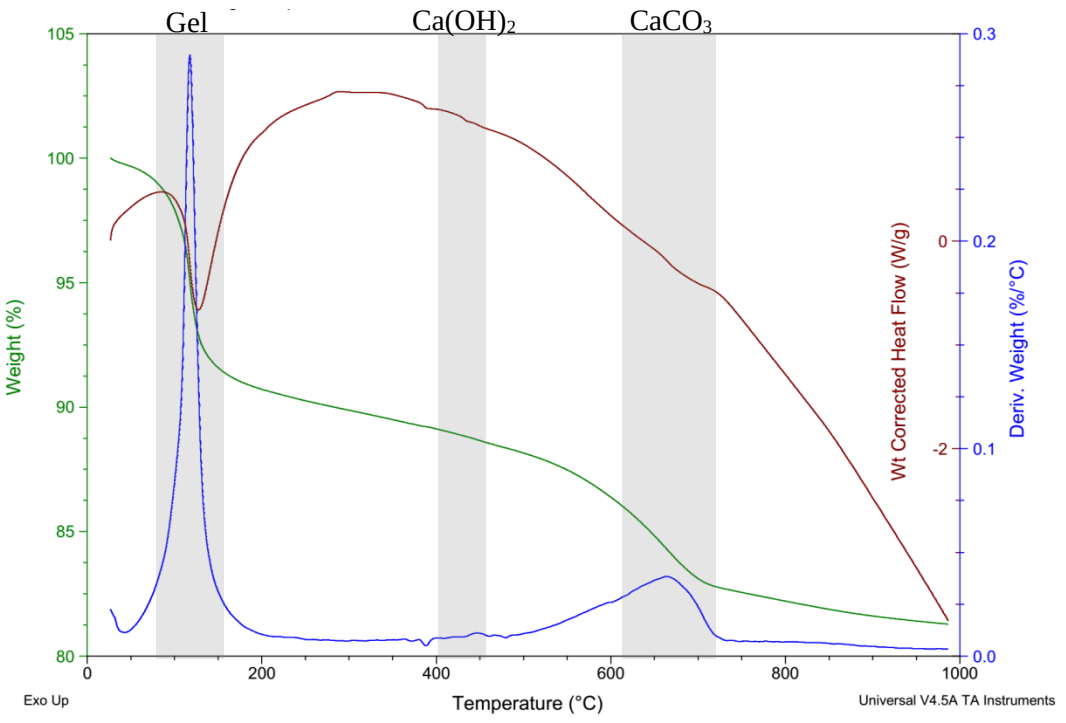

Figure 4-24b: TGA curve SC12|CH10|SF5-[L]

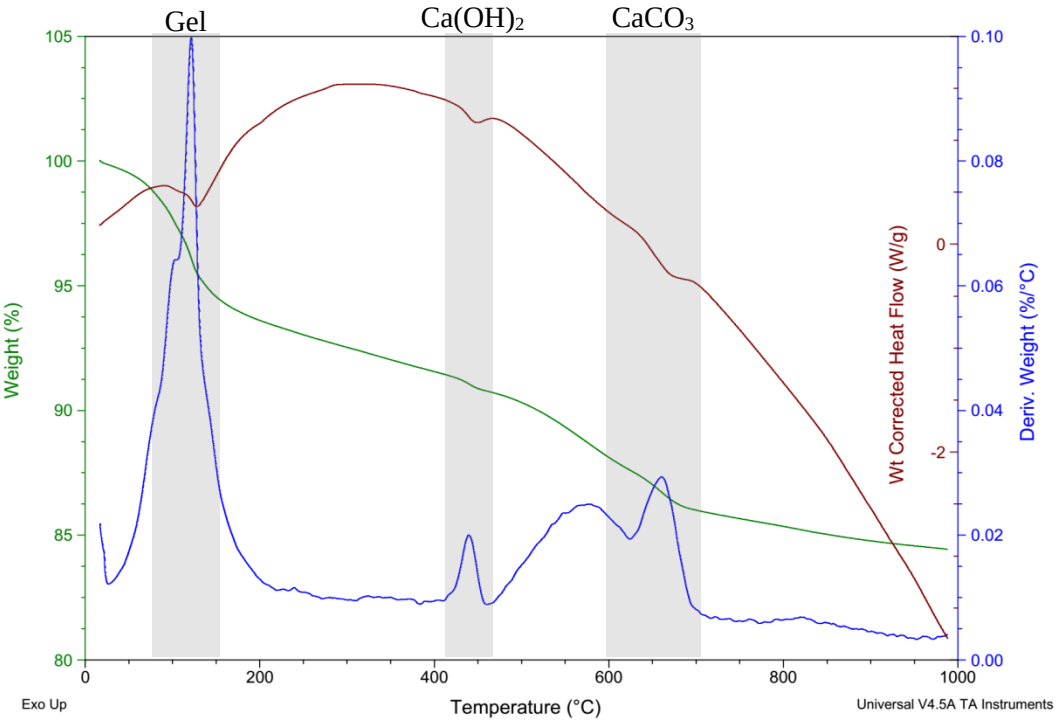

Figure 4-24c: TGA curve SC6|CH20|SF5-[M]

Figure 4-24: TGA curves for chosen samples at 28 days

Weight loss below 200 °C is related to evaporation of free water present in the matrix; the loss around 400 °C is due to the dehydration of $Ca(OH)_2$ and weight loss shown in the region of 600-750 °C is because of the decomposition of carbonate species such $CaCO_3$ (Kim et al., 2017).

In all samples the DTG shows a sharp peak between 75-150 °C in all samples. This can be related the dehydration of the physically bound water present within the pores of the binding gels, which can be CSH or C(A)SH gels. Furthermore, the total weight loss percentage of the sample can be related to the formation of amorphous gel content within the structure (Nedeljkovic et al., 2016; Abdel-Gawwad & Abo-El-Enein, 2014). This is due to the fact that there is a larger quantity of free water present in matrices containing a greater reaction gel. Figure 4-25 collates the weight loss TGA curve for all three samples. Observing the curves for SC12|CH20|SF5-[H] and SC12|CH10|SF5-[L], it can be seen that the weight loss for SC12|CH20|SF5-[H] is larger than SC12|CH10|SF5-[L] which explains the difference in strength observed. However, the mass loss for SC6|CH20|SF5-[M] is less than SC12|CH20|SF5-[H] and SC12|CH10|SF5-[L]. This should suggest that the gel formation in this mixture is low and should attain the lowest strength but it was not the case.

In the range around 400-450 °C, it is related to the decomposition of $Ca(OH)_2$. For SC12|CH20|SF5-[H] (Figure 4-24a) there is a small hump noticed on the DTG curve whereas for SC12|CH10|SF5-[L] (Figure 4-24b) there is no noticeable hump. For SC6|CH20|SF5-[M], the peak is more prominent showing there was a larger decomposition of $Ca(OH)_2$.

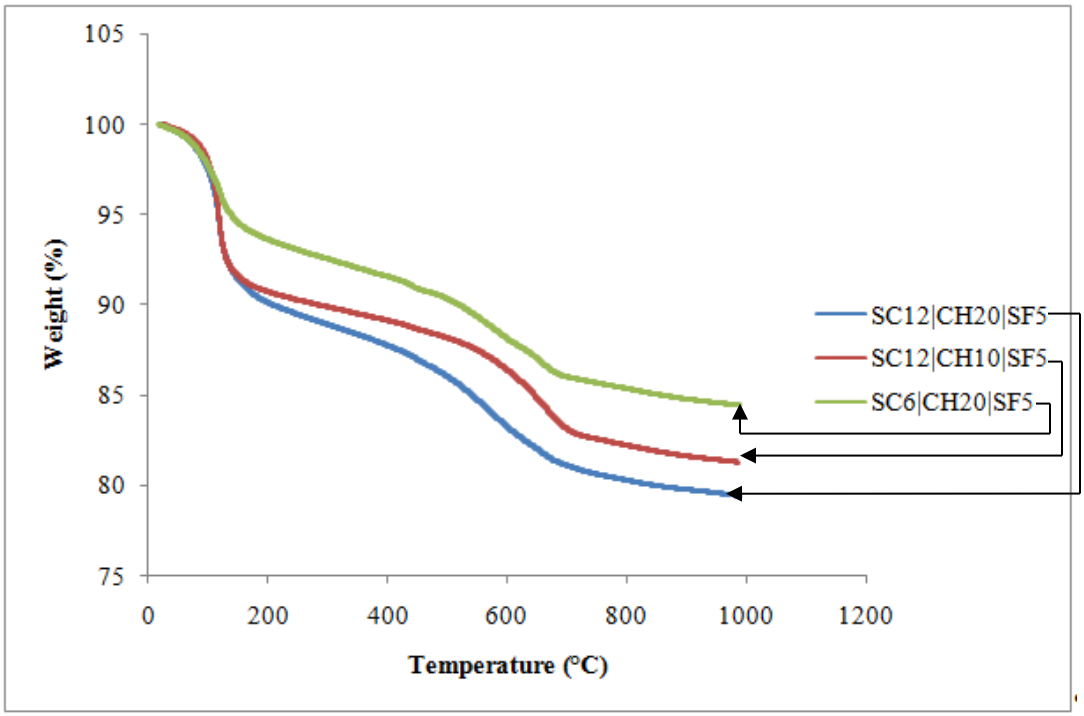

Figure 4-25: Weight loss TGA curves of all chosen samples at 28-day

The weight loss between 600-750 °C is caused by the presence of carbonated compounds like calcite, which was formed due to the reaction between $Ca(OH)_2$ and Na_2CO_3. There is a boarder hump noticed in SC12|CH20|SF5-[H] than SC12|CH10|SF5-[L]. A sharper hump is seen for SC6|CH20|SF5-[M]. This confirms the results from the XRD and FTIR analysis. From quantitative XRD, there is a greater formation of calcite in SC6|CH20|SF5-[M] than SC12|CH20|SF5-[H], and SC12|CH10|SF5-[L] showed no formation of calcite.

These observations can all be tied to the gaylussite reaction mentioned in section 4.4.2. In Section 4.4.2. Gaylussite forms due to the reaction of Ca^{2+} with CO_3^{2-} which releases hydroxide ions that aid in increasing the pH of the system and facilitate activation. It was also mentioned gaylussite is a transient phase that will form to carbonate species at later stage. Thus, it can be deduced that there is an early reaction with lower Na_2CO_3 content, which causes a lower quantity of gel formation but an

earlier reaction phase and could be the cause of the high strength at early age as was the case with SC6|CH20|SF5-[M]. It did not gain the highest strength at 28 days as the lower quantity of SC meant a smaller pH increasing effect. The $Ca(OH)_2$ hump noticed can attributed to leftover amount for the reaction phase. This observation was the opposite for sample SC12|CH20|SF5-[H]. Higher SC content meant larger pH effect and hence more activation potential. The drawback being the lower early age strength as the CO_3^{2-} needs to be exhausted before activation reactions occur (Bernal et al., 2014). The difference in the range of calcite humps noticed in the DTG curves gives a good indication of the extent of gaylussite reactions occurring and also explaining the difference in the strength of the samples. Whether the formation of calcite itself affects the strength is an area requiring further investigation since it is suggested that it can have a pore-refining effect.

5 CONCLUSIONS AND RECOMMENDATIONS

This study focused on testing dry binder blends of fly ash, silica fume, sodium carbonate and calcium hydroxide to obtain an insight into the possibility of producing feasible fly ash based alkali-activated materials (cements) that can attain sufficient strength when cured under ambient conditions. The following conclusions can be drawn from this study:

- It is possible to produce FA|SF|CH|SC blends with compressive strength up to 44.2 MPa at 28 days.
- Sodium carbonate and calcium hydroxide were the main factors that positively affected the 28-day mechanical strength of the fly ash based alkali-activated cements with increasing content. However, sodium carbonate negatively affected the early age strength (3-day) with increasing content whereas calcium hydroxide had little to no effect.
- Silica fume had a small to neutral effect on the system.
- From the characterisation techniques, the mechanism noticed is the formation of gaylussite due to the reaction of Ca^{2+} with CO_3^{2-} for all samples. This releases hydroxide ions which aid in increasing the pH of the system and facilitate activation. Furthermore, this reaction can also explain the consumption of portlandite, which is calcium hydroxide from binder composition, with increasing age as seen in the XRD diffractograms.
- Activation reactions proceeds once the CO_3^{2-} have been exhausted in the system. Hence samples that gained high strength at 3 days but did not undergo much reaction afterward was because of early reaction due to the lower SC content. This causes a lower quantity of gel formation but an earlier reaction phase. Therefore, the gaylussite had a longer time to transform to its stable carbonate species, such as calcite, which enabled the mixes to gain better strength as seen by the characterization techniques.

Different local South African fly ash needs to be tested for alkali-activated materials. Comparing fly ash from different sources can help with the wide application of AAM.

A detailed statistical analysis with response surface methodology to better understand the dynamics of the system and inform on the effects of each component on the strength better.

Durability studies should be conducted on the developed fly ash-based alkali-activated materials. Measuring strength gain at later dates as well as its performance under corrosive environments can provide a better understanding the system's dynamics.

As the fly ash based AAM can be intermixed and stored, mechanical tests should be done after the material has been in storage for some time and compared to the samples that is cast directly after the materials are mixed together.

As microcracks were present in FA|SF|CH|SC system, possibly due to the use of SF, shrinkage behaviour should be considered. Early age shrinkage can affect the mechanical performance of the material and should be quantified in order to reduce its effects.

A detailed inspection on the carbon emission of fly ash based AAM should be conducted to study its ecological impact and justify its usage compared to OPC and other AAM blends.

In conclusion, this system of FA|SF|CH|SC proposes a possibility of creating sustainable alkali-activated materials that gains notable strength under ambient conditions. It also uses low impact activators that are cheaper; easier to handle and less environmentally impactful than sodium hydroxide and sodium silicate which are commonly used to produce fly ash based AAM . Moreover, the activators used in this study are not hygroscopic in nature allowing for intermixing and storage in bags just like ordinary Portland cement.

With further investigation and proper standards setup, this type of system can prove to be a welcoming alternative to OPC and drive its acceptance within the cement industry.

6 REFERENCES

Abdalqader, A.F. Jin, F. & Al-Tabbaa, A. 2016, 'Development of greener alkali-activated cement: utilisation of sodium carbonate for activating slag and fly ash mixtures', *Journal of Cleaner Production*, vol 113, pp. 66-75.

Abdalqader, A.F. Jin, F. & Al-Tabbaa, A. 2015, 'Characterisation of reactive magnesia and sodium carbonate-activated fly/slag paste blends', *Construction and Building Materials*, vol 93, pp. 506-513.

Abdel-Gawwad, H.A. & Abo-El-Enein, S.A. 2016, 'A novel method to produce dry geopolymer cement powder', *HBRC Journal*, vol 12, pp. 13-24.

Aboulayt, A. Riahi, M. Touhami, M.O. Hannache, H. Gomina, M. &Moussa, R. 2017, 'Properties of metakaolin based geopolymer incorporating calcium carbonate', vol 28, pp. 2393-2401.

Ali, M.B. Saidur, R.& Hossain, M.S. 2011, 'A review on emission analysis in cement industries', *Renewable and Sustainable Energy Reviews*, no. 15, pp. 2252-2261.

Altan, E, & Erdogan S.T. 2012, 'Alkali-activation of slag at ambient and elevated temperatures', *Cement and Concrete Composites*, vol 34, no. 2, pp. 131-139.

Aydin, S. 2013, 'A ternary optimisation of mineral additives of alkali activated cement mortars', *Construction and Building Materials*, no. 43, pp. 131-138.

Bakharev, T. Sanjayan, J.G.& Cheng, Y-B. 1999, 'Effect of elevated temperature curing on properties of alkali-activated slag concrete', *Cement and Concrete Research*, vol 29, no. 10, pp. 1619-1625.

Benhelal, E. Zahedi, G. Shamsaei, E.& Bahadori, A. 2013, 'Global strategies and potentials to curb CO_2 emissions in cement industry', *Journal of Cleaner Production*, no. 51, pp. 142-161.

Bernal, S.A. de Gutiérreza, R.M. Pedraza, A.L. Provis, J.L. Rodriguez, E.D.& Delvasto, S. 2011, 'Effect of binder content on the performance of alkali-activated slag concretes', *Cement and Concrete Research*, vol 41, no. 1, pp. 1-8.

Bernal, S.A. Provis, J.L. Myersm R.J. San Nicolas, R. & van Deventer, S.J.S. 2015, 'Role of carbonates in the chemical evolution of sodium carbonate-activated slag binders', *Materials and Structures*, vol 48, no. 2, pp. 517-529.

Chi, M. 2012, 'Effects of dosage of alkali-activated solution and curing conditions on the properties and durability of alkali-activated slag concrete', *Construction and Building Materials*, no. 37, pp. 240-245.

Chi, M.& Huang, R 2013, 'Binding mechanism and properties of alkali-activated fly ash/slag mortars', *Construction and Building Materials*, vol 40, pp. 291-298.

Criado, M. *Fernández-Jiménez, A. Sobrados, I. Palomo, A. & Sanz, J. 2012, 'Effect of relative humidity on the reaction products of alkali activated fly ash', Journal of the European Ceramic Society, vol 32, no. 11, pp. 2799-2807*

Dakhane, A. Tweedley, S. Kailas, S. Marzke, R. & Neithalath, N. 2017, 'Mechanical and microstructural characterization of alkali sulfate activated high volume fly ash binder', *Materials and Design*, vol 122, pp. 236-246.

Das, S.K. Mohapatra, A.K.& Rath, A.K. 2014, 'Geo-polymer Concrete–Green Concrete for the Future—A Review', *International Journal of Civil Engineering Research*, vol 5, no. 1, pp. 21-28.

De Silva, P. Sagoe-Crenstil, K.& Sirivivatnanon, V. 2007, 'Kinetics of geopolymerization: Role of Al_2O_3 and SiO_2', *Cement and Concrete Research*, vol 37, no. 4, pp. 512-518.

Deb, P.S. Nath, P.& Sarker, P.K. 2014, 'The effects of ground granulated blast-furnace slag blending with fly ash and activator content on the workability and strength properties of geopolymer concrete cured at ambient temperature', *Materials and Design*, no. 62, pp. 32-39.

van Deventer, J.S.J. Provis, J.L.& Duxson, P. 2012, 'Technical and commercial progress in the adoption of geopolymer cement', *Minerals Engineering*, no. 29, pp. 89-104.

Doughlas, E. & Brandstetr, J. 1990, 'A preliminary study on the alkali activation of ground granulated blast furnace slag', *Cement and Concrete Research*, vol 20, pp. 746-756.

Dutta, D. Thokchom, S. Ghosh, P.& Ghosh, S. 2010, 'Effect of silica fume additions on the porosity of fly ash geopolymers', *ARPN Journal of Engineering and Applied Sciences*, vol 5, no. 10, pp. 74-79.

Duxson, P. Provis, J.L. Lukey G.C. Mallicoat S.W. Kriven W.M. & van Deventer J.S.J. 2005, 'Understanding the relationship between geopolymer composition, microstructure and mechanical properties', *Colloids and Surfaces A: Physicochemical and Engineering Aspects*, vol 269, pp. 47-58.

Duxson, P. Fernandez-Jimenez, A. Provis, J.L Lukey, G.C. Palomo, A. & van Deventer, J.S.J., 2007, 'Geopolymer technology: the current state of the art', *J. Mater. Sci.*, Vol 42, pp. 2917-2933

Erdem, T.K.& Kırcab, Ö. 2008, 'Use of binary and ternary blends in high strength concrete', *Construction and Building Materials*, vol 22, no. 7, pp. 1477-1483.

Eskom 2017, *Eskom Integrated Report 2017* viewed 10 August 2018, <http://www.eskom.co.za/IR2017/Documents/Eskom_integrated_report_2017.pdf >.

Fernández-Jiménez, A. Palomo, J.G & Puertas, F. 1999, 'Alkali-activated slag mortars mechanical strength behaviour', *Cement and Concrete Research*, vol 29, pp. 1313-1321.

Fraay, A.L.A and Bejen, J.M. 1989, 'The reaction of fly ash in concrete: A critical examination,' *Cement and Concrete Research*, no. 19, pp. 235-246.

Gao, K. Lin, K-L. Wang, D. Hwang, C-L. Shiu, H-S. Chang, Y-M.& Cheng, T-W. 2014, 'Effects SiO_2/Na_2O molar ratio on mechanical properties and the microstructure of nano-SiO_2 metakaolin-based geopolymers', *Construction and Building Materials*, vol 53, no. 28, p. 2014.

Gao, T. Shen, L. Shen, M. Chen, F. Liu, L.& Gao, L. 2014, 'Analysis on differences of carbon dioxide emission from cement production and their major determinants', *Journal of Cleaner Production*, pp. 1-11.

Gao, X. Yu, Q.L.& Brouwers, H.J.H. 2015, 'Reaction kinetics, gel character and strength of ambient temperature cured alkali activated slag–fly ash blends', *Construction and Building Materials*, vol 80, pp. 105-115.

Garcia-Lodeiro, I. Palomo, A. *Fernández-Jiménez, A. & Macphee, D.E. 2011, 'Compatibility studies between N-A-S-H and C-A-S-H gels. Study in the ternary diagram Na_2O-CaO-Al_2O_3-SiO2-H_2O', Cement and Concrete Research, vol 41, pp. 923-931.*

Gibbs, M.J. Soyka, P.& Connely, D. 2000, 'CO_2 emissions from cement production', *Good Practice Guidance and Uncertainty Management in National Greenhouse Gas Inventories* , pp. 175-182.

Habert, G. d'Espinose de Lacaillerie, J.B.& Roussel, N. 2011, 'An environmental evaluation of geopolymer based concrete production: reviewing current research trends', *Journal of Cleaner Production*, no. 19, pp. 1229-1238.

Huang, S. & Cheng, J. 1986, 'Kinetic of reaction in the system of fly ash-$Ca(OH)_2$-H_2O,' *The Journal of Chinese Ceramic Society*, vol 14, no. 1, pp. 191-197.

IEA & WBSCD 2009, *Cement Technology roadmap 2009: Carbon emissions reductions up to 2050*, viewed 08 January 2015, <http://www.wbcsdcement.org/pdf/technology/WBCSD-IEA_Cement%20Roadmap.pdf>.

IPCC n.d., *EFDB*, viewed 16 May 2015, <http://www.ipcc-nggip.iges.or.jp/EFDB/main.php>.

Ismail, I. Bernal, S.A. Provis, J.L. Hamdan, S.& van Deventer, J.S.J. 2013, 'Drying-induced changes in the structure of alkali-activated pastes', *Journal of Materials Science*, vol 48, no. 9, pp. 3566-3577.

Ismail, I. Bernal, S.A. Provis, J.L. Nicolas, R.S. Brice, D.G. Kilcullen, A.R. Hamdan, S.& van Deventer, J.S.J. 2013, 'Influence of fly ash on the water and chloride permeability of alkali-activated slag mortars and concretes', *Construction and Building Materials*, vol 48, pp. 1187-1201.

Jang, J.G. Lee, N.K.& Lee, H.K. 2014, 'Fresh and hardened properties of alkali-activated fly ash/slag pastes with superplasticizers', *Constrution and Building Materials*, vol 50, pp. 169-176.

Jang, J.G. & Lee, H.K. 2016, 'Effect of fly ash characteristics on delayed high-strength development of geopolymers', *Construction and Building Materials*, vol 102, pp. 260-269.

Jambhulkar, H.P.Shaikh, S.M.S. & Kumar, S.M. 2018, 'Fly ash toxicity, emerging issues and possible implications for its exploitation in agriculture; Indian scenario: A review',*Chemosphere*, vol. 213, pp. 333-344.

Jeon, D. Jun, Y. Jeong, Y. & Oh J.E. 2015, 'Microstructural and strength improvements through the use of Na_2CO_3 in a cementless $Ca(OH)_2$-activated Class F fly ash system', *Cement and Concrete Research*, vol 67, pp. 215-225.

Jin, F.&Al-Tabbaa, A. 2015, 'Strength and drying shrinkage of slag paste activated by sodium carbonate and reactive MgO',*Construction and Building Materials*, vol. 81, pp. 58-65.

Kani, E.N. Allahverdi, A. & Provis, J.L. 2012, 'Efflorescence control in geopolymer binders based on natural pozzolan', *Cement and Concrete Composites*, vol 34, pp. 25-33.

Ke, X. Bernal S.A. & Provis, J.L. 2016, 'Controlling the reaction kinetics of sodium carbonate-activated slag cements using calcined layered double hydroxides', *Cement and Concrete Research*, vol 81, pp. 24-37.

Khale, D.& Chaudhary, R. 2007, 'Mechanism of geopolymerization and factors influencing its development: a review', *J Mater Sci*, no. 42, pp. 729-746.

Khater, H.M. 2013, 'Effect of silica fume on the characterization of the geopolymer materials', *International Journal of Advanced Structural Engineering*, vol 5, no. 12.

Kim, E.H. 2012, 'Understanding effects of silicon/aluminum ratio and calcium hydroxide on chemical composition, nanostructure and compressive strength for metakaolin geopolymers', Thesis, University of Illinois at Urbana-Champaign, Illinois.

Kirca, O. Yaman, I.O. & Tokyay, M. 2012, 'Compressive strength development of calcium aluminate cement-GGBFS blends', *Cement and Concrete Composites*, vol 35, no. 1, pp. 163-170.

Komljenović, M.Baščarević, Z.&Bradić, V. 2010, 'Mechanical and microstructural properties of alkali-activated fly ash geopolymer', *Journal of Hazardous Materials*, vol 181, no. 1-3, pp. 35-42.

Kovtun, M. Kearsley, E. & Shevkovtsova, J. 2013, 'Producing alkali-activated slag concrete in South Africa', *UKIERI Concrete Congress - Innovations in Concrete Construction*, University of Pretoria, South Africa, pp. 919-928.

Kumar, S. Mucsi, G Kristaly, F. & Pekker, P. 2017, 'Mechanical activation of fly ash and its influence on mixro and nano-structural behaviour of resulting geopolymers', *Advanced Powder Technology*, vol 28, pp. 805-813.

Lee, N.K.& Lee, H.K. 2013, 'Setting and mechanical properties of alkali-activated fly ash/slag concrete manufactured at room temperature', *Construction and Building Materials*, vol 47, pp. 1201-1209.

Lee, W.K.W. & Van Deventer, J.S.J. 2002, 'The effects of inorganic salt contamination on the strength and durability of geopolymers', *Colloids and Surfaces A: Physiochemical and Engineering Aspects*, vol 211, no. 2-3, pp. 115-126.

Lee, N.K. Koh, K.T. Kim, M.O. An, G.H. & Ryu, G.S. 2017, 'Physicochemical changes caused by reactive MgO in alkali-activated fly ash/slag blends under accelerated carbonation', *Ceramics International*, vol 43, pp. 12490-12496.

Lee, B. Kim, G. Kim, R. Chom B. Lee, S. & Chon, C.M. 2017, 'Strength development properties of geopolymer paste and mortar with respect to amorphous Si/Al ratio of fly ash', *Construction and Building Materials*, vol 151, pp. 512-519.

Li, C. Sun, H.& Li, L. 2010, 'A review: The comparison between alkali-activated slag (Si+Ca) and metakaolin (Si+Al) cements', *Cement and Concrete Research*, no. 40, pp. 1341-1349.

Li, D. Chen, Y. Shen, J. Su, J. & Wu, X. 2000, 'The influence of alkalinity on activation and microstructure of fly ash', *Cement and Concrete Research*, vol 30, pp. 881-886.

Li, Y. & Sun, Y. 2000, 'Preliminary study on combined-alkali-slag paste materials', *Cement and Concrete Research*¸ vol 30, pp. 963-966.

Madlool, N.A. Saidur, R. Hossain, M.S.& Rahim, N.A. 2011, 'A critical review on energy use and savings in the cement industries', *Renewable and Sustainable Energy Reviews*, no. 15, pp. 2042-2060.

Marjanović, N. Komljenović, M. Baščarević, Z. Nikolić, V.& Petrović, R. 2015, 'Physical–mechanical and microstructural properties of alkali-activated fly ash–blast furnace slag blends', *Ceramics International*, vol 41, no. 1, pp. 1421-1435.

Martin, K.G. 2014, *Actually, you can interpret some main effects in the presence of an interaction*, viewed 13 May 2015, <http://www.theanalysisfactor.com/interpret-main-effects-interaction/>.

MathWorks, 2019. *Response Surface Designs - MATLAB*, 17 September 2019, <https://www.mathworks.com/help/stats/response-surface-designs.html>

Mclellan, B.C. Williams, P.R. Lay, J. van Riessen, A.& Corder, G.D. 2011, 'Costs and carbon emissions for geopolymer pastes in comparison to ordinary portland cement', *Journal of Cleaner Production*, no. 19, pp. 1080-1090.

Montgomery, D.C. 2011. *Applied Statistics and Probability for Engineers*. 5th Edition. John Wiley & Sons, Asia.

Mustafa Al Bakri, A.M. Kamarudin, H. Bin Hussain, M. Khairul Nazir, I. Zarina, Y.& Rafiza, A.R. 2011, 'The Effect of Curing Temperature on Physical and Chemical Properties of Geopolymers', *Physics Procedia*, no. 22, pp. 286-291.

Mustafa Al Bakri, A.M. Kamarudin, H. Bnhussain, M. Khairul Nizar, I. Rafiza, A.R.& Izzat, A.M. 2011, 'Chemical Reactions in the Geopolymerisation Process Using Fly Ash–Based Geopolymer: A Review', *Australian Journal of Basic and Applied Sciences*, vol 5, no. 7, pp. 1199-1203.

Nath, S.K. & Kumar, S. 2013, ' Influence of iron making slags on strength and microstructure of fly ash geopolymer', *Construction and Building Materials*, vol 38, pp. 924-930.

Nath, P.& Sarker, P.K. 2014, 'Effect of GGBFS on setting, workability and early strength properties of fly ash geopolymer concrete cured in ambient condition', *Construction and Building Materials*, no. 66, pp. 163-171.

Nath, P.& Sarker, P.K. 2015, 'Use of OPC to improve setting and early strength properties of low calcium fly ash geopolymer concrete cured at room temperature', *Cement and Concrete Composites*, vol 55, pp. 205-214.

Nedeljokovic, M. Arbi, K. Zuo, Y. & Ye, G. 2016, 'Microstructural and Mineralogical Analysis of Alkali Activated Fly Ash-Slag Pastes', *3rd International RILEM Conference on Microstructure Related Durability of Cementitious, pp. 1-10.*

NPC. 2012, *Executive summary-National Development Plan 2030 - Our future - Make it work,* viewed 30 October 2017, < https://www.gov.za/sites/default/files/Executive%20Summary-NDP%202030%20-%20Our%20future%20-%20make%20it%20work.pdf>

Nuruddin, M.F. Qazi, S. Shafiq, N.& Kusbiantoro, A. 2010, 'Compressive strength & microstructure of polymeric concrete incorporating fly ash & silica fume', *Canadian Journal on Civil Engineering*, vol 1, no. 1.

Okoye, F. Durgaprasad, J. and Singh, N. 2016, 'Effect of silica fume on the mechanical properties of fly ash based-geopolymer concrete',*Ceramics International*, vol 42, no.2, pp.3000-3006.

Okoye, F.N. Prakash, S. & Singh, N.B. 2017, 'Durability of fly ash based geopolymer concrete in the presence of silica fume', Journal of Cleaner Production, vol 149, pp. 1062-1067.

Olivia, M.& Nikraz, H. 2012, 'Properties of geopolymer concrete designed by Taguchi method', *Materials and Design*, no. 36, pp. 191-198.

Pacheco-Torgal, F.Castro-Gomes, J. & Jalali, S. 2008. Alkali-activated binders: A review. Part 2. About materials and binders manufacture. *Construction and Building Materials*, vol 22, no.7, pp. 1315-1322.

Pacheco-Torgal, F. Castro-Gomes, J. & Jalali, S. (2008). Alkali-activated binders: A review. *Construction and Building Materials*, vol 22, no.7, pp.1305-1314.

Palomo, A. Grutzeck, M.W.& Blanco, M.T. 1999, 'Alkali-activated fly ashes: A cement for the future', *Cement and Concrete Research*, no. 29, pp. 1323-1329.

Panias, D. Giannopoulou, I.P.& Perraki, T. 2007, 'Effect of synthesis parameters on the mechanical properties of fly ash-based geopolymers', *Colloids and Surfaces A: Physicochem. Eng. Aspects*, no. 301, pp. 246-254.

Part, W.K. Ramli, M. & Cheah, C.B. 2015, 'An overview on the influence of various factors on the properties of geopolymer concrete derived from industrial by-products', *Construction and Building Materials*, vol 77, pp. 370-395

Peyne, J. Gautron, J. Doudeau, J. Joussein, E. & Rossignol, S. 2017, 'Influence of calcium addition on calcined brick clay based geopolymers: A thermal and FTIR spectroscopy study', *Construction and Building Materials*, vol 152, pp. 794-803.

Poon, C.S. Kou, S.C. Lam, L. & Lin, Z.S. 2001, 'Activation of fly ash/cement using calcium sulfate anhydrite', *Cement and Concrete Research*, col 31, no. 6, pp. 873-881.

PPC 2017, *PPC Integrated Report 2017*, viewed 15 August 2017, <http://www.ppc-reports.co.za/iar-2017/pdf/full.pdf>.

Provis, J.L.& Bernal, S.A. 2014, 'Geopolymers and Related Alkali-Activated Materials', *Annual Reviews*.

Puligilla, S.& Mondal, P. 2013, 'Role of slag in microstructural development and hardening of fly ash-slag geopolymer', *Cement and Concrete Research*, vol 43, pp. 70-80.

Rangan, V. 2010, 'Fly Ash-Based Geopolymer Concrete', *Proceedings of the International Workshop on Geopolymer Cement and Concrete*, pp. 68-106.

Rashad, A.M. 2013, 'A comprehensive overview about the influence of different additives on the properties of alkali-activated slag – A guide for Civil Engineer', *Construction and Building Materials*, no. 47, pp. 29-55.

Rashad, A.M.Bai, Y. Basheer B.A.M. Milestone, N.B. & Collier N.C. 2013, 'Hydration and properties of sodium sulfate activated slag', *Cement and Concrete Composites*, vol 37, pp. 20-29.

Rashad, A.M. 2014, 'A comprehensive overview about the influence of different admixtures and additives on the properties of alkali-activated fly ash', *Materials and Design*, no. 53, pp. 1005-1025.

Rashad, A.M.& Khalil, M.H. 2013, 'A preliminary study of alkali-activated slag blended with silica fume under the effect of thermal loads and thermal shock cycles', *Construction and Building Materials*, vol 40, pp. 522-532.

Rattanasak, U. Chindaprasirt, P. & Suwanvitaya, P. 2010, 'Development of high volume rice husk ash alumino silicate composites', *International Journal of Minerals, Metallurgy and Materials*, vol 17, no. 5, pp. 654-659.

Ravikumar, D. Peethamparan, S.& Neithalath, N. 2010, 'Structure and strength of NaOH activated concretes containing fly ash or GGBFS as the sole binder', *Cement and Concrete Composites*, vol 32, no. 6, pp. 399-410.

Reig, L. Soriano, L. Borrachero, M.V. Monzo J. & Paya J. 2016, 'Influence of calcium aluminate cement (CAC) on alkaline activation of red clay brick waste (RCBW),' *Cement and Concrete Composites*, vol 65, pp. 177-185

Reig, L. Sanz, M.A. Borrachero, M.V. Monzo, J. Soriano, L. & Paya, J. 2017, 'Compressive strength and microstructure of alkali-activated mortars with high ceramic waste content', *Ceramics International*, vol 43, pp. 13622-13634.

Reinard, J.C. 2006, 'Factorial Analysis of Variance', in *Communication Research Statistics*, SAGE Publications.

Roy, D.M. 1999, 'Alkali-activated cements: Opportunities and challenges', *Cement and Concrete Research*, no. 29, pp. 249-254.

Ryu, G.S. Lee, Y.B. Koh, K.T.& Chung, Y.S. 2013, 'The mechanical properties of fly ash-based geopolymer concrete with alkaline activators', *Construction and Building Materials*, vol 47, pp. 409-418.

Ryu, G.S. Lee, Y.B. Koh, K.T.& Chung, Y.S. 2013, 'The mechanical properties of fly ash-based geopolymer concrete with alkaline activators', *Construction and Building Materials*, no. 47, pp. 409-418.

Sayed, M.& Zeedan, S.R. 2012, 'Green binding material using alkali activated blast furnace slag with silica fume', *HBRC Journal*, vol 8, no. 3, pp. 177-184.

Sato, T. & Beaudoin, J.J. 2011, 'Effect of nano-$CaCO_3$ on hydration of cement containing supplementary cementitious materials', *Advances in Cement Research*, no. 23, pp. 33-43.

Shekhovtsova, J. Kovtun, M.& Kearsley, E. 2014, 'Effect of activator dosage, water-to-binder-solids ratio, temperature and duration of elevated temperaturecuring on the compressive strength of alkali-activated fly ash cement pastes', *Journal of the South African Institution of Civil Engineering*, vol 56, no. 3, pp. 44-52.

Shi, C. & Day, R.L. 2000, 'Pozzolanic reaction in the presence of chemical activators: Part I. reaction kinetics', *Cement and Concrete Research*, vol 30, no. 1, pp. 51-58.

Shi, C. & Day, R.L. 2000, 'Pozzolanic reaction in the presence of chemical activators: Part II. reaction products and mechanism', *Cement and Concrete Research*, vol 30, pp. 607-613.

Silva, S.V.A. Arachchi, J.N.J.K. Wijewardena, C.L.& Nanayakkara, S.M.A. 2013. '*Development of Fly Ash Based Geopolymer Concrete*', Experimental investigation, Department of Civil Engineering, University of Moratuwa.

Silva, P.D. Sagoe-Crenstil, K. and Sirivivatnanon, V. 2007, 'Kinetics of geopolymerization: role of Al_2O_3 and SiO_2', *Cement Concrete Research*, vol 37, no. 4, pp. 512-518.

Siyal, A.A. Azizli, K.A. Main, Z. Ismail, L. & Khan, M.I. 2016, 'Geopolymerization kinetics of fly ash based geopolymers using JMAK model', *Ceramics International*, vol 42, pp. 15575-15584.

Songpiriyakij, S. Pulngern, T. Pungpremtrakul, P.& Jaturapitakkul, C. 2011, 'Anchorage of steel bars in concrete by geopolymer paste', *Materials and Design*, vol 32, no. 5, pp. 3021-3028.

Stevens, J.J. 2000, *Interactions Effects in Regression*, viewed 13 May 2015, <http://pages.uoregon.edu/stevensj/interaction.pdf>.

Torgal, F.P. Gomes, J.C.& Jalali, S. 2008, 'Alkali-activated binders: A review Part 1. Historical background, terminology, reaction mechanisms and hydration products', *Construction and Building Materials*, no. 22, pp. 1305-1314.

Turner, L.K.& Collins, F.G. 2013, 'Carbon dioxide equivalent (CO_2-e) emissions: A comparison between geopolymer and OPC cement concrete', *Construction and Building Materials*, no. 43, pp. 125-130.

U.S. Geological Survey. 2017, 'Mineral Commodity Summaries 2017: Soda Ash', < https://doi.org/10.3133/70180197>

Vadapalli, V.R.K. Klink M.J. & Etchebers, O. 2008, 'Neutralization of acid mine drainage using fly ash, and strength development of the resulting solid residues', *Chemical Engineering Journal*, vol. 104, pp. 317-322

Vafaei, M. & Allahverdi, A. 2016, 'Influence of calcium aluminate cement on geopolymerization of natural pozzolan', *Construction and Building Materials*, vol 114, pp. 290-296.

de Vargas, A.S. Molin, D.C.C.D. Maseuro, A.B. Vilela, A.C.F. Castro-Gomes, J. & de Gutierrez, R.M. 2014, 'Strength development of alkali-activated fly ash produced with combined NaOH and $Ca(OH)_2$ activators', *Cement and Concrete Composites*, vol 53, pp. 341-349.

Wang, S-D. Pu, X-C. Scrivener, K.L.& Pratt, P.L. 1995, 'Alkali-activated slag cement and concrete: a review of properties and problems', *Advances in cement research*, vol 7, no. 27, pp. 93-102.

Wang, S-D. Scrivener, K.L.& Pratt, P.L. 1994, 'Factors affecting the strength of alkali-activated slag', *Cement and Concrete Research*, vol 24, no. 6, pp. 1033-1043.

Wang G.C. 2016. '*The Utilization of Slag in Civil Infrastructure Construction*'. Woodhead Publishing.

Wardhono, A. Gunasekara, C. Law, D.W. & Setunge, S. 2017, 'Comparison of long term performance between alkali activated slag and fly ash geopolymer concretes', *Construction and Building Materials*, vol 143, pp. 272-279

Walkley, B. Nicolas, R.S. Sani, M.A. Rees, G.J. Hanna J.V. van Deventer J.S.J. & Provis J.L. 2016, 'Phase evolution of C-(N)-A-S-H/N-A-S-H gel blends investigated via alkali-activated of synthetic calcium aluminosilicate precursors', *Cement and Concrete Research*, vol 89, pp. 120-135.

WBSCD 2009, *Recycling Concrete*, viewed 08 January 2018, <http://www.wbcsdcement.org/pdf/CSI-RecyclingConcrete-FullReport.pdf>.

Xie, T.& Ozbakkaloglu, T. 2015, 'Behavior of low-calcium fly and bottom ash-based geopolymer concrete cured at ambient temperature', *Ceramics International*, vol 41, no. 4, pp. 5945-5958.

Xu, W. Yiu Lo, T. Wang, W. Ouyang, D. Wang, P. & Zing, F. 2016, 'Pozzolanic reactivity of Silica Fume and Ground Rice Husk Ash as reactive silica in a Cementitious Study: A Comparative Study', *Materials (basel)*, vol 9, no. 3.

Ya-min, G. Yong-hao, F. Duo, Y. Yong-fan, G.& Chen-hui, Z. 2015, 'Properties and microstructure of alkali-activated slag cement cured at below- and about-normal temperature', *Construction and Building Materials*, vol 79, pp. 1-8.

Yuan, X-H. Chen, W. Lu, Z-A.& Chen, H.2014, 'Shrinkage compensation of alkali-activated slag concrete and microstructural analysis', *Construction and Building Materials*, vol 66, pp. 422-428.

Yuan, B. Yu, & Q. Brouwers, H.J.H. 2017, 'Assessing the chemical involvement of limestone powder in sodium carbonate activated slag', *Materials and Structures*, vol 50, no. 2, pp. 1-14.

Zhang, Z.H. Yang, T. & Wang, H. 2014, 'The effect of efflorescence on the mechanical properties of fly ash-based geopolymer binders', *23rd Australasian Conference on the Mechanics of Structures and Materials (ACMSM23)*, vol. Im Byron Bay, NSW, 9-12 December, Southern Cross University, Lismore, NSW, pp. 107-112.

Zhu, Q. 2011, *CO_2 abatement in cement industry*, viewed 08 January 2014, <http://www.iea-coal.org.uk/documents/82745/8189/co2-abatement-in-the-cement-industry>.

Živic, V. 2007, 'Effects of type and dosage of alkaline activator and temperature on the properties of alkali-activated slag mixtures', *Construction and Building Materials*, vol 21, no. 7, pp. 1463-1469.